AD-A071 369 H-TECH LABS INC SANTA MONICA CA F/G 18/3
THE DESIGN OF SUBTERRANEAN INSTRUMENTATION CABLES TO SURVIVE LA--ETC(U)
JUL 78 B A HARTENBAUM DNA001-77-C-0213
UNCLASSIFIED DNA-4636F NL

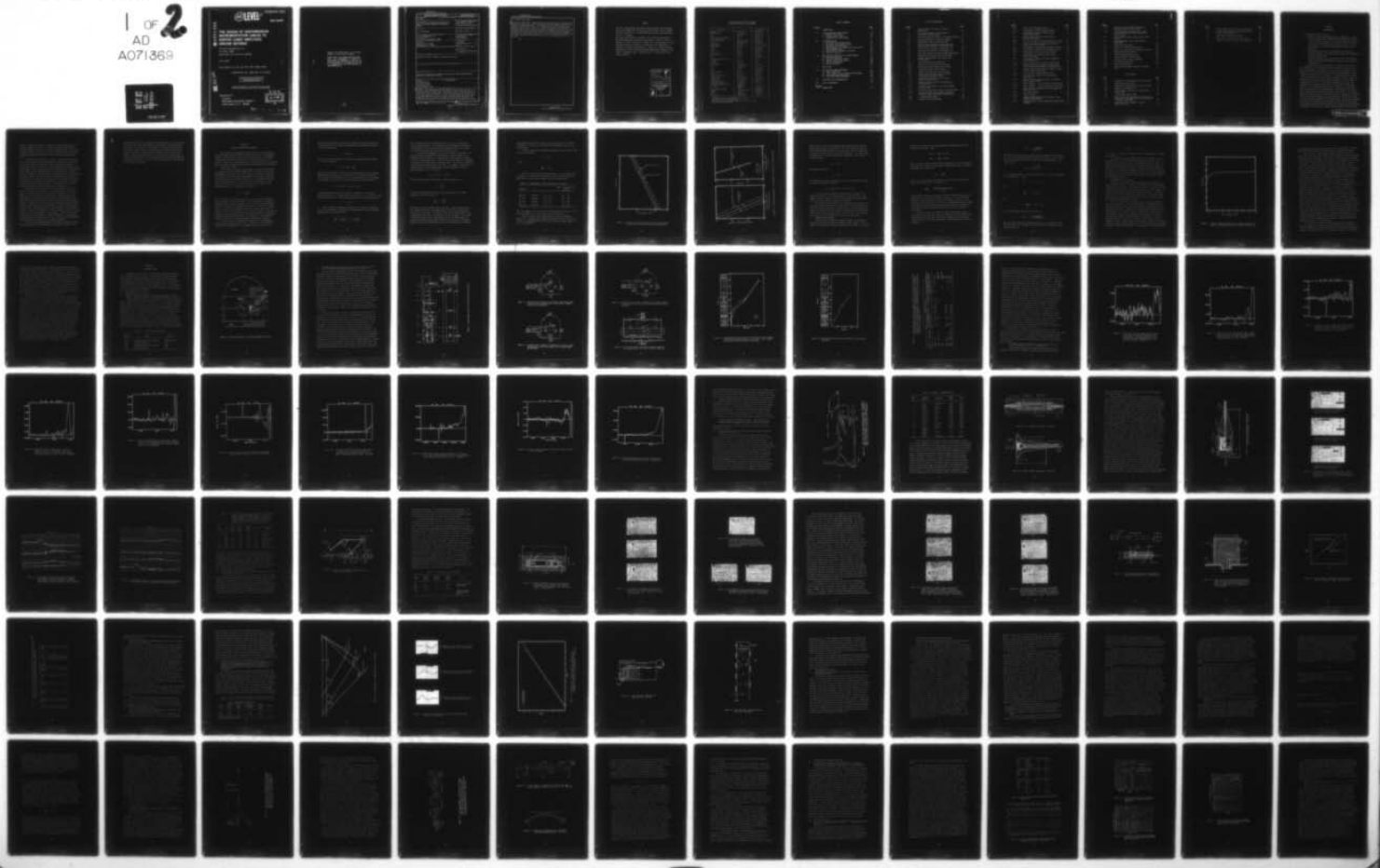

1 OF 2

AD

A071369

(12) LEVEL III

DNA 4636F

THE DESIGN OF SUBTERRANEAN INSTRUMENTATION CABLES TO SURVIVE LARGE AMPLITUDE GROUND MOTIONS

H-Tech Laboratories, Inc.
P.O. Box 1686
Santa Monica, California 90406

July 1978

Final Report for Period June 1977—May 1978

CONTRACT No. DNA 001-77-C-0213

APPROVED FOR PUBLIC RELEASE;
DISTRIBUTION UNLIMITED.

THIS WORK SPONSORED BY THE DEFENSE NUCLEAR AGENCY
UNDER RDT&E RMSS CODE B344077462 J11AAXSX35250 H2590D.

Prepared for
Director
DEFENSE NUCLEAR AGENCY
Washington, D. C. 20305

Destroy this report when it is no longer needed. Do not return to sender.

PLEASE NOTIFY THE DEFENSE NUCLEAR AGENCY, ATTN: TISI, WASHINGTON, D.C. 20305, IF YOUR ADDRESS IS INCORRECT, IF YOU WISH TO BE DELETED FROM THE DISTRIBUTION LIST, OR IF THE ADDRESSEE IS NO LONGER EMPLOYED BY YOUR ORGANIZATION.

UNCLASSIFIED

SECURITY CLASSIFICATION OF THIS PAGE *(When Data Entered)*

REPORT DOCUMENTATION PAGE	READ INSTRUCTIONS BEFORE COMPLETING FORM
1. REPORT NUMBER: DNA 4636F	2. GOVT ACCESSION NO. / 3. RECIPIENT'S CATALOG NUMBER
4. TITLE *(and Subtitle)*: THE DESIGN OF SUBTERRANEAN INSTRUMENTATION CABLES TO SURVIVE LARGE AMPLITUDE GROUND MOTIONS	5. TYPE OF REPORT & PERIOD COVERED: Final Report for Period June 1977—May 1978 / 6. PERFORMING ORG. REPORT NUMBER
7. AUTHOR(s): B. A. Hartenbaum	8. CONTRACT OR GRANT NUMBER(s): DNA 001-77-C-0213
9. PERFORMING ORGANIZATION NAME AND ADDRESS: H-Tech Laboratories, Inc. P.O. Box 1686 Santa Monica, California 90406	10. PROGRAM ELEMENT, PROJECT, TASK AREA & WORK UNIT NUMBERS: NWET Subtask J11AAXSX352-50
11. CONTROLLING OFFICE NAME AND ADDRESS: Director Defense Nuclear Agency Washington, D.C. 20305	12. REPORT DATE: July 1978 / 13. NUMBER OF PAGES: 140
14. MONITORING AGENCY NAME & ADDRESS *(if different from Controlling Office)*	15. SECURITY CLASS *(of this report)*: UNCLASSIFIED / 15a. DECLASSIFICATION/DOWNGRADING SCHEDULE

16. DISTRIBUTION STATEMENT *(of this Report)*

Approved for public release; distribution unlimited.

17. DISTRIBUTION STATEMENT *(of the abstract entered in Block 20, if different from Report)*

18. SUPPLEMENTARY NOTES

This work sponsored by the Defense Nuclear Agency under RDT&E RMSS Code B344077462 J11AAXSX35250 H2590D.

19. KEY WORDS *(Continue on reverse side if necessary and identify by block number)*

Cables
Instrumentation
Electrical Cables
Underground Tests
Nuclear Weapons Tests
Ground Motion

20. ABSTRACT *(Continue on reverse side if necessary and identify by block number)*

Analyses, both mathematical and experimental, are developed to assist in the rational design of subterranean instrumentation cables that must survive pressures of two to three kbars, large axial strains of the order of 40 percent, and severe shear offsets, to allow the measurement of late-time displacements induced by large explosions. Reports on underground tests and other pertinent literature are reviewed and analyzed for the purpose of documenting the design of instrumentation cables, the performance of cables,

→over

DD FORM 1 JAN 73 1473 EDITION OF 1 NOV 65 IS OBSOLETE

UNCLASSIFIED

SECURITY CLASSIFICATION OF THIS PAGE *(When Data Entered)*

20. ABSTRACT (Continued)

and cable problem areas. Both past and current cable practices are also documented from discussions on cable techniques with experimenters involved in the fielding of underground tests. The state-of-the-art in subterranean instrumentation cable design is set forth. Uncertainties both in current design procedures and in the performance of hardware components are pointed out. The review indicates that no proven technique is currently available for providing reliable data transmission in the large strain, high pressure environment imposed by an underground nuclear test. A program to advance the state-of-the-art, which emphasizes logical design, analysis, and experimental tests, is laid out.

PREFACE

This work was sponsored by the Defense Nuclear Agency under Government Contract No. DNA001-77-C-0213 and was authorized under Project J11AAXS, Task X352, Work Unit 50. The DNA Contracting Officer's Representative was Mr. T. E. Kennedy.

The author appreciates the assistance of the following individuals: R. Shunk (Electromechanical Systems of New Mexico), R. Bass, W. Cook, B. Benjamin, C. Smith, H. Miller, L. Vortman, and R. Reed (Sandia), H. Kratz (Systems, Science and Software), D. Smith and J. Day (Waterways), J. LaComb and R. Sherky (Field Command), F. Sauer and C. Vincent (Physics International), Major Volberding (Defense Communications Agency), P. Dai (TRW), G. Abrahamson (SRI), M. Nowak (H-Tech), C. Finney (DDC), and C. Gonzalez (DASIAC).

Conversion factors for U.S. customary to metric (SI) units of measurement.

To Convert From	To	Multiply By
angstrom	meters (m)	1.000 000 X E -10
atmosphere (normal)	kilo pascal (kPa)	1.013 25 X E +2
bar	kilo pascal (kPa)	1.000 000 X E +2
barn	meter^2 (m^2)	1.000 000 X E -28
British thermal unit (thermochemical)	joule (J)	1.054 350 X E +3
calorie (thermochemical)	joule (J)	4.184 000
cal (thermochemical)/cm^2	mega joule/m^2 (MJ/m^2)	4.184 000 X E -2
curie	giga becquerel (GBq)*	3.700 000 X E +1
degree (angle)	radian (rad)	1.745 329 X E -2
degree Fahrenheit	degree kelvin (K)	$t_K = (t° f + 459.67)/1.8$
electron volt	joule (J)	1.602 19 X E -19
erg	joule (J)	1.000 000 X E -7
erg/second	watt (W)	1.000 000 X E -7
foot	meter (m)	3.048 000 X E -1
foot-pound-force	joule (J)	1.355 818
gallon (U.S. liquid)	meter^3 (m^3)	3.785 412 X E -3
inch	meter (m)	2.540 000 X E -2
jerk	joule (J)	1.000 000 X E +9
joule/kilogram (J/kg) (radiation dose absorbed)	Gray (Gy)**	1.000 000
kilotons	terajoules	4.183
kip (1000 lbf)	newton (N)	4.448 222 X E +3
kip/inch^2 (ksi)	kilo pascal (kPa)	6.894 757 X E +3
ktap	newton-second/m^2 ($N-s/m^2$)	1.000 000 X E +2
micron	meter (m)	1.000 000 X E -6
mil	meter (m)	2.540 000 X E -5
mile (international)	meter (m)	1.609 344 X E +3
ounce	kilogram (kg)	2.834 952 X E -2
pound-force (lbf avoirdupois)	newton (N)	4.448 222
pound-force inch	newton-meter (N·m)	1.129 848 X E -1
pound-force/inch	newton/meter (N/m)	1.751 268 X E +2
pound-force/foot^2	kilo pascal (kPa)	4.788 026 X E -2
pound-force/inch^2 (psi)	kilo pascal (kPa)	6.894 757
pound-mass (lbm avoirdupois)	kilogram (kg)	4.535 924 X E -1
pound-mass-foot^2 (moment of inertia)	kilogram-meter^2 ($kg·m^2$)	4.214 011 X E -2
pound-mass/foot^3	kilogram/meter^3 (kg/m^3)	1.601 846 X E +1
rad (radiation dose absorbed)	Gray (Gy)**	1.000 000 X E -2
roentgen	coulomb/kilogram (C/kg)	2.579 760 X E -4
shake	second (s)	1.000 000 X E -8
slug	kilogram (kg)	1.459 390 X E +1
torr (mm Hg, 0° C)	kilo pascal (kPa)	1.333 22 X E -1

*The becquerel (Bq) is the SI unit of radioactivity; 1 Bq = 1 event/s.
**The Gray (Gy) is the SI unit of absorbed radiation.

A more complete listing of conversions may be found in "Metric Practice Guide E 380-74," American Society for Testing and Materials.

TABLE OF CONTENTS

LIST OF ILLUSTRATIONS

LIST OF TABLES

SECTION I

INTRODUCTION

The purpose of this work was to:

a. Develop analyses, both mathematical and experimental, to assist in the rational design of subterranean instrumentation cables that will survive pressures of 2 to 3 kbar, large axial strains of the order of 40 percent and severe shear offsets, to allow the measurement of late-time displacements induced by large explosions.

b. Review and analyze reports on underground tests and other pertinent literature to document cable design, cable performance, and cable problem areas.

c. Establish both past and current cable practices by discussing cable techniques with experimenters involved in the fielding of underground tests.

The various aspects of cable design are unfolded in this report in the following way: The general scene is set in Section II where use is made of the geometry of a homogeneous test field and experimental data to establish, in an approximate way, the strains that are imposed on a cable system at the stress levels of interest. It is emphasized that although a cable system must survive the strains and stresses that would arise in a homogeneous field and which can be quite formidable, it will be shown in Sections III and V that it is the offsets and shears that arise in an inhomogeneous, anisotropic geology that are responsible for many cable failures. At the present state-of-the-art, techniques for calculating shear offsets are not well established and it is this deficiency which is partly responsible for making cable design an uncertain art. The entire picture of cable design and cable failure problems is sketched in Section II.3. The outline provides a guide for the present work; it should also be used as a check list by a designer of a new cable system. We have not considered in detail the properties of any one electrical cable and for good reason: In the high stress and large strain region it is almost certain that conduit is necessary to protect cables against the shear offsets that inevitably

develop in geologic formations. As long as the conduit does not fail, it is almost certain that a variety of cables can operate satisfactorily inside the conduit. Not only can various techniques be used, if necessary, to minimize electrical noise, but we believe that fiber-optic cables will eventually supplant copper cables, at least in high data capacity trunk lines.

In Section III the results of a survey of the literature pertinent to the cable survival problem is presented. The literature, for the most part, is not directly concerned with cable performance; nonetheless, a considerable amount of data useful to cable hardening can be gleaned from the documents. We have analyzed reports on underground tests, high explosive tests, communications, and command and control cable systems, composite materials, and material properties tests for applicability to the underground test cable problem. The survey includes information reported directly in the documents, our analyses of data obtained from the documents, and additional information obtained from the authors of the reports to supplement what was found in the reports themselves. The importance of avoiding or resisting shear loads on cables is emphasized in Section III.

An analysis of shear loads on cables is presented in Section IV, where it is found that the results of six different elastic and plastic models do not differ greatly for the shear force imposed on a cable by a backfill that is stressed to the yield surface. The uncertainty in the shear strength properties of backfill material that has suffered large deformations is of the same order as the differences that exist between the analyses. Documentation of both current and past cable fielding practices, obtained by way of meeting with experimenters at several fielding agencies and by personal involvement with some of the experiments, is presented in Section V. There is no consensus as to what constitutes a good cable system. Practices vary from experimenter to experimenter. In some cases there is controversy over the performance of certain components. It is hoped that one of the values of Sections III and V will be to prevent one experimenter from reinventing the past mistakes of another experimenter.

A series of experiments designed to shed light on problems caused by shear and by large axial deformations are discussed in Section VI. The

importance both of backfill properties at the appropriate strains and strain rates and of the proper end conditions is emphasized. The experiments are conceived to test sections of cable conduit to determine the loads imposed on conduit by backfill and also to determine the interactions between the conduit and backfill. The experiments can employ scaled-down sections of conduit to define loads and deformations. The value of an "end-to-end" or complete scaled-down model of a field experiment to determine cable survival is uncertain at present. In Section VII the conclusions and recommendations of this study are presented.

SECTION II

CABLE STRAINS AND CABLE FAILURE

The two main items presented in this section are (a) an analysis of the strains imposed on line elements (cables, if you will) in a homogeneous medium by a point explosion, and (b) a definitive outline of cable design considerations that must be dealt with if a successful design is to be obtained. Whereas the former exposition is an idealization useful for setting ideas, the latter listing includes many practical problems of the real world.

1. RADIAL CABLE STRAINS

For the purpose of making rough estimates a straightforward method of determining the displacements produced by an explosion is to relate the displacements to the size of the cavity produced. Considerable work has been done both in connection with underground nuclear weapons testing and the Plowshare program to determine cavity size as it depends on the yield, depth of burial and geology. A scaling law has been developed for the radius of the cavity, R_c, in terms of the yield, Y, the density of the surrounding material, ρ, and the depth of burial, h,

$$R_c = G \frac{Y^{1/3}}{(\rho h)^{1/4}},$$

where the yield is in kilotons, the density is in grams/cubic centimeter and the lengths h and R_c are in meters[1]. The coefficient G is determined experimentally; values are available for tuff, alluvium, granite, dolomite and salt. For NTS tuff a representative value for G is 76.42; for example, in Logan a yield of 5.4 KT produced a cavity of radius 28 meters and in Blanca a yield of 22 KT produced a cavity of radius 44 meters. The essential dependence on the scaling law is that the radius cubed which represents the volume is proportional to the yield. The coefficient of proportionality between the volume and yield then depends on the material and depth.

The cavity iteslf is produced by displacement of the surrounding material and by squeezing out the voids. A porosity of a few percent is common in the surrounding rock. For example, with a porosity of 3 to 4

percent only about three cavity radii are needed to accumulate enough voids to form the cavity. The relative displacements are determined as follows. Prior to the explosion

$$M = \frac{4}{3} \pi \rho_o r^3 ,$$

where M is the mass of material at density ρ_o contained within the radius r. After the explosion

$$M = \frac{4}{3} \pi \rho_1 \left(R^3 - R_c^3 \right) ,$$

where M is the same mass of material at a compacted density ρ_1 now contained between the cavity radius R_c and the radius R. The relation between the final position of the material, R, and its initial position, r, is determined by the radius of the cavity, the relative densities, and the porosity n,

$$R^3 = R_c^3 + \frac{\rho_o}{\rho_1} r^3 = R_c^3 + (1 - n) r^3 .$$

In this form the displacement is relatively insensitive to the porosity since the density ratio is about unity and independent of the porosity for small values of the porosity. For the incompressible case the relation reduces to

$$R^3 = R_c^3 + r^3 .$$

When the radial displacements are known, it is possible to determine the ratio of an element of length dR after the explosion to that of the same element dr before any motion occurs,

$$\frac{dR}{dr} = \frac{\rho_o}{\rho_1} \left(\frac{r}{R} \right)^2 = (1 - n) \left(\frac{r}{R} \right)^2 .$$

As r increases this ratio increases from zero to ρ_o/ρ_1, which approaches unity for small porosity. This implies that radial elements are subjected to compression only, with the compression being very large at the origin (dR = 0) and decreasing with distance from the zero point.

The preceding development is based on the condition that there is an effective porosity independent of the pressure. However, thermal and mechanical cracking effects will produce dilatancy and oppose the collapse of pores by the pressure field. The effective porosity which can be squeezed out depends on the range from the explosion source. Thus there is a departure from the idealized conditions just described. For example, using the preceding relation for the incompressible case and introducing u for the net displacement, u = R - r, we have

$$R^3 = (r + u)^3 = R_c^3 + r^3 .$$

For relatively small net displacements (u small compared to r),

$$u = \frac{R_c^3}{3r^2} ,$$

so that the displacement falls off as the inverse square of the range. Furthermore, the radial strain is

$$\frac{du}{dr} = -\frac{2}{3}\frac{R_c^3}{r^3} ,$$

which falls off as the inverse cube of the range. These formulas based on the incompressible limit are intended mainly to indicate the theoretical trends which are possible. For design calculations measured values for the displacements must be used as discussed in the next paragraph. For example, to obtain agreement with the experimental data for the displacement at a scaled range of 100 meters a cavity radius of about 20 meters is required. However, according to measurements of cavity size summarized in the scaling

law presented above a yield of about 2.8 KT is required for this radius. The offset, by a factor of 2.8, indicates the approximate nature of the relationships.

A recent compilation of measured displacements, made by Perret[2], can be fit by the relation

$$u = cr^{-a}$$

so that

$$\frac{du}{dr} = -a\,\frac{u}{r}\,.$$

Scaled to one kiloton with the displacement, u, in centimeters and the range, r, in meters, both the constants a and c, and the range over which Perret fit the data are summarized in the following table.

Table 2.1 Displacement vs range regression fit constants.

Material	c	a	Range of Regression Fit ($m/KT^{1/3}$)
Alluvium	$2.22(10)^2$	1.11 ± 0.11	100 - 350
Dry Tuff	$3.80(10)^5$	2.20 ± 0.21	100 - 500
Wet Tuff	$4.90(10)^6$	2.63 ± 0.19	50 - 600
Hard Rock	$8.72(10)^4$	1.88 ± 0.14	70 - 2200

Thus, for example, in the case of wet tuff the exponent in the decay law is 2.63 rather than 2.0 as in the simple model presented above.

A plot of stress versus scaled range for wet tuff is given in Figure 2.1[3]. To examine cable performance between 3 kbar and 0.5 kbar it is necessary to extrapolate Perret's data back to shorter ranges, Figure 2.2, i.e., $r \approx 30$ ($m/KT^{1/3}$).

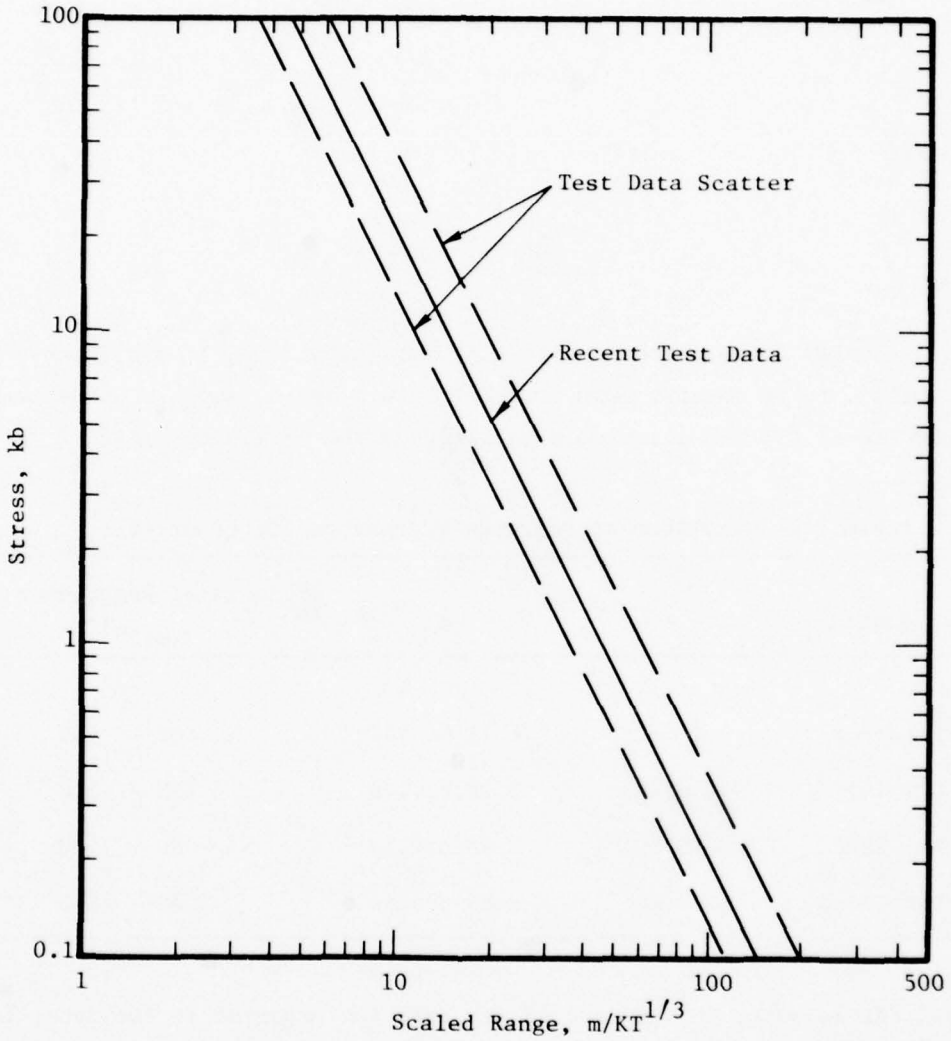

Figure 2.1 Recent wet tuff test data for stress vs scaled range with band of effective maximum and minimum stress.

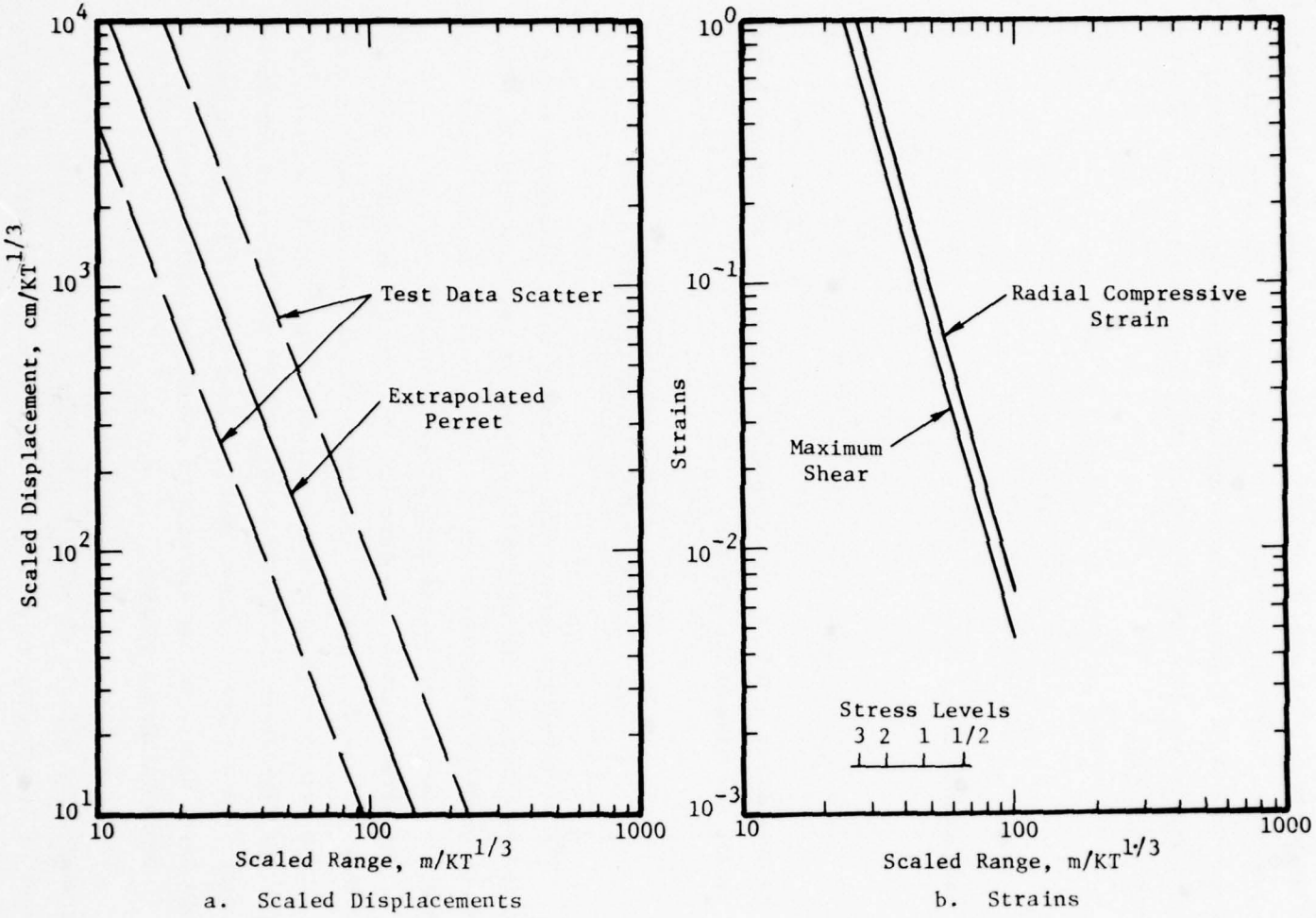

Figure 2.2 Scaled displacements, a, and strains, b, in wet tuff vs scaled range.

Figure 2.2b is a plot of the radial and shear strains obtained from the displacements using a static analysis. The static analysis implies that the peak displacements occurred at the same time. The error inherent in this method can be estimated from machine calculations. The radial strain is compressive and is calculated from the displacement by the relation previously given,

$$\varepsilon_r = -a \frac{u}{r} .$$

The tangential strain is

$$\varepsilon_t = \frac{u}{r} .$$

The maximum shear strain is determined as half of the difference between the radial and tangential strains,

$$\gamma_{max} = \frac{1}{2} \left(\frac{u}{r} + a \frac{u}{r} \right) = \frac{1}{2} (1 + a) \frac{u}{r} .$$

For an idealized underground explosion which is assumed to be spherically symmetric the only displacement is radially outward. This movement produces compressive strains in the radial direction and tensile strains in the two transverse tangential directions.

The strains given in Figure 2.2 each contain an extra factor of 1/r over that for the displacement from which the strains are derived and so the strain versus range relation is rather steep. As can be seen for the ranges out from about the 3 kbar level to less than 0.5 kbar the strains decrease from a value of almost unity to less than 0.01. The 10 percent strain level occurs in the vicinity of the 1 kbar stress level.

2. NONRADIAL CABLE STRAINS

So far we have considered only radial elements. We continue by determining the effects of cable orientation on cable strains. For an element of length with an arbitrary orientation with respect to the radial

direction we can take ds, dS as the differential lengths before and after straining, respectively. Thus

$$(ds)^2 = (dr)^2 + (r\,d\theta)^2$$

$$(dS)^2 = (dR)^2 + (R\,d\theta)^2$$

where r, R and dr, dR have already been introduced and $d\theta$ is the differential polar angle which remains constant during a displacement because of symmetry. Furthermore, we recognize that

$$\tan\alpha = \frac{r\,d\theta}{dr},$$

where α is the angle between the element of length and the radial line in the initial configuration. It follows that,

$$\left(\frac{dS}{ds}\right)^2 = \frac{(dR/dr)^2 + (R^2/r^2)\,\tan^2\alpha}{1 + \tan^2\alpha},$$

which provides the relation between the elements of length before and after straining for an arbitrary orientation. Of course, if $\alpha = 0$ so that the element is in the radial direction then dS/ds reduces to dR/dr. Just as the quantity dR/dr represents the ratio of an infinitesimal element of length after loading to the same element of length before loading for lengths in the radial direction the quantity dS/ds does the same for an arbitrary orientation.

From the relation just derived for dS/ds the remarkable result is obtained that it is possible to choose an orientation for the cable at each radial station such that there is no strain produced in the cable going from the initial to the final configuration! Mathematically we set dS/ds = 1 and obtain

$$\tan^2\alpha = \frac{1 - (dR/dr)^2}{(R/r)^2 - 1} .$$

This relation is theoretically rigorous; the only limitation in determining tan α is how well the displacement is known as a function of range. Using the relation previously derived for dR/dr with the approximation $\rho_o/\rho_1 = 1$ there results

$$\tan \alpha = \frac{r}{R}\sqrt{1 + \frac{r^2}{R^2}} .$$

It is of course possible to use the measured values for the net displacement u to determine tan α. Since

$$R = r + u = r + cr^{-a} ,$$

then

$$\left(\frac{R}{r}\right)^2 - 1 = 2\,\frac{u}{r} + \frac{u^2}{r^2}$$

and

$$1 - \left(\frac{dR}{dr}\right)^2 = 2a\,\frac{u}{r} - a^2\,\frac{u^2}{r^2}$$

so that by using the previously derived relation

$$\tan^2\alpha = a\,\frac{1 - (1/2a)(u/r)}{1 + (1/2)(u/r)} .$$

Thus, for large ranges $\tan^2\alpha$ approaches a and not two as obtained for the incompressible case. Incidently, since the dilation (the change in volume per unit volume) is

$$\varepsilon_r + 2\varepsilon_t = -(a - 2)\frac{u}{r}$$

a value for a not equal to two implies that the incompressibility condition does not hold.

By using these formulas and Perret's data to determine α it can be seen from Figure 2.3 that as one moves further from the point of the explosion it is possible to orient a cable between about 40 to 55° to the radial without producing any strain in the cable. At smaller angles the cable will suffer compressive strains, at larger angles the strains will be tensile. It is almost surely impractical to lay a cable in a curved arc to conform to the zero strain condition. However the zero strain condition may be useful over short sections of cable when it is necessary to alter the direction of a cable.

3. COMPONENTS OF A CABLE SYSTEM

Up to now we have been concerned mainly with an idealization of strains imposed on cables. In Section IV an analysis of the shear loading of cables will be taken up. We continue by noting that in practice a large number of problems must be considered in the design of a cable system, some of which are not readily amenable to mathematical analysis. We believe, however, that an orderly and rational approach which includes both mathematical analysis and experimental tests will provide an expeditious means for improving the survivability of cables.

We find it convenient to consider a cable system to be composed of three major components. The components constitute a nonredundant series system, so that the failure of any component makes the entire data link susceptible to failure. Starting at an instrumentation canister, the first major component is a signal line which is required not to interfere with the mechanical response of the transducers. Many signal lines may be connected into a bundle or multiplexed to form a trunk line. The distinguishing feature of a trunk line is that it is sufficiently far from a canister so that it cannot influence the mechanical response of a transducer. Between the canister and the output end of the trunk line there may be cable connectors, splices, and transitions. The transitions include sections for

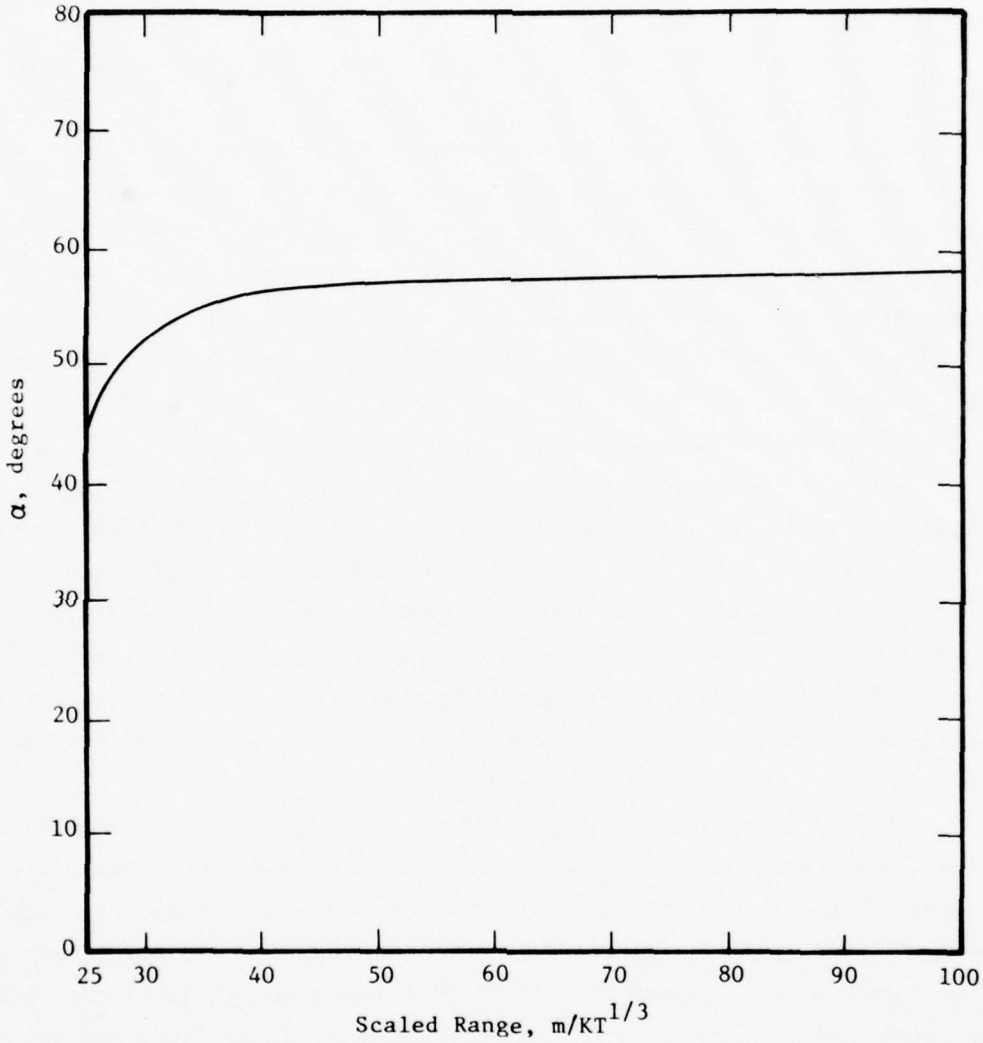

Figure 2.3 Effective angle with respect to the radial direction vs range, for orientation of cable to eliminate axial strain.

the fanning-in and fanning-out of cables to and from trunk lines, for making changes in direction, and for effecting changes in mechanical impedance.

The first step in the mechanical design of a cable system is the definition of the entire cable topology from transducer to recording equipment and the making of an estimate of cable strains. More important than whether a cable is geometrically radial or nonradial is the determination of the loads on the cable. A cable that starts out from a canister along a radial is often made to change its direction to conform to the geometry of access drifts. Line-of-sight pipe expansion and other late-time motions may impose transverse loads on a radial cable. A nonradial topology may be satisfactory; in fact, one experiment with a completely non-radial cable topology (unfortunately it was a small-scale experiment and there are some questions about acaling) experienced no cable failures whatsoever (Section III.5.2). (We note also the very important fact that cable survival issues aside, a non-radial cable topology may result in a rotational acceleration and rotational velocity being induced in free-field motion instrumentation which can cause erroneous results.) Implicit in the radial placement is the assumption that the geology is homogeneous; if a radial line crosses a plane of weakness that will produce a shear offset under load or crosses a construction discontinuity, then the radially placed cable will be subject to failure. A non-radial cable topology, even in a homogeneous medium, will be loaded in shear and be subjected to rotations, but in a homogeneous medium the shears and rotations are almost surely no more significant than the axial loads (which can be quite impressive) placed on a radially oriented cable. The main problem that must be contended with by a non-radial cable is the shear that arises at planes of weakness and at abrupt transitions. Particular attention must be given to differential motions arising at collars, bulkheads, and between multiple pours. Geologic discontinuities are particularly troublesome because of the difficulty in avoiding crossing the multitude of faults, bedding planes, or regions of rapidly changing shear strength that exist in a typical geology.

A wide variety of geologic variables and construction parameters have the potential for influencing the performance of a cable system. It would be advantageous to catalog how cables are affected by the mechanical properties of native rock such as tuff, granite, sandstone, and limestone,

and of construction backfill such as superlean, rock matching, and high strength grouts, sand, and concrete. Of particular interest are the effects of yielding, crushing, extrusion, and water migration. An accurate definition of what function a particular backfill can perform is important, to wit, under certain circumstances lateral support to prevent buckling may be needed, but at other times it might be advantageous to have the backfill flow past the cable. Whether it is feasible or desirable to add reinforcement at weak interfaces is an important problem that needs to be addressed as does the use of crush-space to protect cables. One of the problems, of course, with using crush-space is the uncertainty in the magnitude of the offset that can develop at a weak zone. Similarly, the loads imposed on reinforcements may be so great as to make the scheme impractical.

Although the properties of electrical cables are not analyzed at any length in this report they are certainly important and must be considered in any practical design. A field design must address the following points: (a) elongation to failure, (b) ductility, (c) pressure resistance, (d) effects of voids in the cable, (e) effects of rattle space in conduit, (f) imperviousness to water entry, (g) inertness to chemical attack, e.g., from coal tar and RTV, (h) mechanism for taking up strain, (i) effects of conduit filling materials, and (j) integrity of electrical insulation under mechanical and electrical stress. Some designs have employed stout conduit with a number of mesh armored cables fanning into the conduit or with a number of soft TSP fanning out of the conduit. The fan-in and fan-out sections were in high stress regions and because both the mesh armored and soft TSP cables had failed on previous tests the designs appear illogical to us. The fan-in and fan-out problem needs additional work. Controversy over gas-seal connector performance needs to be resolved. One of the issues is the ability of the internal pins to withstand shock loading. Pressure loading and shock tests need to be performed. Experimenters usually expend some effort on designing the connection between the cable and canister, but test data to document the integrity of the designs are needed.

SECTION III

LITERATURE SURVEY

A broad view of cable failure problems and cable design techniques can be obtained from the literature. In this section various documents are reviewed for data on horizontal line-of-sight tests, high explosive tests, Minuteman and Sanguine communications cable design, the performance of composite materials, and constitutive properties tests. The reviews are specialized to the problem of cable hardening and often contain analyses not found in the documents themselves. Data not pertinent to cable hardening are not discussed in the review.

4. HORIZONTAL LINE-OF-SIGHT TESTS

4.1 POR 6254 "Operation Latch Key, Shot Midi Mist, Project Officer's Report - Project 9.52 Stemming and Containment Dynamics," Vincent, C.

A limited number of gauges were installed for the stemming diagnostics add-on to Midi Mist as indicated in Table 3.1. A typical gauge installation layout obtained from the POR is shown in Figure 3.1. The cables were double braided stainless steel TSP (see Section IV.14) and were installed in the HLOS manway prior to the final grouting operation[4]. The Kaman gauges were sandbagged in place. Crescent data at station 153 was not presented in the POR because of poor data quality. The cables at station 185 failed at 14.2 ms, the time of ground shock arrival as indicated by Sandia slifers. One Kaman gauge recorded for about 1.5 ms. The Crescent gauges at stations 217 and 240 recorded for several milliseconds. The method chosen for data presentation does not allow the reader of the POR to determine cable failure times. Manganin data were not obtained because of a recording system failure.

Table 3.1. Gauge plan, shot Midi Mist.

Station	Gauge	Region
153	Crescent Velocity, SRI Manganin	Matching Grout
185	Kaman Air Pressure	Void
217	Crescent Velocity, SRI Manganin	Sand
240	Crescent Velocity	Sand

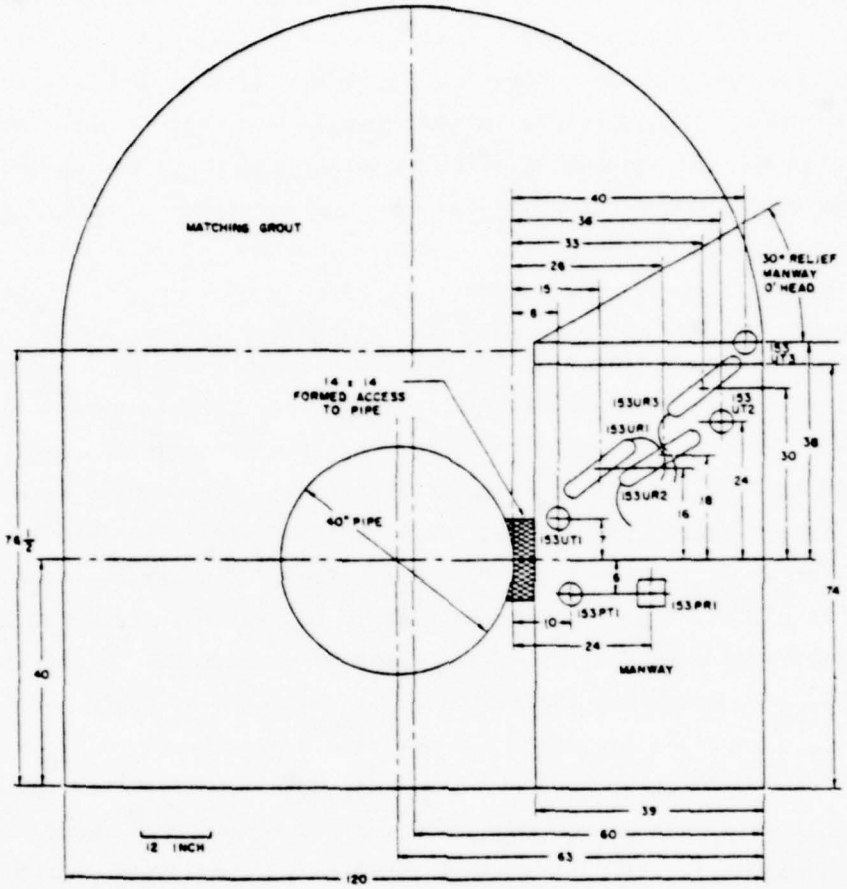

Figure 3.1 Typical gage layout in Midi Mist stemming (POR 6254).

4.2 POR 6389 "Operation Minute Gun, Shot Diana Mist, Project Officer's Report, Stemming and Containment Diagnostics," Vincent, C.

For the purpose of analyzing cable failure we examine the Diana Mist measurements made on the HLOS, in the stemming, and in the free field between 160 and 360 feet from the working point. The region is one of moderately high stress insofar as long term cable survival is concerned. The gauge layout with the implied cable topology is best illustrated by the gauge installation diagrams found in the original POR which are reproduced in Figures 3.2 through 3.6. The cables were double braided stainless steel TSP as noted in the preceding section and were routed inside a trench that ran along the left rib of the HLOS drift[5]. Note that the measurements in the free-field and at the tunnel wall used cable routings that had to turn corners into the stemming material. Ground motion time-of-arrival was measured in the stemming with PZT bimorphs and in the free-field with slifers. Gauges themselves are often used to indicate time-of-arrival, but in Diana Mist the velocity gauges were so noisy as to preclude, in our opinion, determining time-of-arrival. Binary pressure switches with set ranges of either 100 or 1000 or 5000 psi were used to indicate pressure front arrival in the HLOS.

Circuit failure times, which were determined from the plots of the digitized records presented in the POR, and time-of-arrival obtained from reduced data in the POR are summarized in Table 3.2. At station 1+60 the POR text states that cable break occurred at approximately 8 ms, although this cannot be determined from the POR records which extend only to 8 ms. The gauges at station 1+60 were Pace-Wiancko transducers installed in a sand-filled alcove facing the HLOS. The failure of these gauges was apparently caused either by gas shock induced motions or by shrapnel. At station 2+00 the DX velocity gauge records indicate a time to cable failure of 17.4 ± 1.0 ms, which is earlier than the ground shock arrival implied by the PZT TOA's or the slifer (the POR time-of-arrival plots are reproduced in Figures 3.7 and 3.8). The HLOS pipe pressure switches indicate a pressure front in the pipe preceding the ground shock by a considerable amount. The pressure switch set levels were so low, however, that we know only that the pressure exceeded 1000 psi, which almost surely is too low to cause cable

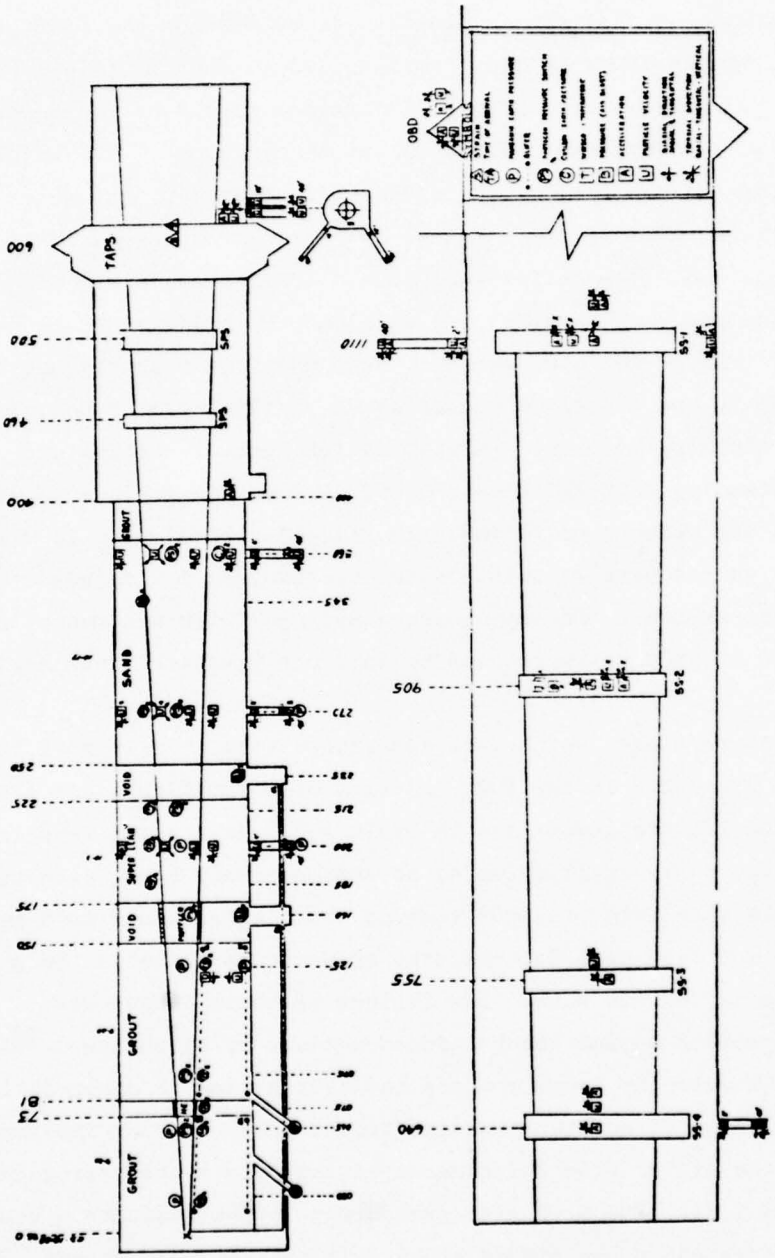

Figure 3.2 Experimental layout on Diana Mist HLOS (POR 6389)

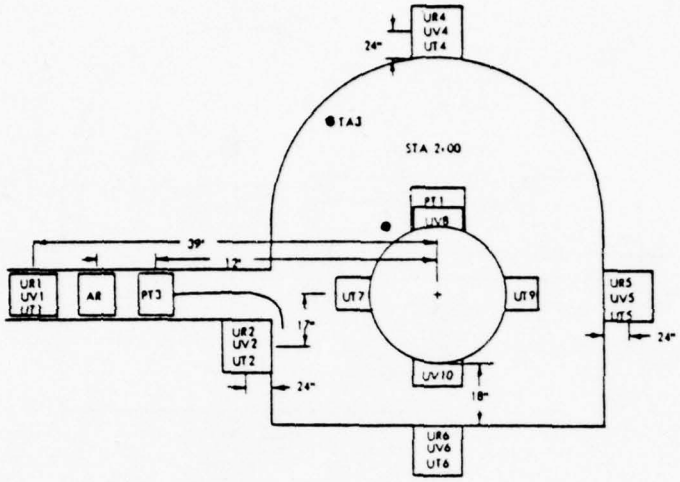

Figure 3.3 Elevation view: Pressure, acceleration, and velocity gage installation in superlean grout, Station 2+00, looking toward the WP (POR 6389).

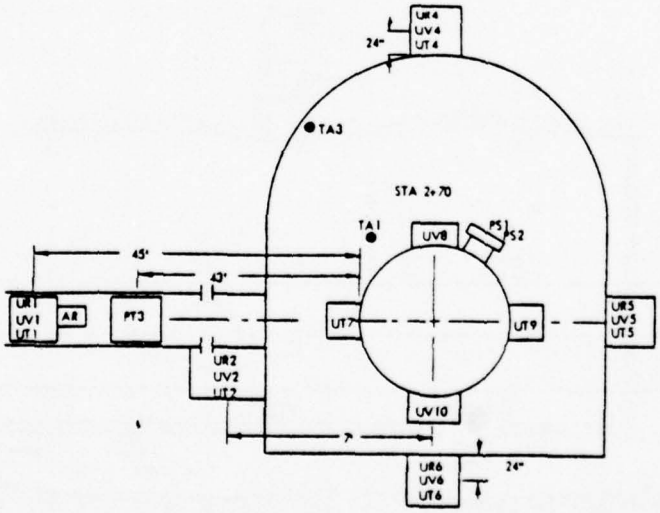

Figure 3.4 Elevation view: Pressure, acceleration, and velocity gage installation in sand stem, Station 2+70, looking toward WP (POR 6389).

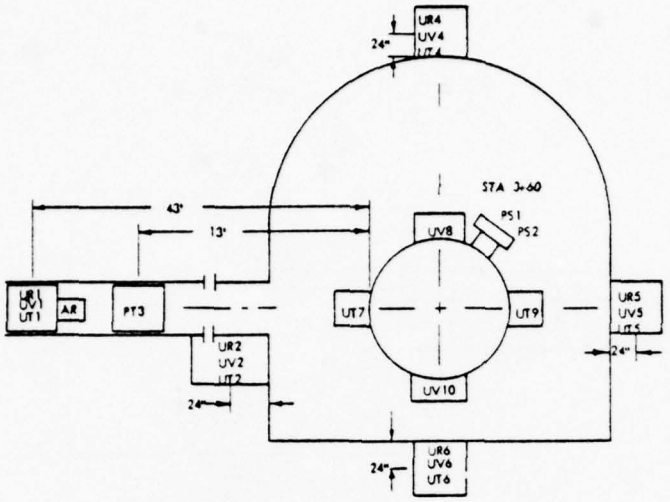

Figure 3.5 Elevation view: Pressure, acceleration, and velocity gage installation in sand stem, Station 3+60, looking toward WP. (POR 6389)

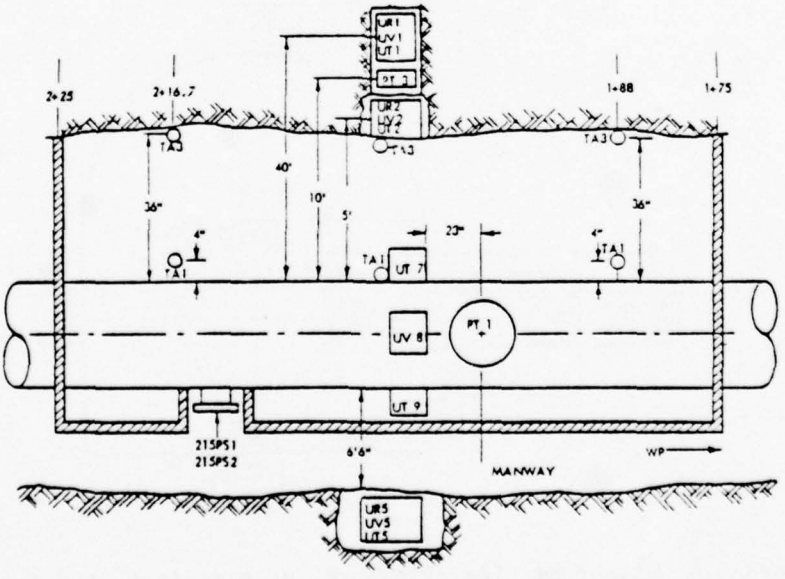

Figure 3.6 Plan view: Pressure and velocity gage installation in superlean grout, 175 feet to 225 feet. (POR 6389)

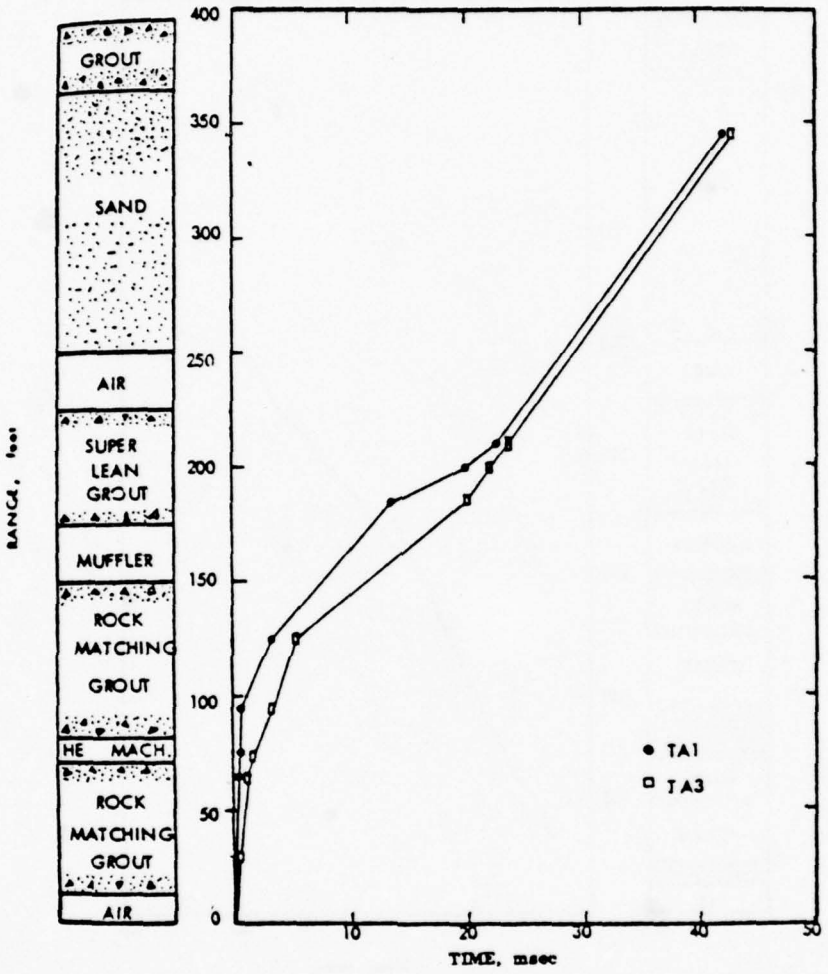

Figure 3.7 Reduced time-of-arrival data from PZT gages in tunnel stemming. The time-of-arrival was taken to be the time of first signal output from the crystal circuit.[7] (POR 6389)

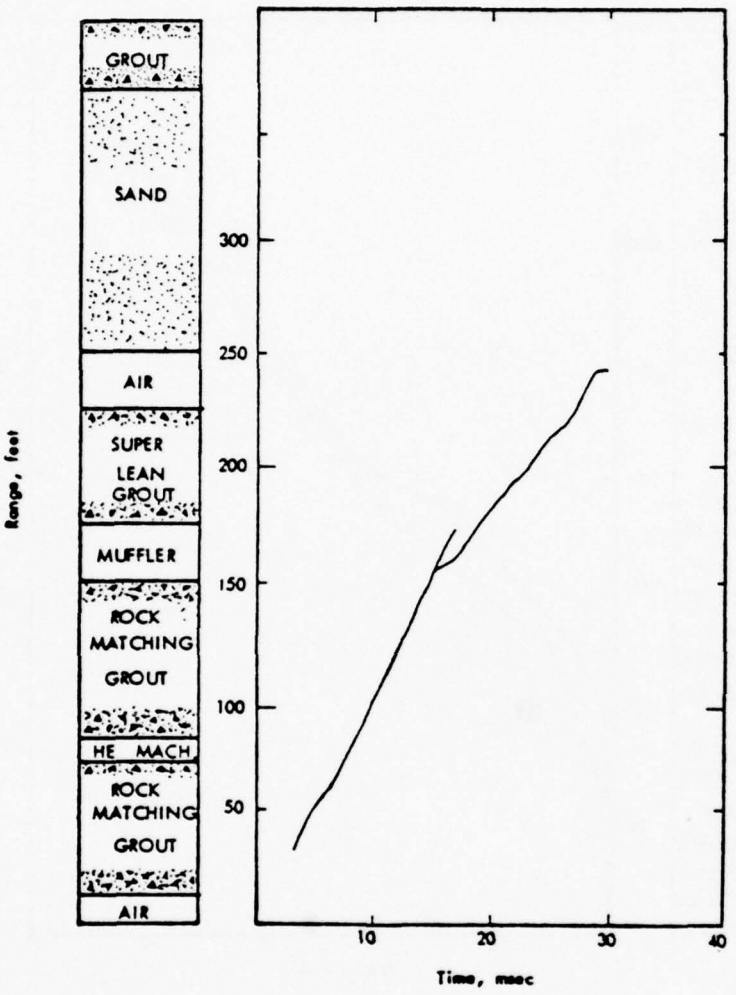

Figure 3.8 Reduced time-of-arrival data from slifers in free-field. (POR 6389)

Table 3.2. Cable break times and various times-of-arrival. All times in milliseconds. PZT TOA's denoted as HLOS were made 8 inches from HLOS; those denoted as wall were made 36 inches from HLOS. HLOS pressure in psia. PZT interpolated time at station 1+60 based on ground motion; pipe rupture may have occurred at approximately 8 ms.

Station	Cable Break	Time-of-Arrival							Stemming Region
		In-Stemming - PZT			Free Field Slifer	HLOS Pressure			
		HLOS	Wall			5000	1000	100	
1+60	~8.	(9.5)	(12.0)	interpolated	17 ± 0.7	7.5	2.0	2.0	Void
2+00	17.4 ± 1.0	21.5	24.8		22.0				Superlean Grout
2+15							10.0		Superlean Grout
2+35	~27.	26.7	27.9	interpolated					Void
2+70	39.5 ± 3.4	30.0	31.0				15.0	8.0	Sand
3+60	>(48.5 to 68.5)	41.0	43.0	extrapolated				72.5	Sand

failure. If cable failure were induced by pipe expansion then it is surprising that the PZT TOA's did not register at earlier times. The reported time-of-arrivals were, in fact, determined from the first signal output from the crystal circuits[6]. We speculate that the cables were cut by the action of the explosive driven sample protection system (SPS's). Some typical DX velocity gauge records are shown in Figures 3.9 through 3.14. Although the records were terminated by cable break before the onset of strong ground motion it is evident that electrical noise was a severe problem, see especially Figure 3.14. Assuming a P-wave speed of 8,000 ft/s and a grout density of 1.9 g/cm^3 the transverse DX gauge records 200 2UT and 200 1UT, Figures 3.12 and 3.15, if taken at face value, imply an outward moving pressure front in excess of 1.4 kbar. This picture of early motion needs to be corroborated by the PZT TOA's and the Manganin stress gauges, but the necessary data are not presented in the POR. The fact that the air pressure gauges in the void at 2+35 did not record any high pressure contradicts the picture of high pressures implied by the 200 1UT and 200 UT gauges. The cables at 2+35 failed at the time of ground shock arrival. At station 2+70 the cables failed at 39.5 ± 3.4 ms. The 8 ± 3.4 ms of recording time is too short for late time measurements. The ground motion environment is moderately severe with radial velocities of the order of 80 ft/s, Figure 3.16. Gauge 270 1UR, Figure 3.16, exhibits a cable break, but the erratic behavior of gauge 270 4UV, Figure 3.17, initially may have arisen from a loose connector. At station 3+60, where the peak radial velocity is down to about 50 ft/s, gauge survival is improved with a few breaks occurring from 7 to 27 ms after ground shock arrival, Figure 3.18.

The POR author, C. Vincent, states in his conclusion that more attention should be paid to cable passage through the tunnel and pipe seal (TAPS). Cable failure caused by SPS's is no longer of practical importance, because SPS's are no longer used. It is significant for future applications, however, that the double braided armored TSP failed so readily on both Midi Mist and Diana Mist.

4.3 POR "Minute Gun Series, Dido Queen Event, Closure Monitor and Tunnel Environment," Wetzel, D., and Sanders, H.

Multiconductor twisted pair (telephone cable) encased in heavy hydraulic hose was used to transmit break-switch and magnetic pickup data

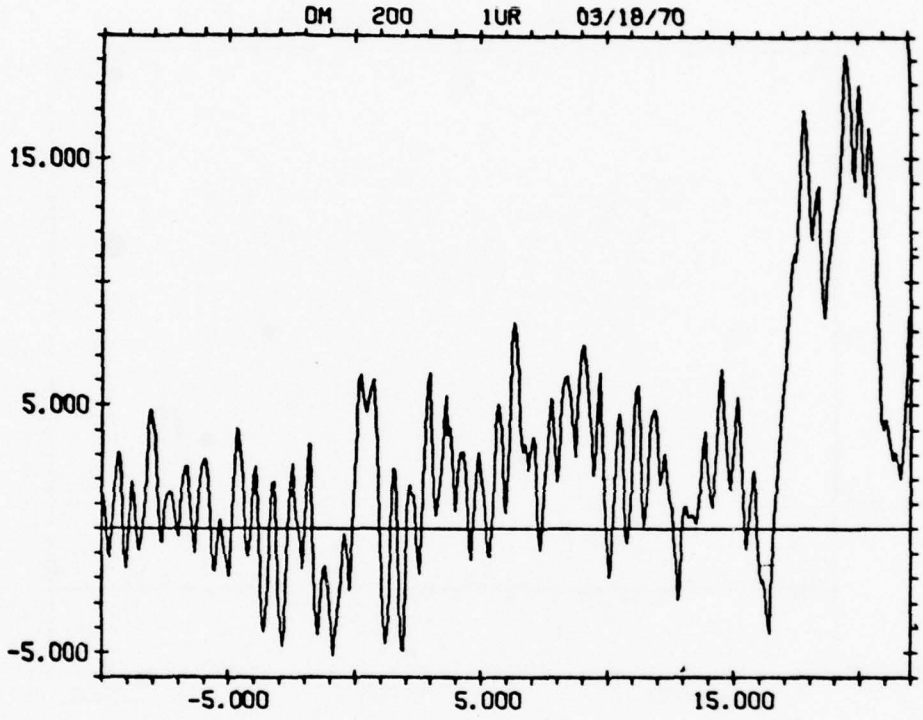

Figure 3.9 Free field DX velocity gage record at Station 2+00. Gage axis radially outward from the working point. The large excursion at 16 ms preceedes the time-of-arrival measured with free-field slifers. (POR 6389)

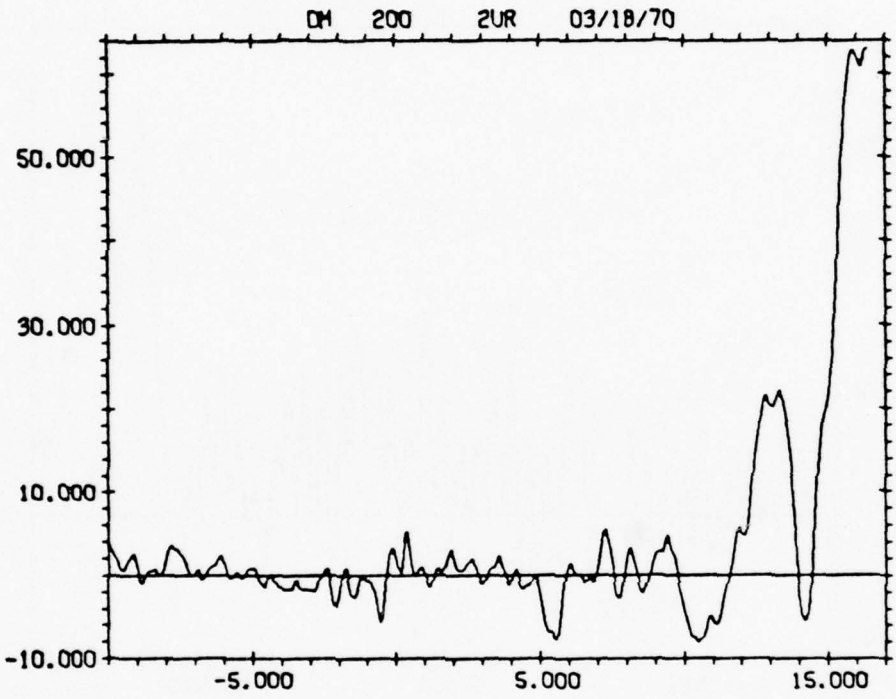

Figure 3.10 Radial DX velocity gage circuit failure. Station 2+00 at left side of tunnel wall. Open circuit condition at 16.5 ms. Time-of-arrival from free-field slifer data at 22 ms. (POR 6389)

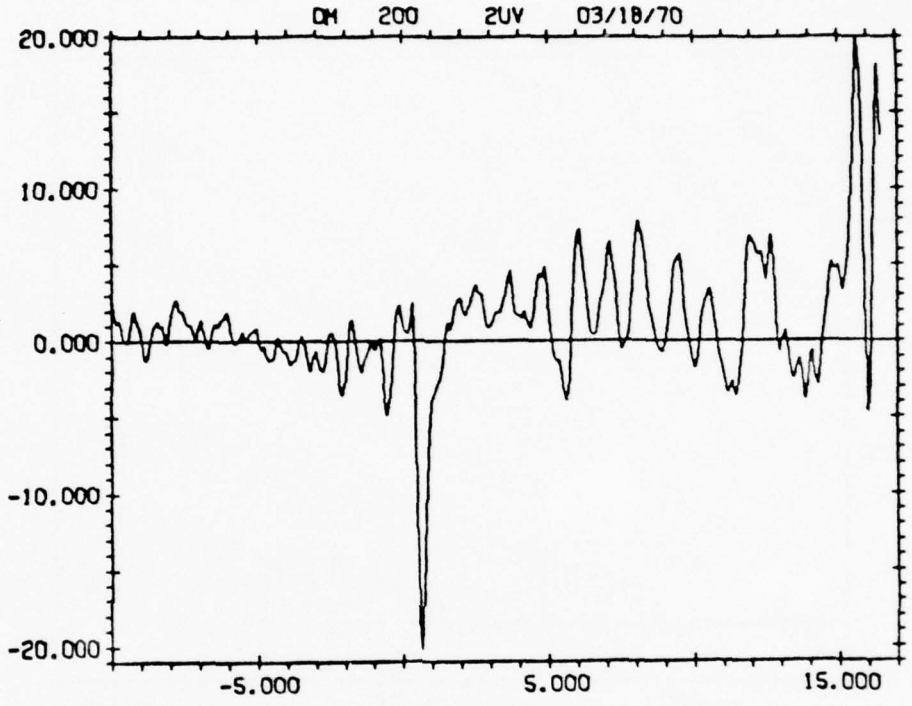

Figure 3.11 Vertical DX velocity gage circuit failure. Station 2+00 at left side of tunnel wall. Open circuit condition at 16.5 ms. Time-of-arrival from free-field slifer data at 22 ms. (POR 6389)

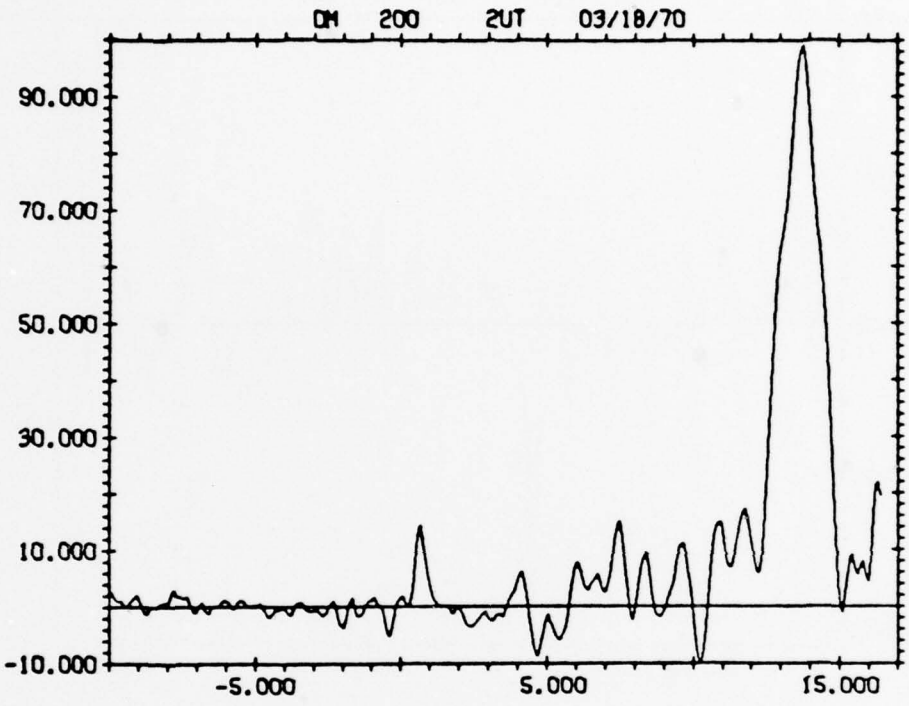

Figure 3.12 Transverse DX gage circuit failure. Station 2+00 at left side of tunnel wall. Open circuit condition at 16.5 ms. Free-field time-of-arrival from free-field slifer data at 22 msec. (POR 6389)

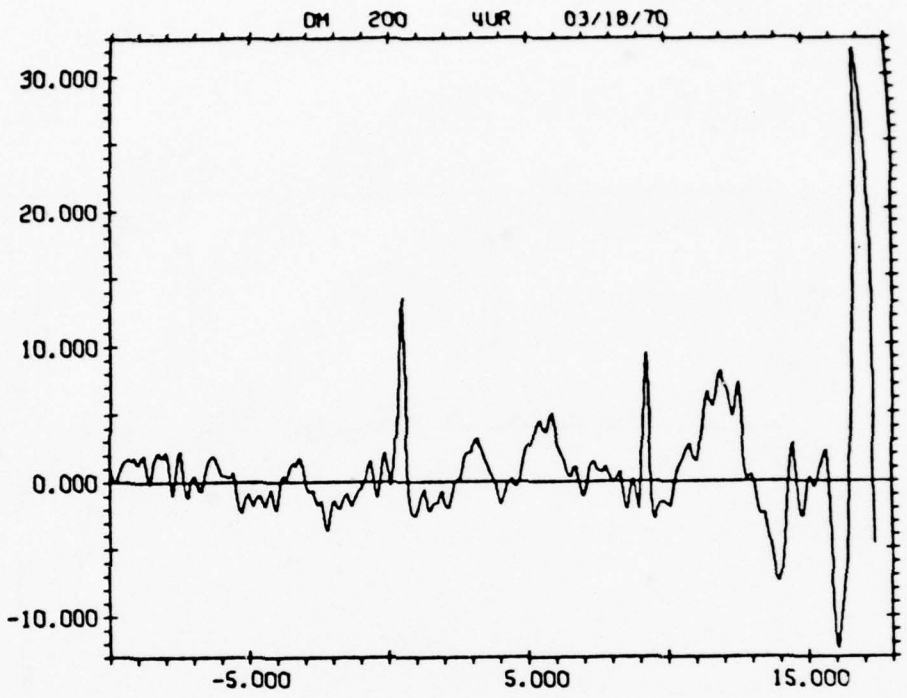

Figure 3.13 Radial DX velocity gage circuit failure. Station 2+00 at top of tunnel wall. Open circuit condition at 16.5 ms. Time-of-arrival from free-field slifer data at 22 ms. (POR 6389)

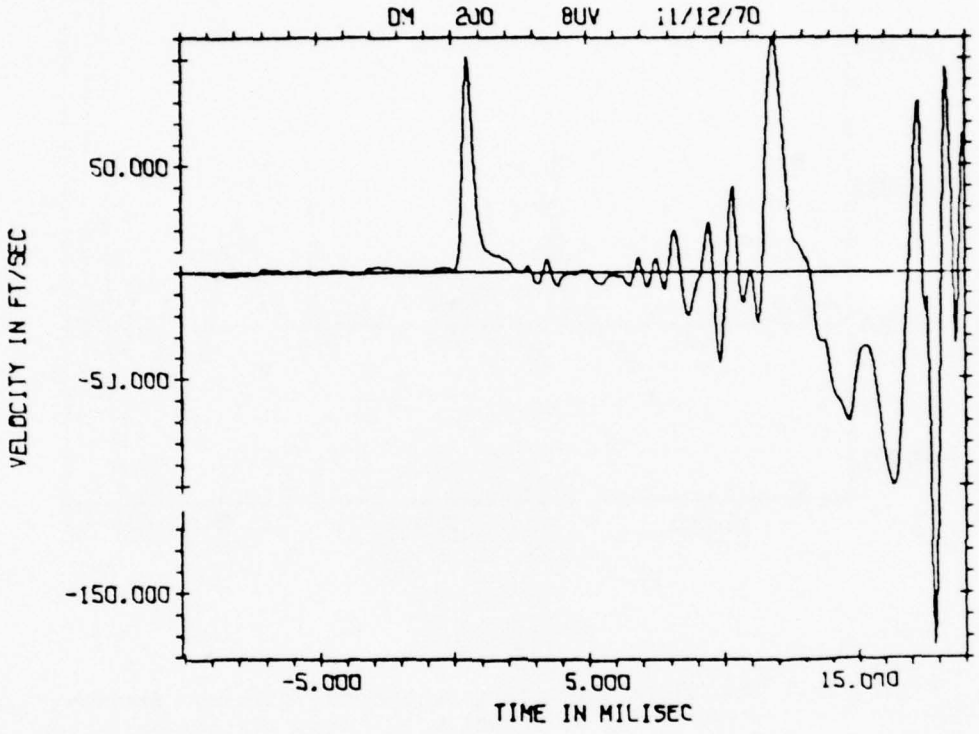

Figure 3.14 Severe electrical noise in circuit of DX velocity gage attached to HLOS at Station 2+00. (POR 6389)

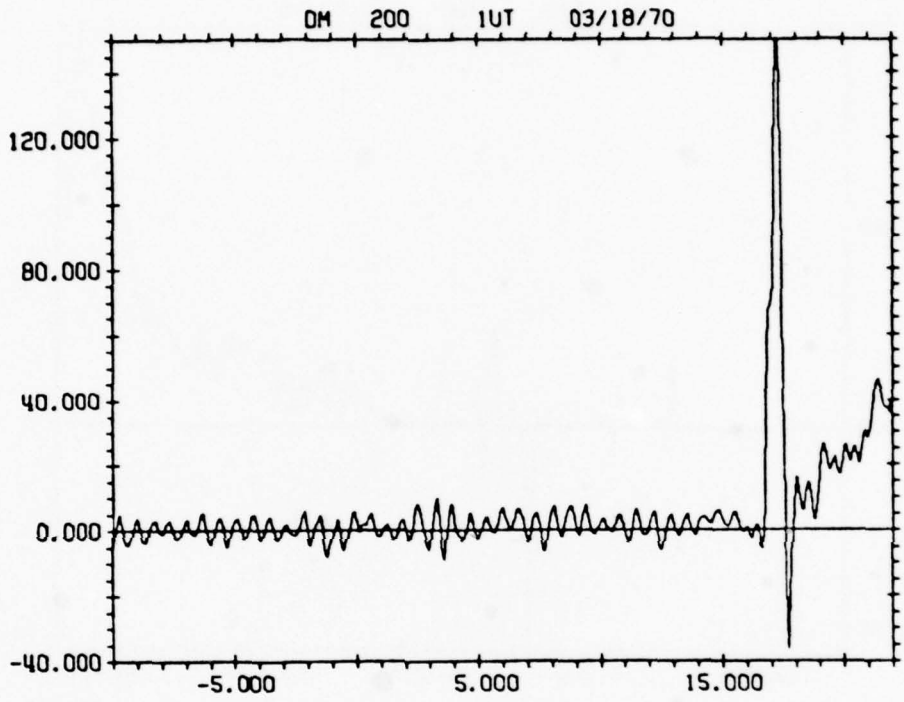

Figure 3.15 Transverse free-field DX velocity gage record at Station 2+00. The record implies an outward moving pressure wave in excess of 1.4 kb prior to main ground shock arrival. (POR 6389)

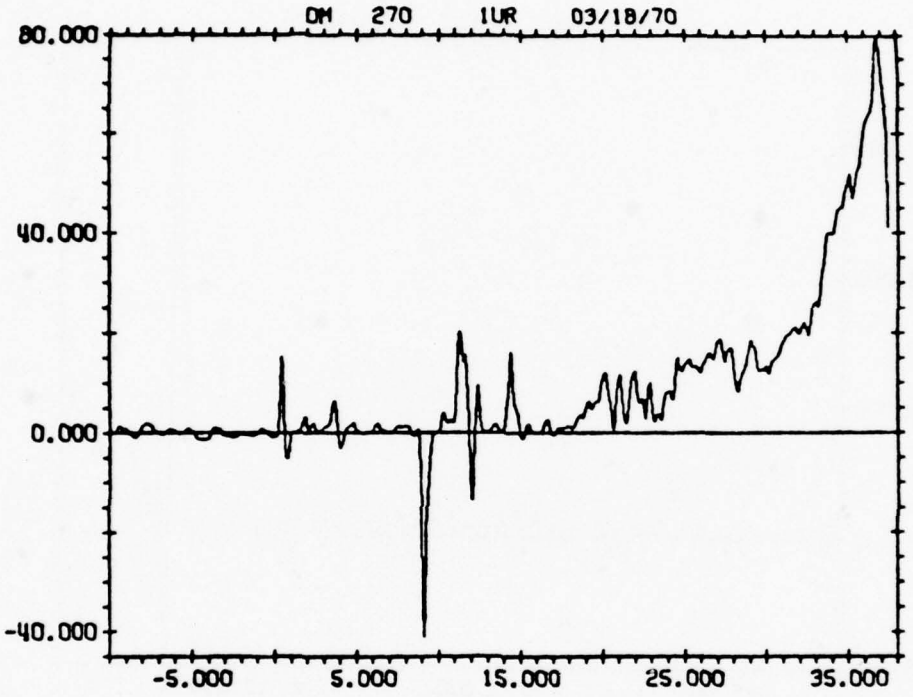

Figure 3.16 Radial velocity away from the working point at Station 2+70. Open circuit condition at 37.5 ms. Time-of-arrival from extrapolated slifer data at 36 ms. (POR 6389)

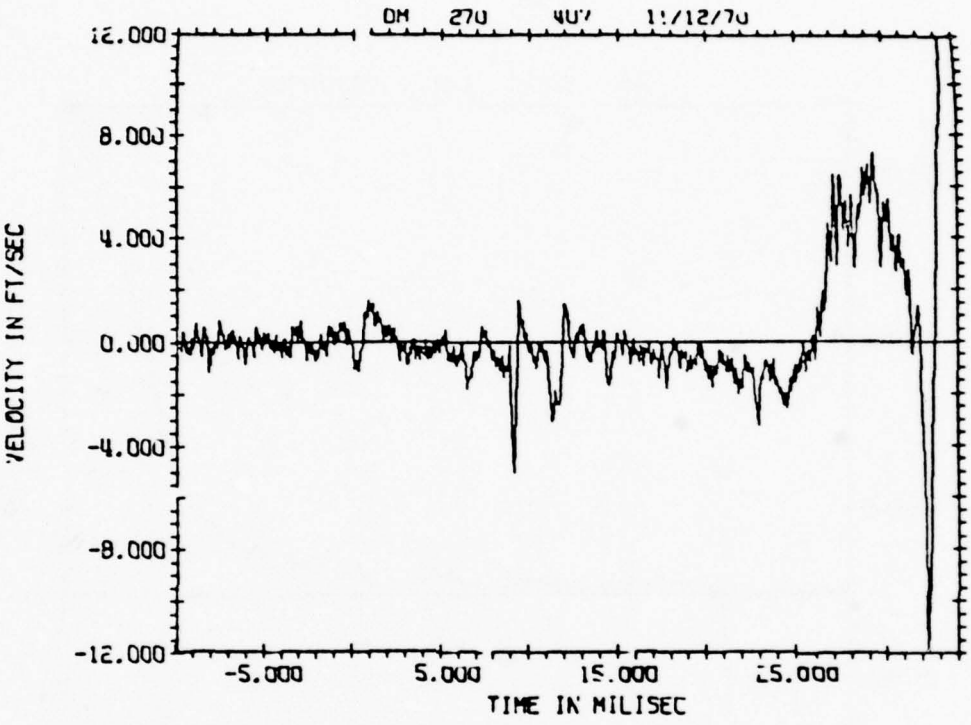

Figure 3.17 Erratic circuit behavior of DX velocity gage at Station 2+70. (POR 6389)

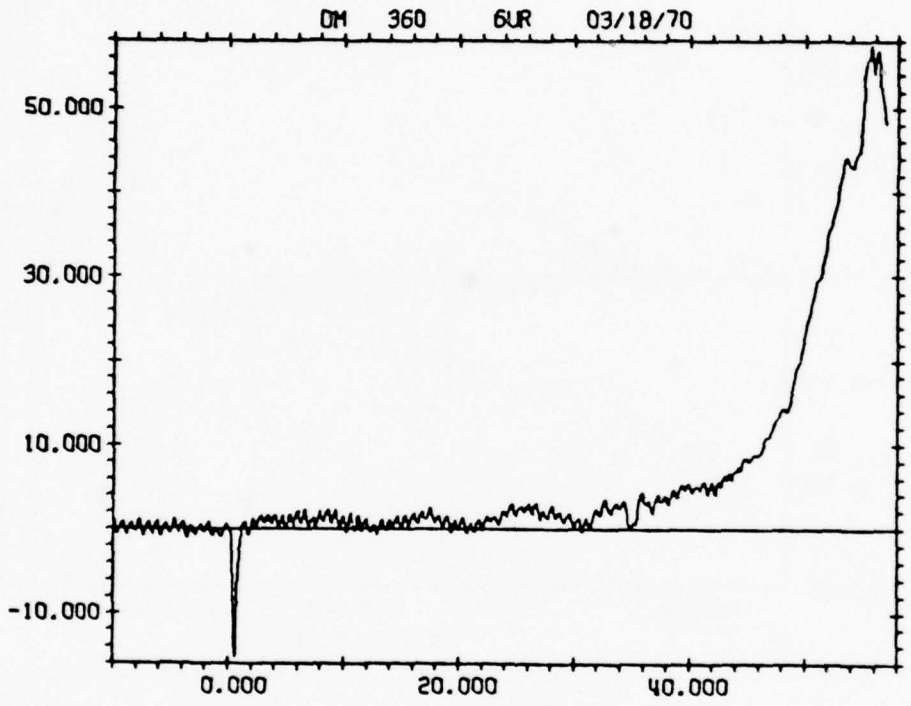

Figure 3.18 DX velocity gage circuit failure at Station 3+60. Open circuit condition at 48.5 ms. (POR 6389)

from the DASA auxiliary closure (DAC's). The hydraulic hose was used to provide protection to the cables during the grout pour and not during ground shock because the DAC data are acquired prior to ground shock arrival. All junction boxes were filled with epoxy to provide waterproofing (and crush protection!).

Although the TAPS cable had to survive ground shock to obtain data the experiment designers "deemed it not necessary to provide special cable protections since most of the cable was buried and the distance from ground zero was over 500 feet. This proved erroneous since the TAPS cables were lost during ground shock." According to the POR, cable failure occurred at 217 ms, which indicates to us that cable failure was induced by late-time motions, rather than by ground shock, even at a location as distant as the gas seals. In our opinion the POR presents contradictory conclusions:

> ...after looking at the tunnel on reentry, it is doubtful that anything would have protected the cables. Additional protection on future events is planned to increase the chance of survival.

Unfortunately, neither the mode of failure nor the failure location was identified in the POR.

4.4 POR 6785 "Minute Gun Series, Dido Queen Event, Stemming Diagnostic Measurements," Rinehart, R.

To analyze cable failures we examine the Dido Queen stress and velocity measurements made in the free-field between the LOS drift and the by-pass drift. Attention is directed to gauge locations which vary between 150 to 297.3 feet from the working point, to cable routings as far as 515 feet from the working point, and to times up to 85 ms from zero time. The gauge layout with the implied cable topology is illustrated in Figure 3.19. Instrument types, locations, and cable types are summarized in Table 3.3. Cables were routed along the left rib of the by-pass drift. A splice box for the subminiature instrumentation coaxial cable (Endevco 3091B) which was used for the quartz stress gauges and for the velocity gauges was located at approximately the 425 foot range in the by-pass drift. Beyond this range all cables (RG22B/U and RG213) were grouted into a trench in the floor of the drift. All boreholes were 3 inches in diameter and dipped downward between 7 to 26 degrees to ensure a competent column of DSRM-2 rock matching grout. The by-pass drift was stemmed with superlean grout.

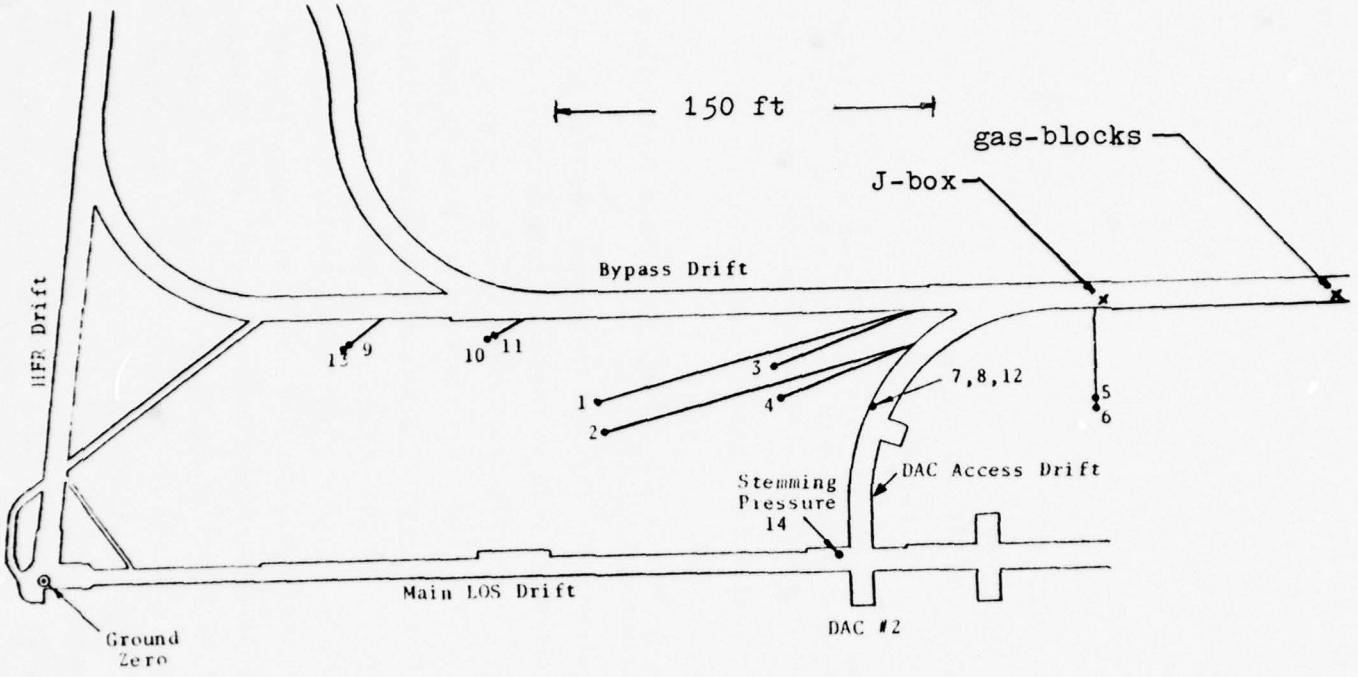

Figure 3.19 Plan view of Dido Queen showing locations of boreholes, gages, gas-blocks and of the junction box. Boreholes used to install gages at locations of gages 13 & 9, 10 & 11, 1, 2, 3, 4, 7 & 8 & 12, and 5 & 6. (POR 6785)

Table 3.3. Summary of instrumentation.

Gauge No.	Gauge Function	Transducer	Range (ft)	Cable
1	stress	ytterbium	229.0	RG213
2	stress	quartz	229.0	armor
3	stress	quartz	297.3	armor
4	velocity	PZT	296.0	armor
5	stress	quartz	449.6	armor
6	velocity	PZT	449.6	armor
7	stress	quartz	332.9	armor
8	velocity	PZT	332.9	armor
9	stress	ytterbium	154.0	RG213
10	stress	quartz	199.2	armor
11	stress (dummy)	quartz	199.8	armor
12	stress (dummy)	quartz	332.9	armor
13	stress	ytterbium	150.0	RG213

A brief description of the gauge circuitry and mechanical layout of the electrical components is necessary because, as will be shown subsequently, not all gauge malfunctions can be attributed to cable failure. The ytterbium gauges, which were installed by Stanford Research Institute, (SRI), followed their standard practice of using coaxial cable (RG213) embedded directly in grout. The quartz stress gauges and velocity gauges, which were built by Systems, Science and Software (S^3), employed armored cable and downhole signal conditioning. The armor is stated to be 0.25 inches OD aluminum tubing and based on past practice we believe that the material was 6061-T6 with an ID of 0.152 inches. An FET driven impedance converter was placed near each quartz stress gauge and velocity gauge. The preamplifiers were potted in epoxy inside a metal housing which in turn was potted in silicone rubber, Figure 3.20. Shock tests indicated that the preamplifier could withstand 3500 g along its axis and 1000 g normal to its axis (presumably

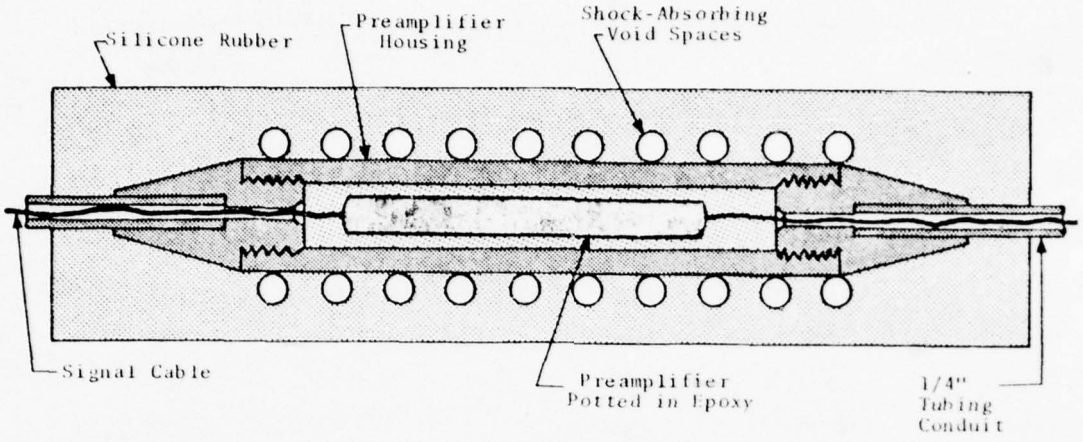

Figure 3.20 S^3 preamplifier housing. (POR 6785)

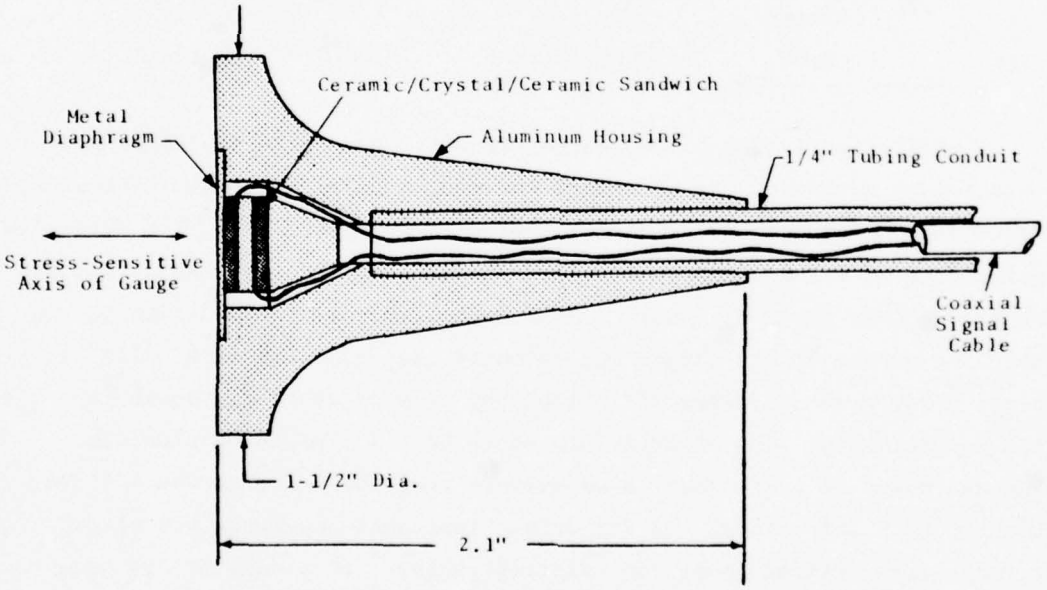

Figure 3.21 Detail of quartz stress gage. (POR 6785)

these are operating limits). Gauge construction and cable dressings are illustrated in Figures 3.21 and 3.22.

Analyses needed in the detective work to ascertain the cause of circuit failure can require a wide variety of information: the time of arrivals of the wavefront, of the peak stress, and of the peak displacement (all at various strategic locations, which include the locations of construction discontinuities, of potentially frangible equipment such as amplifiers and splice boxes, and of natural faults), circuit diagrams, reentry observations, and perhaps even post-shot tests. In this section we shall limit our detective work to investigating whether a circuit failure was caused by a cable or by some other mechanism. The raw data, Figures 3.23 through 3.25 indicate the following: The ytterbium gauges numbers 13 and 9, located at 150 and 154 feet, respectively, suffered intermittent break-make behavior. The ytterbium gauge number 1, located at 229 feet, does not show any failure on the oscillogram, but a replot of the tape readout shows circuit failure at 34.7 ms. Quartz stress gauges numbers 2 and 10, located at 229 and 199.2 feet, respectively, yielded wave forms with discontinuous slopes. The tails of the voltage traces appear to decay with an RC time constant. The circuit behavior does not appear to be caused by cable failure. The behavior of quartz stress gauge number 3 does imply either cable or connector failure. At the time of failure, ground shock was 200 feet beyond the splice box and 115 feet beyond the gas-seal connectors. Based on this rather flimsy evidence, late-time failure caused by differential motions at the gas-seals cannot be ruled out. The raw data do not indicate failure of the velocity gauge circuits, but replotted wave forms in the POR do show failure for times greater than 80 ms. A comparison of the time-of-failure (TOF), with the time-of-arrival of ground shock at the intersection of the instrument boreholes and the by-pass drift, Table 3.4, coupled with the behavior of the wave forms implies that ytterbium gauge cables failed in shear where the RG213 entered the by-pass drift. We note that going strictly by the numbers and using an average wave speed of 8.6 ft/ms determined from an x-t diagram in the POR, gauge 1 failed just prior to shock arrival at the borehole-drift intersection. It is our opinion that this apparent discrepancy is more indicative of an uncertainty in wave speeds than in failure modes

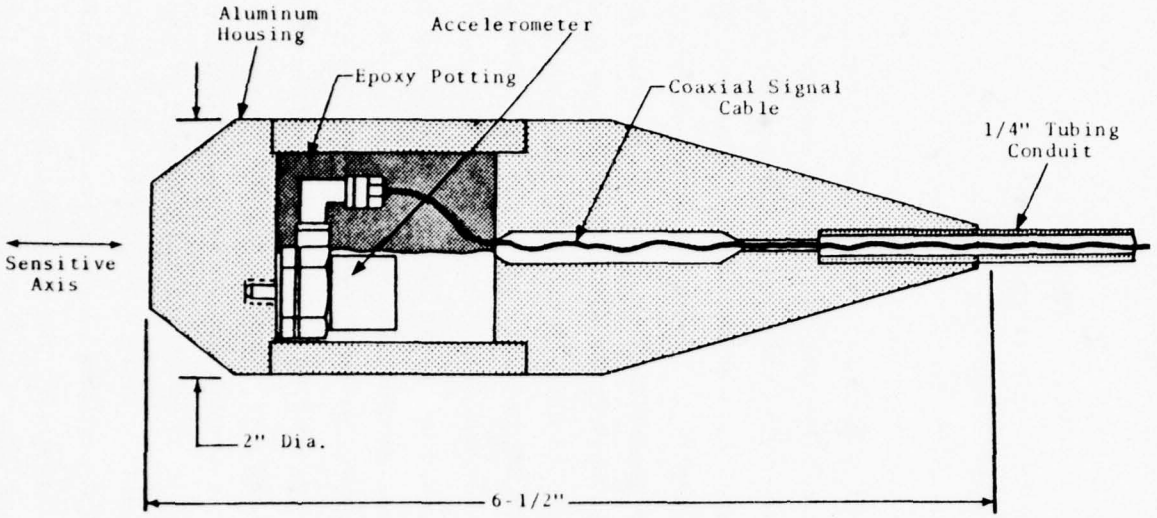

Figure 3.22 Detail of accelerometer canister used to make velocity measurement. (POR 6785)

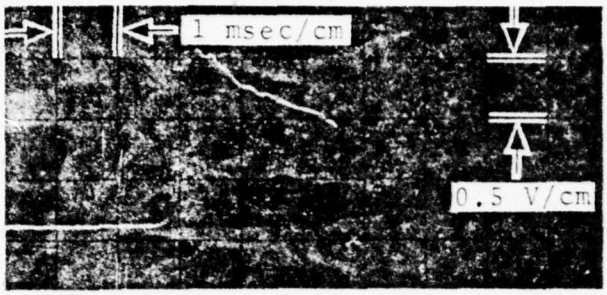

Voltage-time records from ytterbium gage No. 13 at 150 foot range.

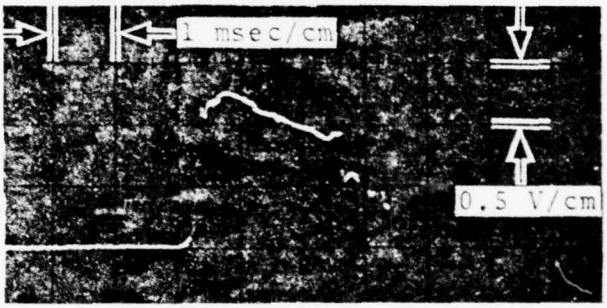

Voltage-time records from ytterbium gage No. 9 at 154 foot range.

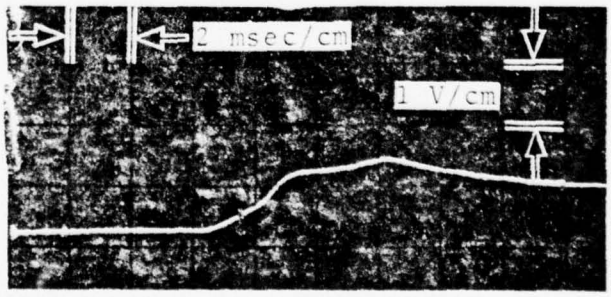

Voltage-time records from ytterbium gage No. 1 at 229 foot range.

Figure 3.23 Oscillograms of ytterbium gage voltages. Gage 13 failed at 15.5 ms, gage 9 failed at 15.8 ms, and gage 1 failed at 34.7 ms (not shown on oscillogram). (POR 6785)

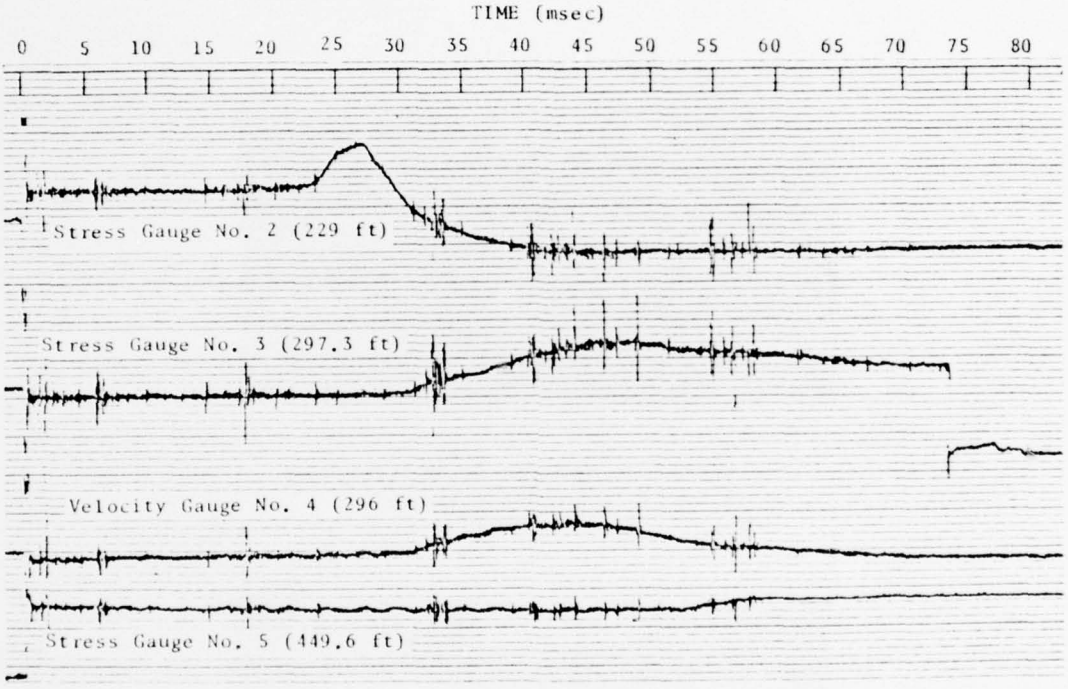

Figure 3.24 Oscillograph records of stress gage and velocity gage signals. The record of gage no. 2 suggests an electronics failure, but gage no. 3 appears to have suffered a cable or connector failure. (POR 6785)

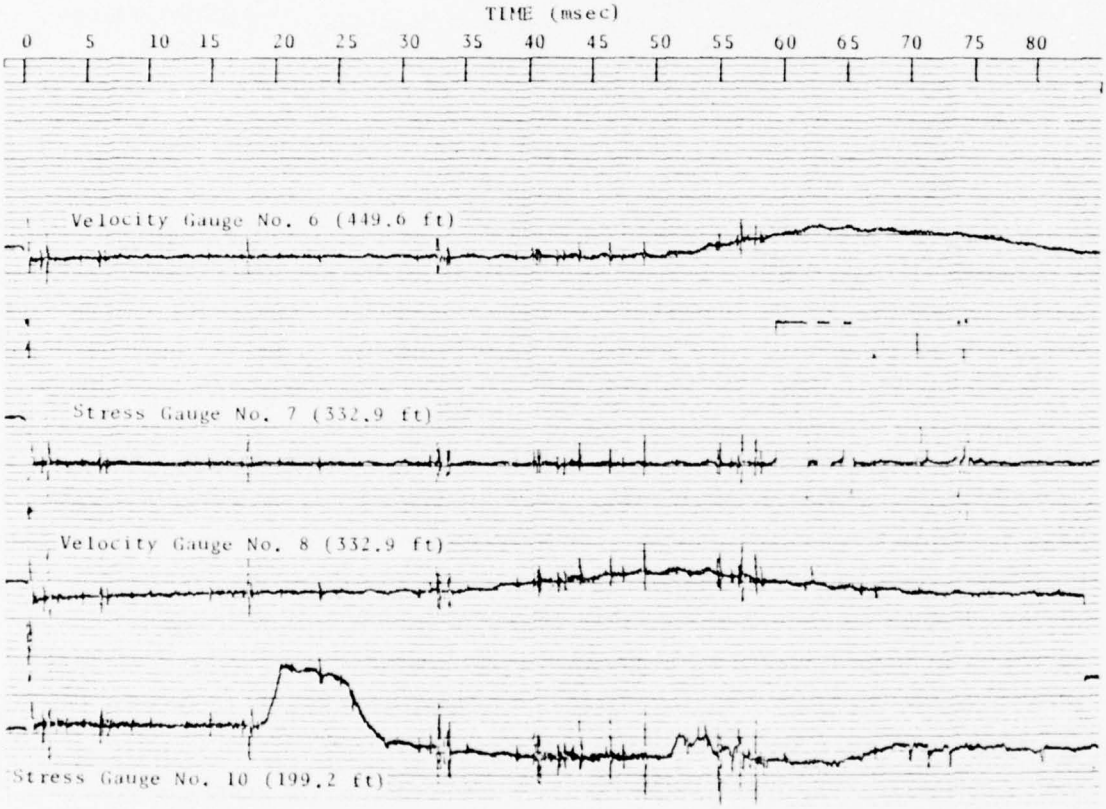

Figure 3.25 Oscillograph records of stress gage and velocity gage signals. The record of gage no. 10 suggests an electronics failure.

Table 3.4. Circuit time of failures, TOF, and possible failure modes. The armor (aluminum conduit) was used to protect subminiature instrumentation coaxial cable (Endevco 3091B). Gauge 3 failure occurred when ground shock was 200 feet beyond the 3091B-RG22B/U splice box and 115 feet beyond the gas-seals.

Gauge No.	Cable	Peak Stress (kbar)	Time of Failure (ms)	Arrival @ Drift (ms)	TOF/TOA	Possible Failure Mode
1	RG213	1.7	34.7	37.5	0.93	cable shear
2	armor	1.1	27.4	36.8	0.74	circuit
3	armor	0.62	73.3	38.0	1.9	cable/connector
9	RG213	4.7	15.8	14.9	1.06	cable shear
10	armor	1.9	28.2	20.4	1.38	circuit
13	RG213	5.0	15.5	14.9	1.04	cable shear

(note that a 0.23 percent increase in wave speed would eliminate the discrepancy). Quartz gauge number 2 failed considerably in advance of the wave reaching the by-pass drift. The waveform suggests that an analysis of preamplifier malfunction would be rewarding. Quartz gauge number 3 failed 38.6 ms after ytterbium gauge number 1 failed, yet both gauges entered the by-pass drift at essentially the same location. The data imply that aluminum conduit is more resistant to shear at low stress levels ($p \sim 0.5$ kbar) than is unprotected coaxial cable.

4.5 SSS-R-75-2631 "Hybla Fair Event, Diagnostic Measurements, Project Officer's Report," H. Kratz.

To analyze cable failures we direct our attention to stress measurements made in the free-field near the bypass drift and to velocity measurements made in the main LOS drift on Hybla Fair. The gauge layout is illustrated in Figure 3.26. The routing of the stress gauge cables in the by-pass drift is not important for our purposes, because as will be shown subsequently, the cables failed at the time the peak of the stress wave had reached the intersection of the gauge boreholes with the bypass drift. The routing of velocity gauge cables is of interest because the velocity

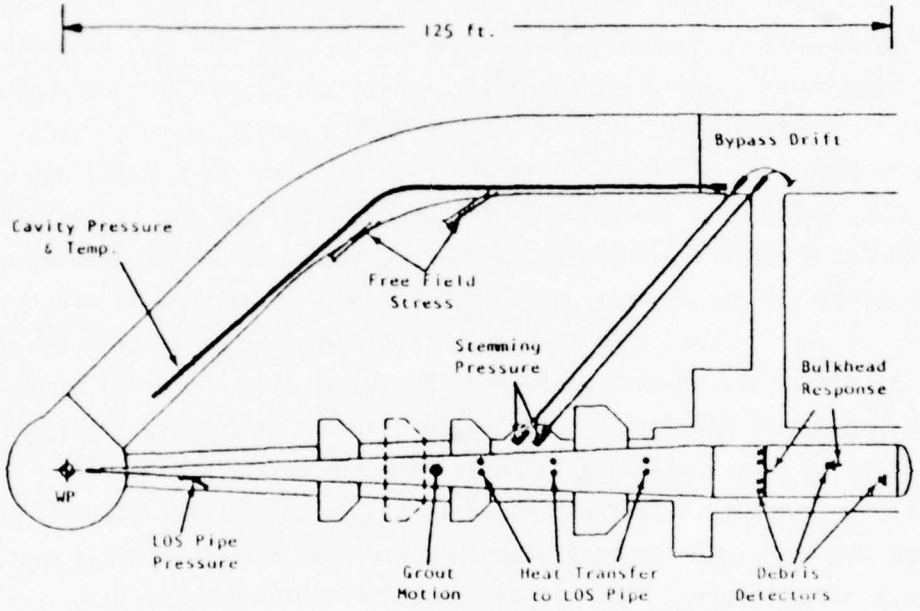

Figure 3.26 Plan view of Hybla Fair showing location of gages. (SSS-R-75-2631)

gauge circuits survived for a considerable period of time ($\gtrsim$26 ms). The velocity gauge cables were routed along the HLOS and then through the cross drift to the bypass drift. The cross drift exit was employed because of the anticipated bursting of the HLOS upon flow stagnation[8].

Two triaxial translational velocity gauges each consisting of three piezoresistive accelerometers and three active integrators were located 50 inches above and 40 inches below the LOS at 0+56. The cable was 4 TSP with a woven stainless steel reenforcing sheath manufactured to S^3 specifications (Section IV.13) by Whitmore Wire and Cable Corp., North Hollywood, CA. Apparently neither performance specifications nor test data on the performance of the cable exist. The stainless cable sheath was clamped to the canister, Figure 3.27. The three circuits in the canister located below the LOS, denoted as PV1, PV2, and PV3, failed at about the same time, Table 3.5 and Figure 3.28, implying a common failure mode. Whether the failure occurred in the canister or in the cable or at the gas blocks cannot be determined from the available data. That gauge PV3 took about 4 ms to fail does not rule out, in our opinion, a cable failure. The absence of a zero-time offset and the spikey nature of the record of PV5, Figure 3.29, suggests to us that the integrator had failed prior to zero-time. Circuit survival for more than 25 ms in the stemming material is a noteworthy achievement. In principle, triaxial translational velocity gauges are not sufficient for unfolding the true translational velocity, but must be supplemented by rotational measurements. The well-behaved nature of the data, Figure 3.28, suggests that rotation is not significant in the stemming material and that the motion may not be as violent as once supposed.

Table 3.5. Velocity gauge failure times.

Gauge No.	Time of Failure (ms)	Time-of-Arrival (ms)	Survival Time (ms)	Note
PV1	34	7.5	26.5	common canister and cable bundle
PV2	34	7	27	
PV3	34-38	7	27-31	
PV5	?	?	?	possible pre-zero time integrator failure

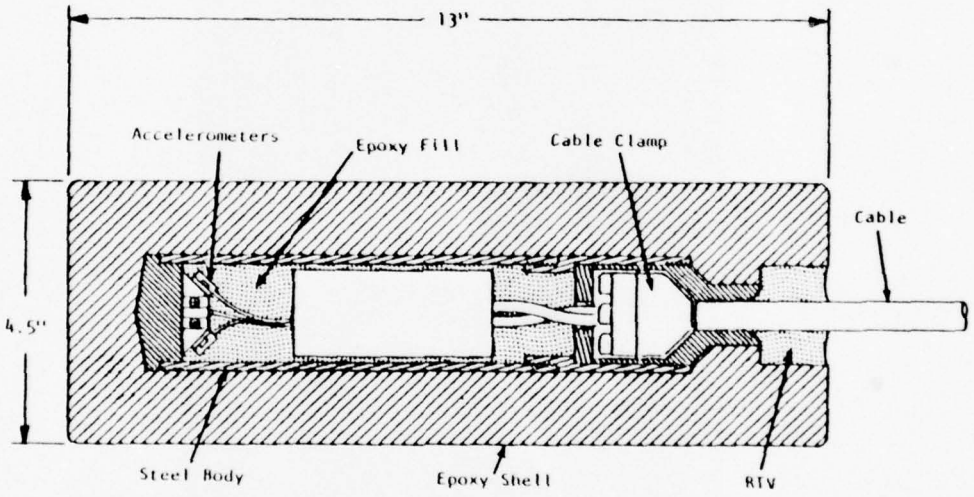

Figure 3.27 Detail of triaxial integrating accelerometer translational velocity gage. The cable was 4 TSP with a woven stainless steel reenforcing sheath. (SSS-R-75-2631)

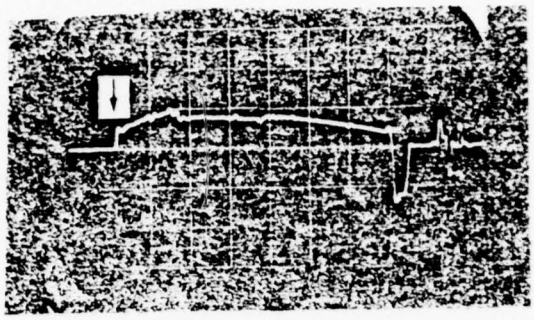

PV1

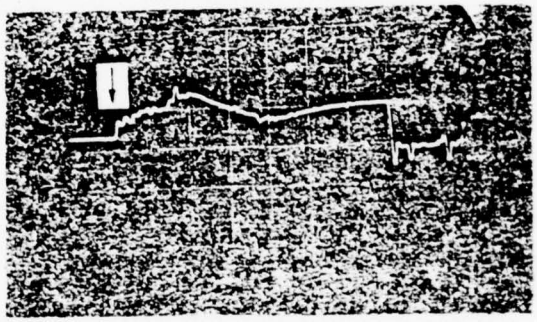

PV2

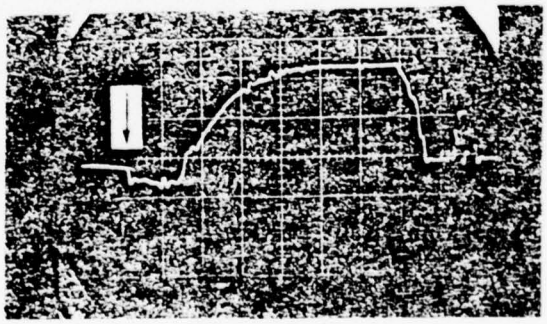

PV3

Figure 3.28 Oscillograms of integrated accelerometer outputs PV1, PV2, and PV3 located 40 inches below the LOS at 0+56. Sweep speed: 5 ms/cm. (SSS-R-75-2631)

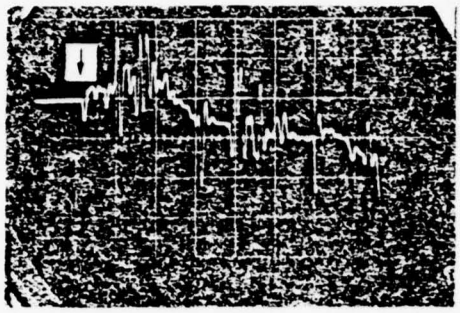

Figure 3.29 Oscillogram of integrated accelerometer output PV5 located 50 inches above the LOS at 0+56. The spikey record and absence of zero-time offset implies that the integrator was inoperative. Sweep speed: 5 ms/cm. (SSS-R-75-2631)

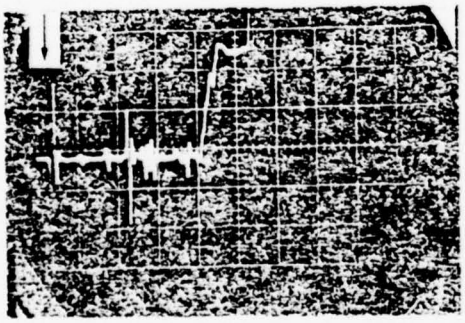

ES7

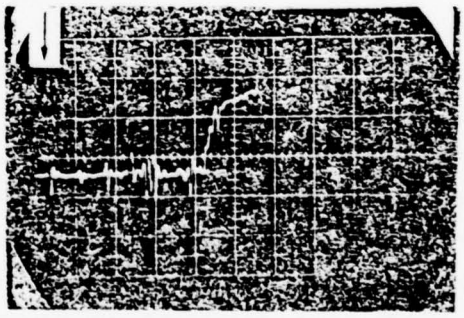

ES8

Figure 3.30 Oscillogram of quartz stress gage outputs ES7 and ES8 embedded in rock matching grout at a range of 70.8 feet. Sweep speed: 2 ms/cm. (SSS-R-75-2631)

Ytterbium and quartz gauges were emplaced in boreholes drilled in the floor of the by-pass drift. The gauges were located at ranges of 55.3, 56.3, 70.8, and 71.3 feet from the working point. The boreholes intersected the drift at ranges of approximately 60.5 and 77 feet from the working point, Figure 3.26. For the measurement of radial stress, rock matching grout was installed in two boreholes. To allow the mean stress to be measured super-lean grout was installed in the remaining two boreholes. Changes from the techniques used in Dido Queen both in the construction of the quartz gauges and their method of installation may have contributed to their short survival time, Figures 3.30 through 3.32. A preamplifier using RG22B/U output cable, Figure 3.33, was employed on Hybla Fair. Coaxial cable protected by aluminum conduit was used on Dido Queen. Both the borehole-drift intersection angle and the stemming material were different on the two shots. A shear box, Figure 3.34, was used in an attempt to prevent shear failure of the cables. The design of the Hybla Fair shear box is quite different from that found in the communications literature and may itself induce shear failure in the vertical direction. Shear boxes proposed for communications cables do not allow a guillotine action to cut cables if the box suffers a partial collapse. Of course, near-surface communications cable plants are not designed to survive at the pressures encountered in Hybla Fair. Analyses and test data on the functioning of the shear box were not included in the POR. Stress gauge failure times and times-of-arrival at the gauges and at the intersection of the boreholes and the by-pass drift are summarized in Table 3.6. Oscillograms which illustrate the failures are shown in Figures 3.30 through 3.32. The failure times are quite close to the time of arrival of the peak of the stress wave at the borehole-drift intersection, estimated on the basis of measured stress wave velocities, Figure 3.35.

The test data indicate that soft cables should not be employed in regions of shearing action. We note that several of the S^3 cable anchors at the transducer rely on epoxy to grip the cables. Although this technique is commonly used, test data on the strength of the epoxy anchor is necessary. If required, the anchor could be strengthened by using a Kellem grip on solid dielectric cable. It is believed that the Kellem gripping action

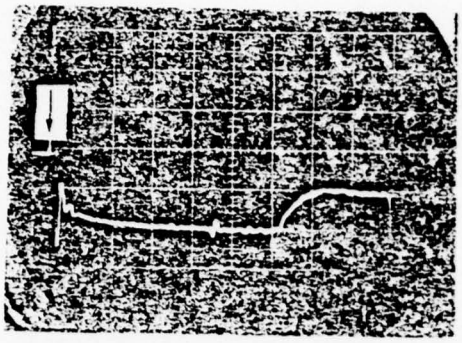

ES1

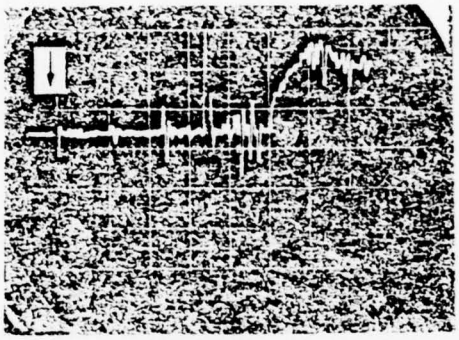

ES2

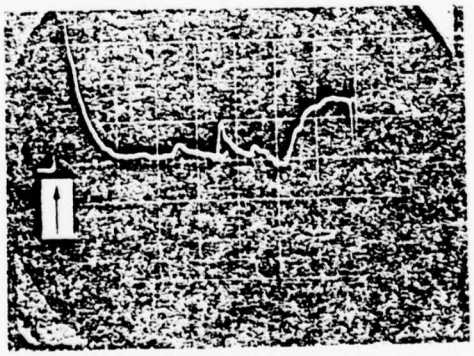

ES3

Figure 3.31 Oscillograms of ytterbium stress gage ES1 and quartz stress gage ES2 embedded in superlean grout at a range of 56.3 feet and ytterbium stress gage 3 embedded in rock matching grout at a range of 55.3 feet. Sweep speed: 1 ms/cm. (SSS-R-75-2631)

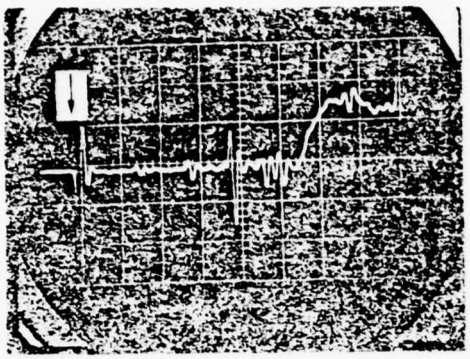

ES4

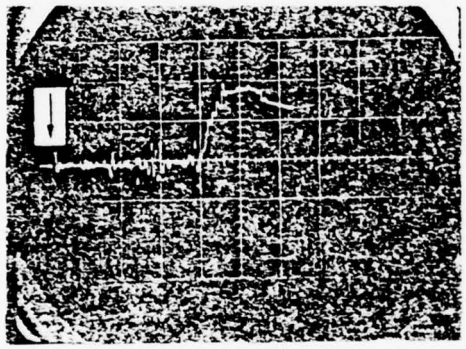

ES5

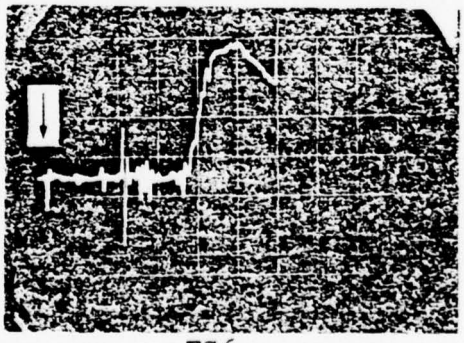

ES6

Figure 3.32 Oscillograms of quartz stress gage ES4 embedded in rock matching grout at a range of 55.3 feet and quartz gages ES5 & ES6 embedded in superlean grout at a range of 71.3 feet. Sweep speed: ES1 = 1 ms/cm, ES2 and ES3 = 2 ms/cm. (SSS-R-75-2631)

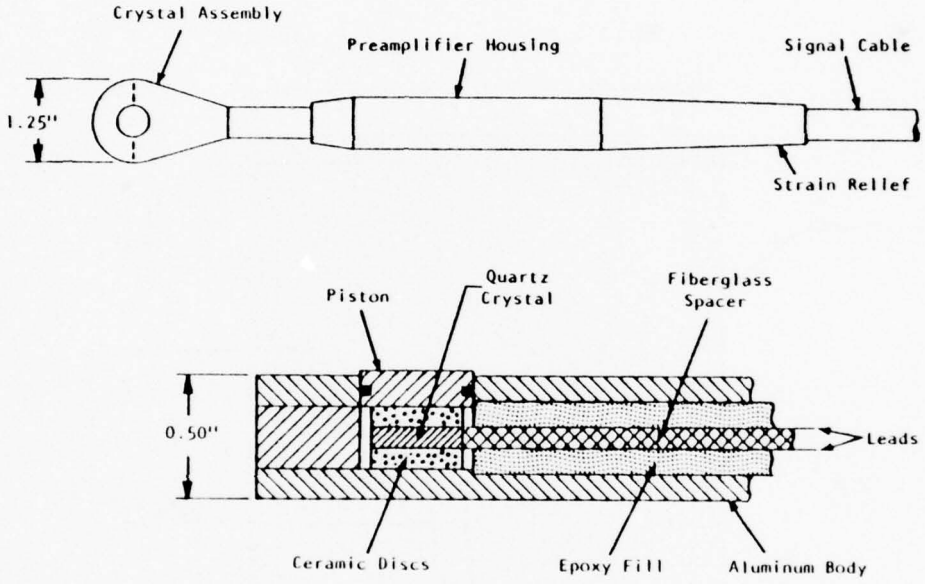

Figure 3.33 Quartz stress gage with built-in preamplifier using RG22B/U output cable. (SSS-R-75-2631)

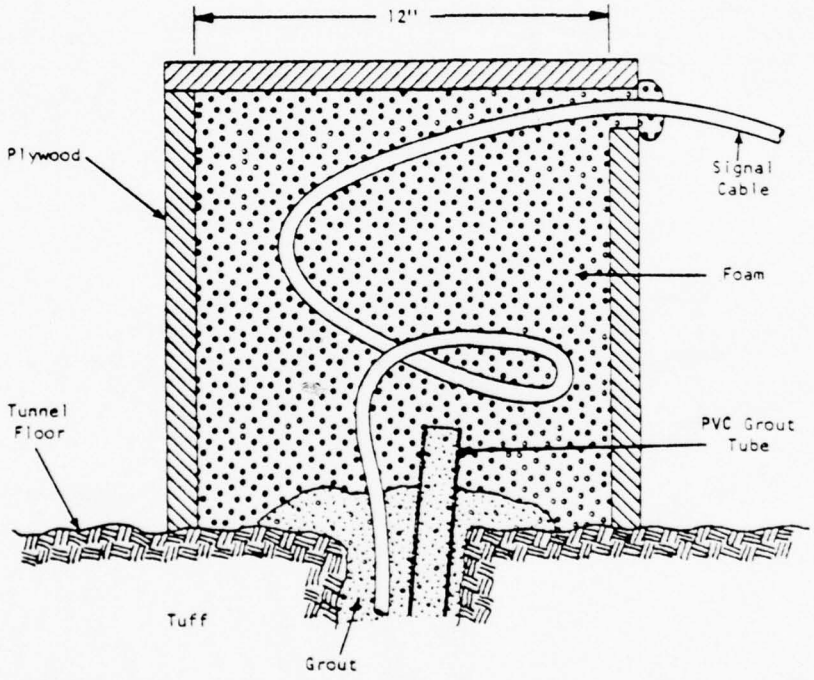

Figure 3.34 Shear box used in an attempt to prevent cable failure where the cables entered the by-pass drift. At the location of the shear box the drift was stemmed with high strength grout. (SSS-R-75-2631)

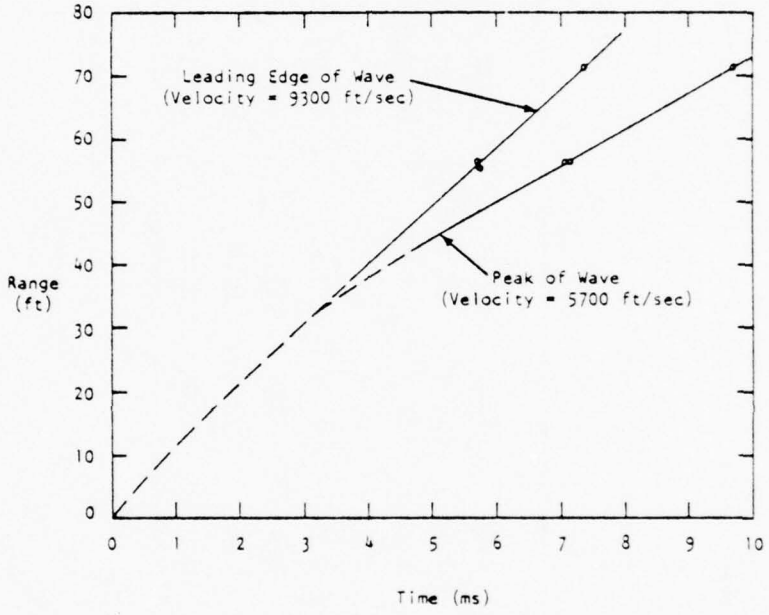

Figure 3.35 Arrival times of leading edge and peak of stress wave as a function of range. (SSS-R-75-2631)

Table 3.6. Gauge failure times and times of arrival (TOA) of the stress wave at the gauges and at the by-pass drift--borehole intersection. The by-pass drift was stemmed with high strength grout near the gauge boreholes[9].

Gauge	Time of Failure (ms)	Time of Arrival (ms)	Survival Time (ms)	Range (ft)	TOA of Peak Stress at Drift (ms)	Transducer	Borehole Grout
ES1	8.45	5.8	2.65	56.3	7.75	ytterbium	SL
ES2	8.0	5.45	2.55	56.3	7.75	quartz	SL
ES3	7.4	5.8	1.60	55.3	7.75	ytterbium	RM
ES4	8.0	5.5	2.5	55.3	7.75	quartz	RM
ES5	12.0	7.2	4.8	71.3	10.5	quartz	SL
ES6	11.6	7.2	4.4	71.3	10.5	quartz	SL
ES7	10.2	7.6	2.6	70.8	10.5	quartz	RM
ES8	10.6	7.8	2.8	70.8	10.5	quartz	RM

could be improved on TSP cable by filling the gripped section of cable with a flexible solid dielectric.

4.6 SSS-R-75-2682, "Dining Car Stemming Diagnostics Post-Shot Instrumentation Report," Rinehart, R.

Rinehart summarizes his experience with cabling problems as follows: "A moderate amount of data was lost in the program due to cabling problems. A number of cables were lost pre-shot but all except two were replaced without loss of data. The cable problems incurred during the event can be divided into two groups: those cables lost in the gauge-to-alcove run due probably to ground shock induced relative motion at those locations where the cables passed through material interfaces; and those cables lost in the alcove-to-mesa run due apparently to drift collapse during ground shock passage. The loss of close-in cabling has always been a problem due to shear motions that can occur at material interfaces and fault planes. The problem of material interfaces can be eased by reducing the number of interfaces through which the cables must pass. These interfaces occur where cables enter trenches, pass through steel or Blaw Knox bulkheads, and pass through grout-to-grout interfaces. More extensive use of cable armoring at further distances from GZ, either by integral armor on the cable or by putting the cables inside heavy pipe, is recommended to alleviate the general poblem of relative motion at interfaces.

The loss of cables due to drift collapse can be prevented by protecting the cables with sandbags or trenching. It is recommended that in the future special attention be paid to the assignment of alcove locations, uphole cable runs, and trailer locations for systems which require late-time data acquisition."

We believe that reducing the number of interfaces traversed by a cable requires an overall cable topology plan that is worked out in the early stages of shot planning. The effectiveness of various techniques for preventing shear induced failure at interfaces needs to be determined.

5. NTS TUNNEL, HIGH EXPLOSIVE SHOTS

5.1 POR 6578 "Mighty Mite Series, Diamond Mine Event, Calibration Shot Ground Motion Measurements," Hartenbaum, B.

One quarter inch OD by 0.152 inch ID 6061-T6 aluminum tubing was used as conduit to protect either RG174/U coaxial cable or Endevco 3090A

low-noise cable. The gauge layout is shown in Figure 3.36. Of the nine cables installed, two failed at late times after data recovery. A comparison of the time-of-failure with the time-of-arrival of first motion, peak velocity, and maximum displacement at the entrance of the cables into the tunnel floor, Table 3.7, strongly suggests that cable failure was induced by shearing action at the tunnel floor at the time of peak displacement. The two velocity records that show cable failure are reproduced in Figure 3.37, along with a record of an earth pressure gauge. (The anomalous unloading response of the gauge at station 15.7 was analyzed in the POR as resulting from a high conductance path at the gauge and attributed to failure of the canister water seals. The earth pressure gauge was used to estimate the time of maximum displacement at station 15.7.) The graph of measured (first) time-of-arrival of the precursor is reproduced in Figure 3.38.

5.2 POR 6666 "Mighty Mite Series, Mine Dust Event, Stemming Mechanics Study Series: Stemming Mechanics Study Three," Grote, B. Appendix A, "Stress Wave and Particle Velocity Experiments in the Mine Dust High Explosive Test," Kratz, H., Rinehart, R. and Hartenbaum, B.

One-quarter inch OD by 0.152 inch 6061-T6 aluminum tubing was used as conduit to protect either Endevco 3090A or 3091B low-noise cable. The cable armoring technique was improved over that used in the Diamond Mine HE test: Stress concentrations were eliminated at the junction of the canister and the cable and the armor was made flexible by bending it into a wave pattern for about 18 inches from the 2 inch diameter canisters. The gauge layout is shown in Figures 3.39 and 3.40. The design was successful; not only were signals recorded for the duration of the shot, but all gauges were operative after the shot. The improved performance of the Mine Dust HE cables over the Diamond Mine HE cables may have resulted from a different

Table 3.7. Cable failure time compared to various times-of-arrival.

Station (ft)	TOA: Cable-Tunnel Intersection			Cable Failure (ms)	Notes
	First Arrival (ms)	Peak Velocity (ms)	Peak Displacement (ms)		
11.3	2.55	4.2	7.2	7.6	
15.7	3.4	4.8	9.8	9.8	a

[a] based on pressure record.

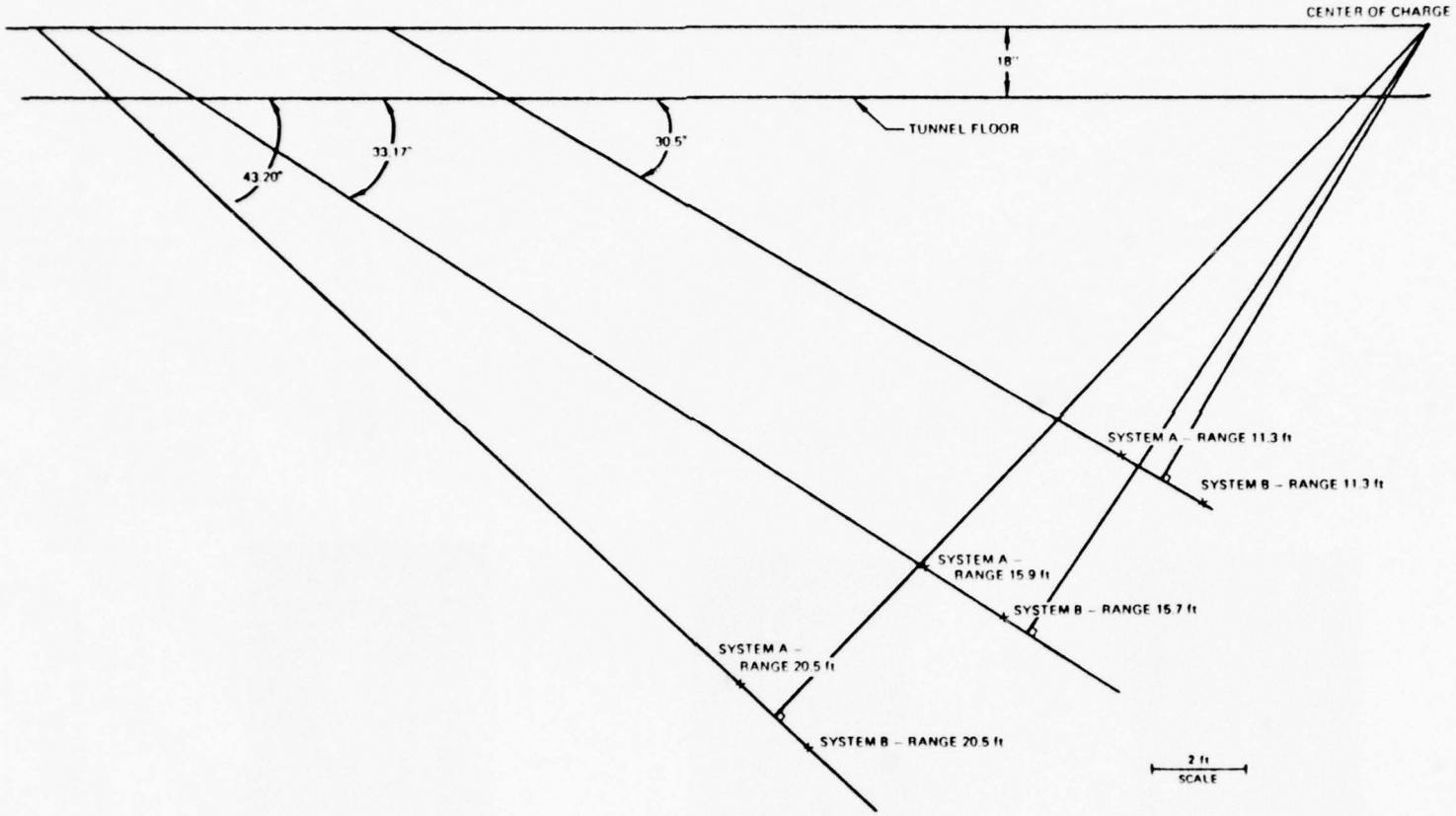

Figure 3.36 Cable topology - Diamond Mine HE test. (POR 6578)

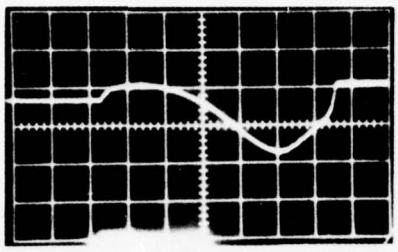

(a) Range 11.3 feet. Sweep rate 1 ms/cm. Vertical deflection 13.1 f.p.s./cm.

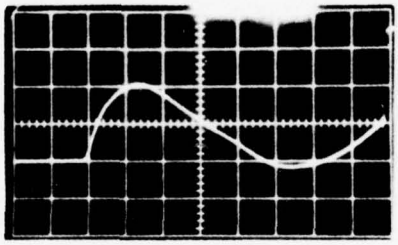

(b) Range 15.7 feet. Sweep rate 1 ms/cm. Vertical deflection 6.24 f.p.s./cm.

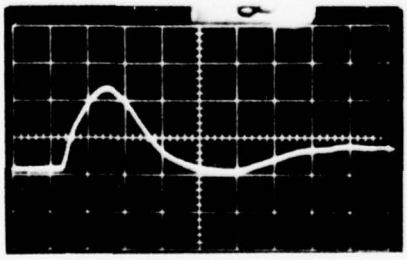

(c) Range 21.5 feet. Sweep rate 2 ms/cm. Vertical deflection 0.041 kb/cm.

Figure 3.37 Late-time cable failure (a & b) and earth pressure gage record (c). (POR 6578)

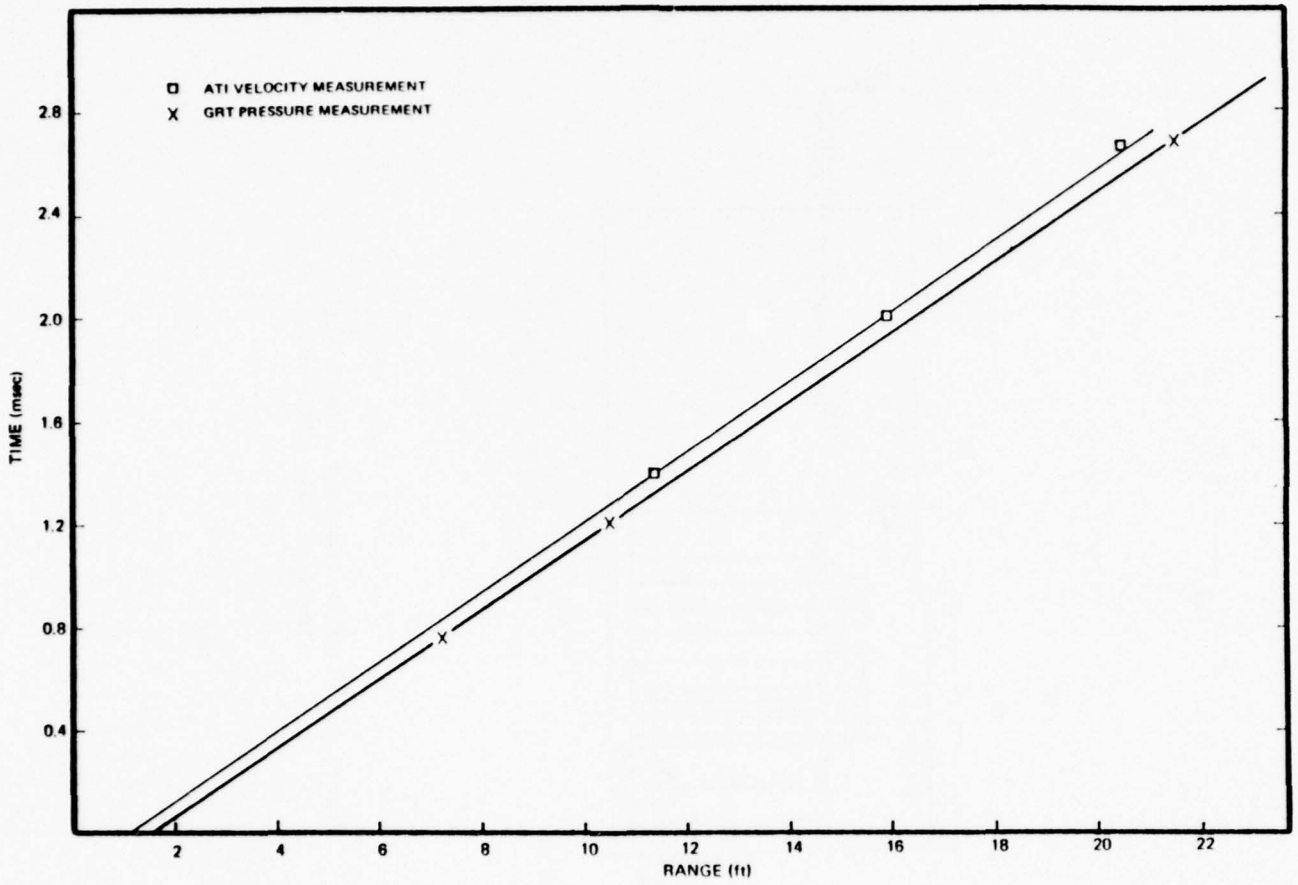

Figure 3.38 Measured (first) time-of-arrivals of precursor wave at gage locations used to calculate arrival times at the entrance of cables into the tunnel floor. (POR 6578)

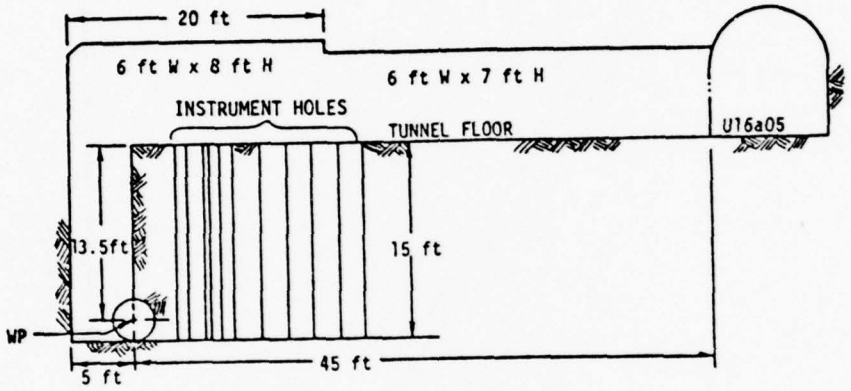

Figure 3.39 Cable topology - Mine Dust HE - elevation view (POR 6666)

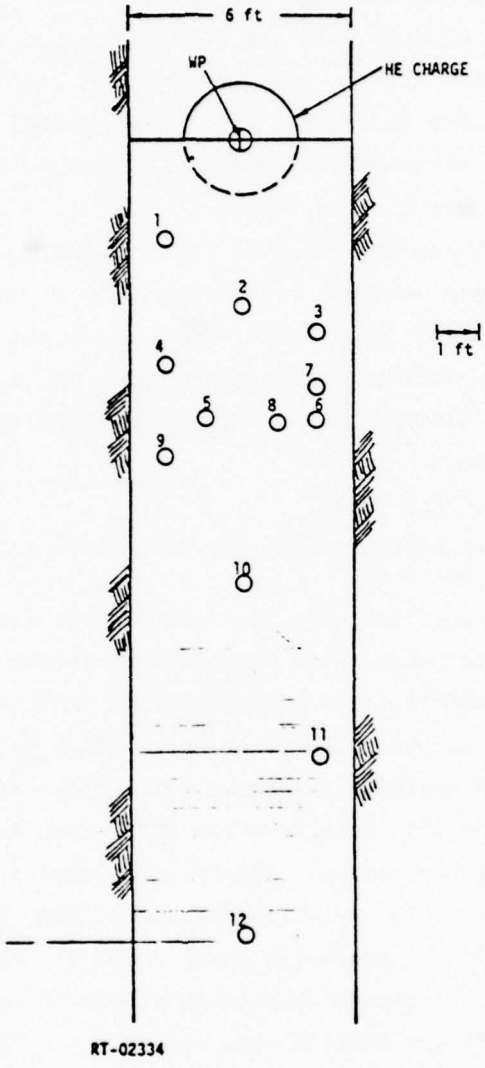

Figure 3.40 Cable topology - Mine Dust HE test - plan view. (POR 6666)

cable topology, e.g., compare Figure 3.36 with Figure 3.39, rather than from design changes in the cabling near the canister. As noted in the review of the Diamond Mine HE test the time of failure of the two cables that broke (seven cables did not fail) occurred at the time of maximum ground displacement where the cables entered the tunnel floor. The data demonstrated that the canister and cable could withstand ground motions at the 0.9 kbar level from a 0.5 ton yield.

A comparison of the Mine Dust HE and Diamond Mine HE tests with the Mighty Epic nuclear test suggests the possibility of using relatively small-scale high explosive shots for the test and development of cable systems that are to be used on full-scale nuclear tests. The idea of scaled tests and the current uncertainties in the interpretation of such tests are discussed in Section VI.

6. HIGH EXPLOSIVE FIELD TESTS

6.1 POR 6908 "Middle North Series, Pre-Dice Throw II, Stress Gauge Measurements," Smith C.

Ytterbium stress gauges were emplaced several feet below the ground surface at or below the water table in soils consisting of sand, clay, and silt or silt and gravel. The high explosive induced pressures varied from 14.8 to 1.2 kbar at the gauge locations. RG8/U (currently designated RG213/U) coaxial cable employed a tapered polythylene dielectric to produce a gradual transition in thickness from the 0.405 inch diameter cable to the 0.056 inch thick gauge paddle. Flexane 60 Epoxy--a rubber-like epoxy--was used to encase the cable transition at the paddle, for it was found by experience that to do so prolonged gauge records. The RG8/U made a 30 degree angle with the plane of the gauge paddle to form a strain relief loop but did not employ any special type of cable protection. Gauges were grouted in place taking care to prevent the entrapment of air in the grout. All of the cables survived long enough to allow the entire pressure wave form to be recorded, but all of the cables eventually failed. We believe that the data indicate that high pressure is in itself not detrimental to the performance of large diameter coaxial cable.

7. COMMUNICATIONS, AND COMMAND AND CONTROL CABLES

7.1 RM-2503 "Some Considerations About Hardening of Underground Cables," Laupa, A., Rand, February 1960 (For Official Use Only).

Laupa's report, which apparently was unknown to the UGT community until the present time, addresses the survivability of near-surface communications cables. The methods for analyzing near-surface cable failure modes and the techniques suggested for building survivable cables also bear directly on the problems of deeply buried cables. Much of what is in Laupa's report was discovered independently by UGT experimenters. The report is based on analyses and literature reviews; the need for experimental data is recognized.

Possible failure modes are identified as crushing and elongation. We add that large compressions along the axis of a cable may also induce failure on an underground test. Based on the use of solid polyethylene dielectric cables in transoceanic service to depths where the hydrostatic pressure is 7000 psi, crushing is thought not to be a problem--at least to pressures of several tens of thousands of psi. Likewise, acceleration has no particular effect on cable hardness. Ground displacement is one of the most important parameters of ground shock in connection with the hardness of underground cables. Flexible underground cable cannot offer any independent resistance to ground displacement and consequently suffers axial strain. Cable ductility is crucial in preventing failure. On the average, ductility is based on a strain that can be tolerated uniformly throughout the cable, rather than on strain to failure data which include localized necking. Without having good test data at hand it was estimated that polyethylene insulated copper cable could take 10 percent elongation, with the exact figure depending on cable construction. This figure turns out to be a mid-point value; some special cables can withstand 20 percent elongation, but others can handle but a few percent. The controlling importance of local irregularities or inhomogeneities which can produce large local strains is emphasized. If properties vary gradually then a long length of cable can be available to accommodate displacements. The length of cable can be estimated by balancing the skin friction, τ, along the length of the cable, L, with the stress, σ_y, acting on the cable cross section, A, so that $L = A\pi y/\pi d\tau$.

Whether or not this is a practical scheme in, say, tuff needs to be demonstrated. A fault zone may introduce considerable lateral displacements within a distance that is no more than a few feet in extent. High localized differential displacements may be encountered where a cable terminates in an underground structure: the movement of the structure may be different and out of phase with the free field. (Recall the failures attributed to trying to pass cables through a TAPS.)

The remedy to cable failures centers on increasing the length of cable that is available to accommodate displacements. The use of slack, armor wires, and conduit is suggested. A helical configuration is thought to be one of the most effective methods of providing slack. A planar sinusoidal modification of the helical scheme was tested on the Husky Pup cable experiment (Section III.8). Armor wires may decrease the overall ductility of a cable. Only if armor is arranged in a mesh pattern that retains the ductility of unarmored cable is the use of armored cable likely to be beneficial. A cable of this type has been used by Physics International since 1968 (Section IV.14). Conduit design is not spelled out in any detail but it is noted that a reduced frictional bond between the cable and the conduit is required. Conduits have been used on several underground tests. Slack is Laupa's preferred method, but the large shear strength of tuff compared to that of soil makes a system employing slack more difficult to engineer for a UGT than for a near surface installation. Slack pull-out tests are recommended. It is noted that Pacific Telephone uses slack in the form of an "S" when crossing the San Andreas fault. An alternate method of providing slack is to wrap electrical cables in a helix around a rubber core. This type of cable, known as Sandia stretch cable, was first employed on a nuclear test circa 1965. After about a decade of service on underground tests, stretch cable fell into disfavor and is no longer used at Sandia Laboratories (Section IV.11).

It is our opinion that Laupa's analyses point out the need for experiments: all of the techniques reviewed by Laupa have been tried on underground tests and all have failed in the large strain regime.

7.2 Review of Documents on the Survivability of Command and Control Cables.

Certain items from the command and control literature which might assist UGT cable design are presented in this subsection, as is also an

overview of the relationship between the UGT and command and control efforts. Many of the details are concerned either with the use of open boreholes in rock or with installations in soil, which although interesting do not bear directly on the subject at hand and are not reported in this review.

UGT cables are often required to survive large average axial strains, e.g., approximately 40 percent compressive strain at 2 kbar in tuff. Commercial cables fail at between a fraction of 1 percent to a few percent extensional strain; their capabilities under compressive strains are even less. The Minuteman cable specification is 20 percent extensional strain. An adaptation of the Minuteman cable technique might prove worthwhile for underground tests for it would allow both slack and take-up space to be decreased.

It was proposed in the literature that splice cases which allow access for servicing (which is not needed either for command and control installations or for underground tests) be done away with and that strong "factory-type" splices be used. Apparently "factory-type" splices were never developed. Although no details are given we assume that such a splice would entail brazing of the conductor and fusing of insulation such that the mechanical strength of the joint would be 85 to 90 percent of continuous wire and that the dielectric strength would not be diminished. Strong splices would appear to be an improvement over current UGT junction box design, but we note that in a UGT splices are often made between different cable types and more importantly we have not found evidence of splice failures.

It is our opinion that several of the conclusions stated in the literature should not be carried over to UGT design, for the conclusions are applicable only to certain specific tests and lack generality. For example, certain test results can be applied only to crush resistance (which we believe to be of lesser importance than, say, shear in a UGT) and do not give any guidance as to the axial compressibility and elongation performance of cables. From the data presented in the reports it appears that pre-shot faults intersecting boreholes were not mapped so that post-shot correlations between fault orientations and observed offsets could not be made.

The use of armored cable is often mentioned and it is important to understand the function of armor. It is our belief that most armor is designed to provide axial tensile strength, not either crushing resistance or axial compressibility. Crushing resistance is obtained either from protective conduit or from the intrinsic incompressibility of void-free materials subjected to hydrostatic stress. For example, based on our reentry observations of Dido Queen, we believe that the helically wrapped armor wires of well logging cable separate under the high stresses produced by local asymmetric loadings. The flattening of armored cable also supports the view that the armor itself does not impart crushing resistance to cables.

Newcomers to UGT cable design often inquire as to why boreholes are backfilled instead of being left open. Insofar as cable survival is concerned the answer has been that at the stresses of interest in tuff an open borehole would either spall or collapse. The resulting debris would produce high localized loads on a cable which would almost surely cause cable failure. Recently this view has been partially substantiated by laboratory tests[10]. (The laboratory tests themselves were idealizations which did not include all of the failure modes that can occur in a deforming and translating borehole.) To increase the stress levels at which long term displacement measurements can be made, UGT design has turned to thick-walled cable conduit which in itself can withstand the applied stress field without collapsing. Command and control cable design has relied upon an open borehole maintaining its integrity, relatively thin-walled conduit, and the strength of the cable itself.

7.3 NCEL-CR-69.015 "Vulnerability of Buried Cables to Nuclear Detonations," Karagozian, J.

Some of the techniques used to analyze the survival of shallow buried communications cables at overpressure levels between 1,000 and 10,000 psi are of interest to UGT cable design. Airblast produces a transverse loading of buried cable, causing the cable to deflect in a manner similar to that of a beam. The airblast loading of a homogeneous medium outside of the crater region has such a slow spatial variation that variations in the deflection of a cable are so small as to cause no distress in the cable.

To analyze cable failure the concept of a rapidly varying random displacement arising from inhomogeneities in the ground is invoked from soils engineering. One datum on random displacements is given as the sole justification for the calculations: It is noted that differential displacements of up to 50 percent of the maximum displacement can occur between two foundation footings separated by 25 feet. This separation distance is considered to be one-half of a "wavelength" used to characterize the scale of inhomogeneities. Two limits are placed on the random displacement. As the wavelength becomes vanishingly small the random displacement, Δ_λ, must also vanish. As the wavelength becomes arbitrarily large, Δ_λ cannot exceed the systematic displacement, u. At λ = 50 feet, Δ_λ must equal u/2. Thus,

$$\Delta_\lambda = \frac{u}{1 + B/\lambda} ,$$

where B = 50 feet for soils, u is the free-field displacement and λ is essentially a floating parameter.

The cable itself is modeled as a beam using plastic limit design in which plastic hinges are formed at x = 0, $\lambda/2$, and λ. The deflection of a cable is

$$\Delta_c = \frac{M_p \lambda^2}{12\ EI} .$$

M_p, the plastic hinge moment is given by

$$M_p = \sigma_y\ d^3/6 = w\lambda^2/16 ,$$

where σ_y is the yield strength of the cable and w is the distributed load on the cable. For a circular cable the deflection is

$$\Delta_c = 0.28\ \frac{\sigma_y}{E}\ \frac{\lambda^2}{d} .$$

To obtain numerical results at large strains, σ_y/E is set equal to the strain to failure. At short wavelengths the critical deflection is less than the random displacement which implies cable failure. However, it is noted that the loads which induce cable failure at small λ may exceed the shear strength of the backfill, allowing the cable to slip through the backfill and limiting the (beam) deflection, i.e., cable failure does not occur. The maximum shear stress in the backfill is assumed to act on the surface of the cable, producing a cable loading of

$$F = 2S_o d ,$$

which is the same result obtained using a different model in Section V.

Generally, UGT cable design has not been concerned with random displacements in the same sense as used in communication cable design. (To be sure, random shears along slip planes are of great concern, but that is a different type of random displacement.) The systematic strains that occur during an underground test are in themselves impressive enough to cause cable failure. It is of interest to pursue the random displacement concept for a moment because of a possible nonscalability in going from kiloton nuclear shots to HE shots a thousand times smaller. By setting the random displacement equal to the critical displacement an equation for the critical failure wavelength is obtained,

$$\left(\frac{\lambda}{d}\right)^2 + \left(\frac{B}{d}\right)\left(\frac{\lambda}{d}\right) - \frac{1}{f}\left(\frac{u}{d}\right) = 0 ,$$

where d is the cable diameter and $f = 0.283\ \sigma_y/E$. The B = 50 foot wavelength introduces a nonscalable factor into the equation. At the present time it is thought that the large systematic strains in a UGT are far more important than the random displacements, so that departures from scalability introduced by randomness should not unduly affect scaled tests. Moreover, the 50 foot wavelength was introduced in an ad hoc manner and both its applicability and numerical value needs to be determined for underground tests. Based on a review of foundation engineering in soils we have not

found evidence supporting the wavelength concept. The determination of differential settlements is not well established. On the one hand, an approach that is very rough, in our opinion, is employed[11]. Differential settlements are simply estimated to be 3/4 of the computed maximum settlement for any one location and then both maximum allowable differential and total settlements are specified. For example, the greatest allowable differential settlement in clay is 1-3/4 inches and in sand is 1-1/4 inches for both piers and rafts. A characteristic length is implied by requiring the angular deflection or final building tilt to be less than some number ranging from, say, 0.0007 to 0.005. The maximum allowable settlement is also specified to be between 2 to 5 inches, depending upon the soil and type of foundation. On the other hand, a qualitative, but deterministic explanation of differential settlement in homogeneous soils has been proposed[12]. It has been noted that interactions between footings with the same nominal design loading can modify the stress distribution in the soil around the footing to produce differential settlement. Furthermore, considerable differential settlement can occur during construction because of different incremental loadings up to identical final loads.

Laboratory tests of cable loadings with cables embedded in soils, similar to the tests discussed in Section V are suggested.

8. CABLE HARDENING TESTS

8.1 PYU-3654 "Project Officer's Report: Husky Pup Hardened Cable Experiment," Wilkinson, W. and Abrahamson, G., Stanford Research Institute (unpublished).

Four different cable designs, all employing some means for allowing the cable to stretch or contract were fielded to test their ability to accommodate a strain field similar to that expected on Mighty Epic, which was then in the planning stage. A fifth design which relied upon tensile strength rather than upon an effective ductility was also fielded. All of the cables failed within 0.3 to 1.5 ms of ground shock arrival at the intersection of the bypass drift and the cable boreholes, Figure 3.41. To add insult to injury all of the cables also failed at the gas seal connectors. Without visual inspection of the failed parts, which can be obtained only by a reentry operation, the exact causes of failure will remain uncertain. Nonetheless, it is believed that at the drift-borehole intersection the

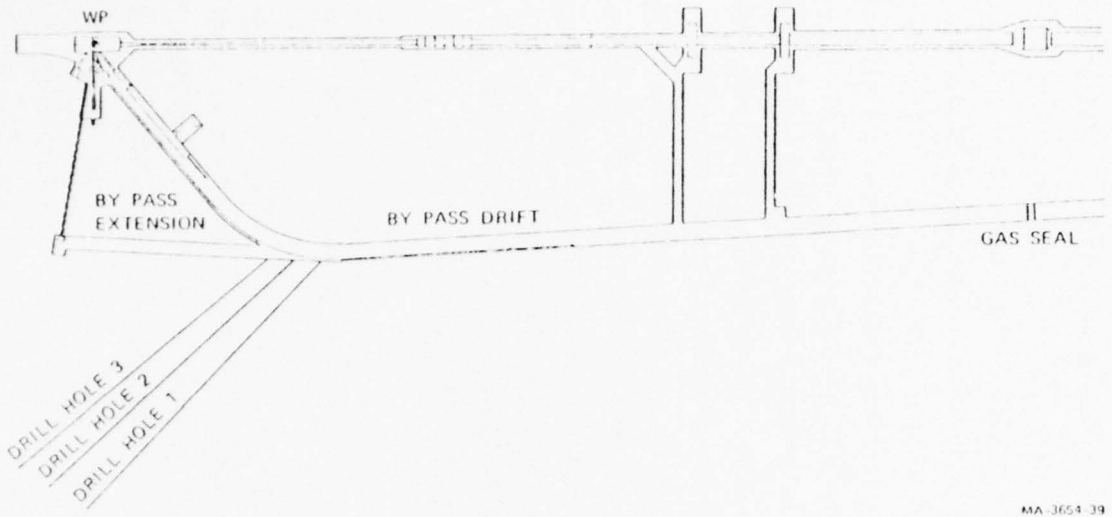

Figure 3.41 Husky Pup cable hardening experiment emplaced in drill holes 1-3. Design stress in the by-pass drift at drill hole 3 is 2.5 kb and at drill hole 1 is 2 kb. Design stress at far end of drill holes is 1 kb. (PYU-3654)

cables failed in shear. It is our opinion that the Husky Pup cable experiment illustrates two major uncertainties in cable design: shear induced failure and connector failure.

Although the experiment yielded no successful design it is of value to examine the cable designs to illustrate the state-of-the-art. At the time the experiment was planned, no agreement on the best cable type could be reached amongst experienced experimenters, so five different cable configurations were employed. A striking omission from the test is the braided stainless steel armored cable used by Physics International. Some of the designs as actually employed are controversial. The principal features of the five designs are discussed below.

8.1.1 Slip Joint. The design is indicated in Figure 3.42. The dimensions were chosen to prevent buckling at 2.7 kbar, which required a ratio of wall thickness to inside radius not less than 1.2. "O"-ring seals were used to prevent water and grout entry into the cable take-up space. Shear pins with a 6900 lbf design were used to facilitate loading. A PVC cap was used to prevent cable damage during straining. The coupling lengths were designed for 20 percent extension and 10 percent elongation. It is stated in the draft POR that the 16 TSP cable (type DOD/DNA-MP-13) contained in the conduit was tested to 12.5 percent extension and 25 percent compression without open or short circuiting. Resistivity and capacitance change measurements are not reported so that the transmission characteristics of the cable at the rather large reported strains cannot be ascertained. We note that the strain capabilities of cables tested in different laboratories show a fair amount of scatter. Although the extensional capability of the conduit exceeded that of the cable no provision was made for storing slack cable within the couplings because the expected strains did not exceed the strain capabilities of the 16 TSP.

8.1.2 Meander or "Slack" Aluminum Conduit. The design, illustrated in Figure 3.43, is based on the fact that the axial compressibility of a pipe with "U" bends is much greater than that of a straight pipe and that the length of the conduit can be changed with a relatively small force to accommodate strains in the material in which the conduit is embedded. It is thought that the main advantage of "slack" conduit over slip joints

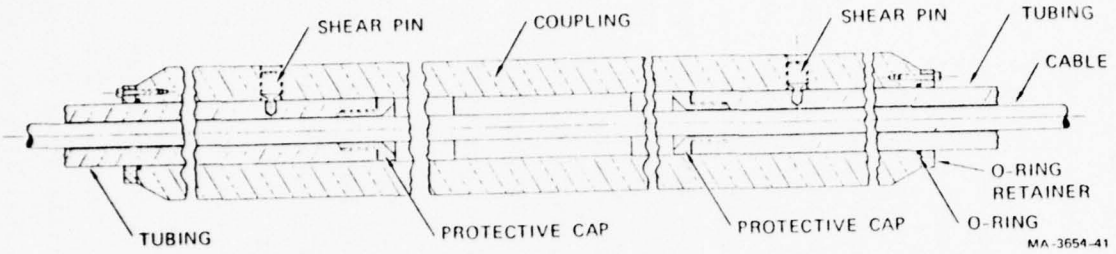

Figure 3.42 Slip joint assembly. Sections are 10 ft long. The tubing is 1.75 inch o.d. with a 0.5 inch wall. The coupling is 3.75 inch o.d. with a 1.0 inch wall. The material is 6061-T6 aluminum. The design pressure is 2.7 kb. (PYU-3654)

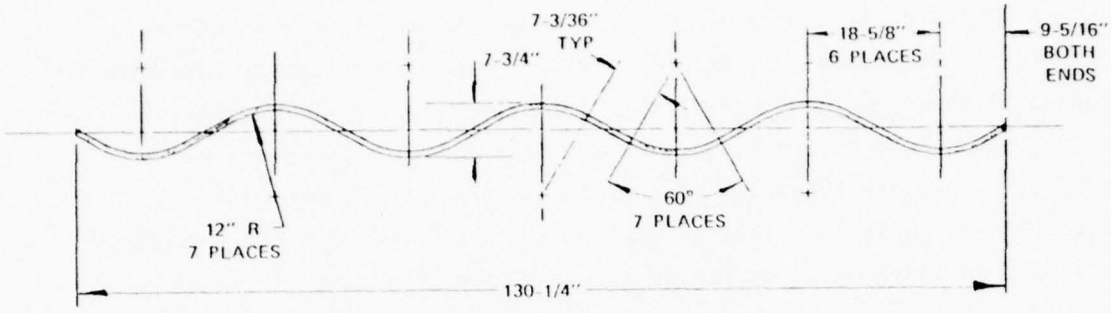

Figure 3.43 "Slack" conduit. Conduit o.d. is 0.875 inches with a wall thickness to inside radius ratio = 1.3. (PYU-3654)

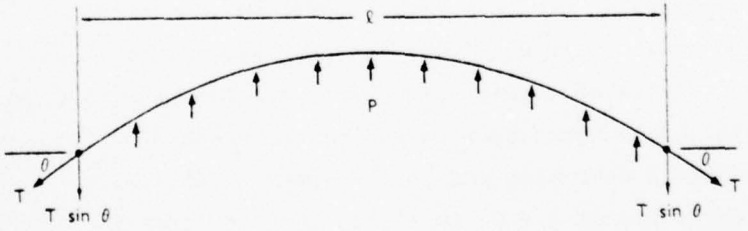

Figure 3.44 Diagram for estimating forces required to pull tubing through material. (PYU-3654)

is that the former design provides slack distributed continuously over the length of the cable whereas the latter lumps the compliance at discrete locations. Thus shear offsets might be accommodated better by the "slack" conduit. Experimental proof of this intuitive concept is required.

Tensile tests indicated that a 6000 pound force is required to produce 11 percent extension in the configuration of Figure 3.43. To estimate the additional force needed to pull the conduit through backfill a simple analysis based on Figure 3.44 was used to derive the relation

$$T = PLd/2 \sin \theta ,$$

where T is the tension in the conduit, L is the arc length of conduit, d is the conduit diameter and P is the pressure resisting the movement of the tube through the grout. We assume that P is essentially equal to the maximum stress difference, $\sigma_1-\sigma_3$, that can be supported in the backfill. The experiment designers set P = 300 psi, and with the geometry of Figure 3.43 determined that the initial force required to strain the conduit is 5000 lbf. Adding the 5000 lbf generated by the backfill resistance to the 6000 lbf required to straighten the conduit results in a force which exceeds by 100 lbf the strength of the welded couplings.

Several aspects of the design are uncertain: Based on triaxial compression tests performed at Terra-Tek, the maximum stress differences that can be supported in properly mixed superlean grout, HSSL-1, is 190 ± 15 psi, not 300 psi. It is difficult to set P exactly in a simple analysis because of the effects of strain rate, large deformations, and pre-failing. Thus the initial grout resistance is reduced to about 3200 lbf. As the conduit stretches, θ decreases and for a constant value of $\sigma_1-\sigma_3$, the force increases, e.g., at $\theta = 6°$ the grout induced force is 15,000 lbf. Using handbook values, the 6061 aluminum conduit in the T-6 condition can develop 20,000 lbf at the yield point. The as-built Husky Pup welded couplings reduced the strength of the conduit by about a factor of two, which checks with the ultimate strength of 6061-T0 aluminum. Should the "slack" conduit test ever be repeated (under less time pressure to get the experiment in the field), then we believe that couplings must either be

formed from double butted tubing or welded and then heat treated back to the T-6 condition.

To compensate for the reduced strength of the welded couplings the conduit was encased in sealed trays containing gelled water. For an actual field experiment such a technique appears to us to be cumbersome and somewhat impractical.

The approximate calculations of the tensile force in the conduit differ from each other by a factor that is less than two, depending upon the value used for the shear strength. Both the amount of strain and the strain rate affect the plastic behavior of grout. Rather than attempt to incorporate the effects of large deformations, strain rate, and pore water migration into calculations, a direct measurement of the force-strain characteristics of "slack" cable pulled through grout in various strain states is called for.

8.1.3 Well-Logging Cable. Seven conductor well-logging cable (Vector type 7-J-46RB) was used in two configurations. One cable with slack was placed alongside the "slack" conduit inside the gel trays to allow this low ductility cable to accommodate strains. A second straight cable was embedded directly in grout to test the ability of the cable to force grout and tuff to flow around the cable.

The well-logging cable was tested under hydrostatic pressure to 2.7 kbar without displaying either an open or short circuit condition. The manufacturer's specifications give a minimum tensile strength of 11,300 lbf with a 1 percent elongation to failure. Because of uncertain performance and difficulty in fielding stiff armored cable both Sandia Laboratories and Physics International discontinued using well-logging cable several years ago. Our post-shot inspection of well-logging cable used on the Dido Queen test revealed flattening and local separation of the armor wires, but whether the damage resulted from ground motion or the reentry mining operation could not be determined.

8.1.4 Sandia Stretch Cable. Six TSP wound around a compressible neoprene core and sheathed in neoprene (Vector type AEC-NV-IV-24) was embedded directly in rock matching grout. The cable specifications state that a 20 percent extension can be accommodated. Stretch cable is no longer considered worth using by experienced personnel at Sandia Laboratories.

9. THE ANALYSIS OF COMPOSITE STRUCTURES

9.1 R-1070-PR "High Performance Composite Materials for Vehicle Construction: An Elastoplastic Analysis of Crack Propagation in a Unidirectional Composite," Adams, Donald F., Rand, March 1973.

A finite element code was applied to the determination of the flow and failure around a fiber in the matrix of a composite material according to the Prandtl-Reuss elastic-plastic theory. The two dimensional plane strain problem was investigated for a square section of the matrix with the circular cross-section of the fiber at its center. The matrix was loaded by forces applied at its edges, and so this case is almost an exact analog of the problem of the relative transverse motion of a cable through a backfill. Numerical results were obtained for the elastic response, the onset of yielding, the ultimate yielding and the propagation of the failure surface through the material. The numerical solution technique is far from cut and dry: A large number of test cases had to be run to make certain that the observed propagation of the failure surface was physically accurate and not due to the zoning. There is a fair amount of commentary in the report on various methods for the numerical description of crack propagation. A large amount of work has been done in recent years on the mechanical response of composite materials, such as stress distribution and propagation, and it is important to recognize the close analogy with the loading of a cable in a backfill. The numerical techniques appear to be more powerful than are currently required in view of the relatively small spread between the analytic results and the uncertainties that exist in specifying the yield surface of the matrix material (grout).

10. MATERIAL PROPERTIES

10.1 DNA 3870F-1 "Material Properties in Support of the Nevada Test Site Nuclear Test Program," Volume 1, Butters, S., Dropek, R., Green, S., and Jones, A.

Test data on grout properties required both for the analysis of cable-backfill interactions and for the design of cable hardening experiments are presented. Based on our analysis, the strength of grout, in particular superlean grout, can play a crucial role in determining whether or not a cable system fails. The Terra-Tek experiments provide numerical values for the strength of grout and document factors affecting the

strength of grout, which must be taken into account when designing cable tests.

The compositions of the grouts that were tested are listed in Table 3.8 and their physical properties are listed in Table 3.9. The maximum stress difference that can be supported by superlean grout in a triaxial compression test varies between 9 and 13 bars, depending upon the value of the confining pressure, Figure 3.45. The shear strength, $(\sigma_1-\sigma_3)/\sqrt{3}$, increases about 28 percent as the pressure increases from 0 to 0.5 kbar and then increases only about 12 percent to the maximum test pressure of 4 kbar. Thus the grout induced forces on a cable should decrease during the unloading phase of an underground explosion, i.e., as the displacements increase the grout resistance decreases. The unconfined compression strength of superlean grout increases about 5 percent to 10 percent for each decade increase in strain rate, Figure 3.46. Thus, the initial value of shear strength to be used for design calculations should be about 30 percent greater than that indicated by the triaxial tests. Large strain tests indicate a gradual decrease in shear strength with increasing strain--about a 25 percent decrease at 30 percent axial strain, Figure 3.47. At small values of strain both the high strength grout and rock matching grout tests are in agreement with the small strain tests, but the superlean grout test shows a larger value of $\sigma_1-\sigma_3$ at corresponding strains than do the small strain tests. The discrepancy apparently is caused by a variation in the superlean grout mixtures[13] and points out the importance of strict control of grout mixing procedures in the field. Extrusion tests with area reductions of 78, 300, and 610 percent and extrusion rates of 5.6×10^{-3} to 6.65×10^{-2} inches/second determined that an elastic plastic model characterized the grout response and that a viscous model did not. A mathematical model based on the work of Avitzur[14] indicated that for elastic-plastic behavior $\sigma_1-\sigma_3$ is independent of extrusion velocity, but for viscous behavior $\sigma_1-\sigma_3$ is linearly dependent on the extrusion velocity. The range of extrusion rates was too narrow to reveal the strain rate dependence which, based on unconfined compression tests, is believed to occur.

Type	Constituents	lbs/ft^3	% By weight
Superlean	Cement-Type G	3.46	3.17
(SLG)	Bentonite gel	2.48	2.26
same as	NTS desert fine sand	79.55	72.55
HSSL-1	CFR-2 (Cement friction reducing agent)	0.037	0.03
	water	24.1	21.98
Rock-matching	Cement-Type G	23.06	18.09
(RMG)	Sand 20-40	24.73	19.40
same as	Barite	42.04	32.97
DSRM-2	Bentonite	3.23	2.53
	CFR-2	.09	.07
	water	34.35	26.94
High Strength	Cement-Type G	23.30	18.35
(HSG)	Chem Stress II	6.82	5.37
same as	Fly Ash	15.75	12.40
DSHSG	Sand 20-40	53.73	42.37
(CSII-6.82)	Bentonite	2.29	1.80
	CFR-2	.29	0.23
	AVI (air entraining)	.04	0.03
	water	24.78	19.51

Table 3.8 Typical design constituents of grout mixtures. (DNA 3870F)

Type	As Rec.	Density gm/cc		H_2O by Wet Wgt. %	Saturation %	Porosity Total %	Air Voids %	Meas. Perm Comp. %	Velocity (Ft/Sec)	
		Dry	Grain						Long	Shear
SLG	Meas.	Calc.	Meas.	Meas.	Calc.	Calc.	Calc.	Meas.	Meas.	Meas.
14-45* Day Age	1.74 ±0.03	1.25 ±0.03	2.63 ±0.02	28 ±2.0	94	52	3	2-4	5800	2600
RMG										
14-45* Day Age	2.04 ±0.03	1.51 ±0.03	3.20 ±0.02	26 ±2.0	100	53	0	2-4	7400	3600
Full** Strength	2.02	1.62	3.20	20	82	49	7	7	8300	4500
HSG										
Full** Strength	1.95	1.68	2.70	14	56	38	11	10+	11500	6800

* Average of about 10 batches for physical properties and permanent compactions and one batch only for velocities.
** One batch only for all values. For the RMG, see RMG test data section for explanations of the change in physical properties with age.

Table 3.9 Physical properties and ultrasonic velocities of three grout mixtures. (DNA 3870F)

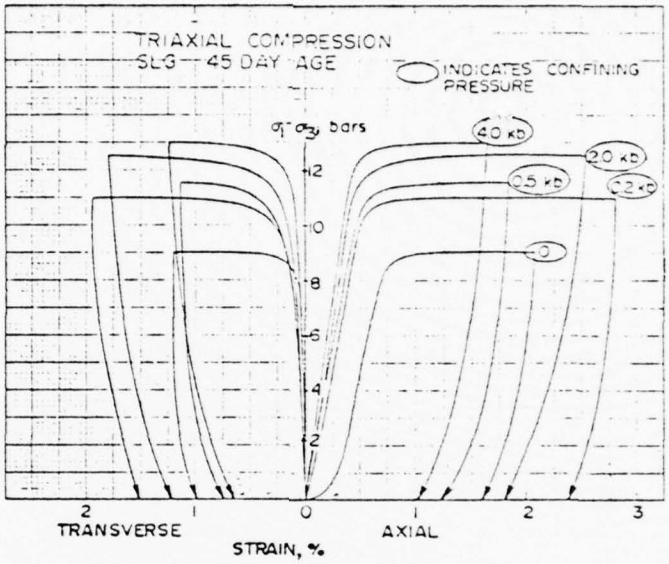

Figure 3.45 Superlean grout; triaxial compression stress-strain response (45-day age). (DNA 3870F)

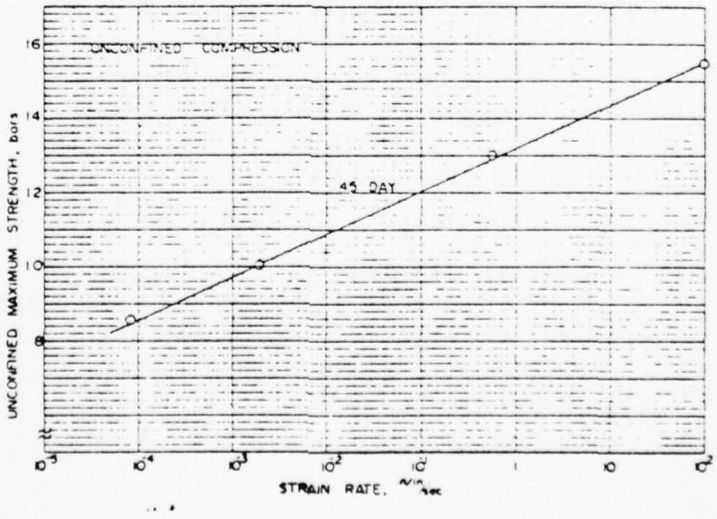

Figure 3.46 Superlean grout; unconfined compressive strength at various strain rates (45-day age). (DNA 3870F)

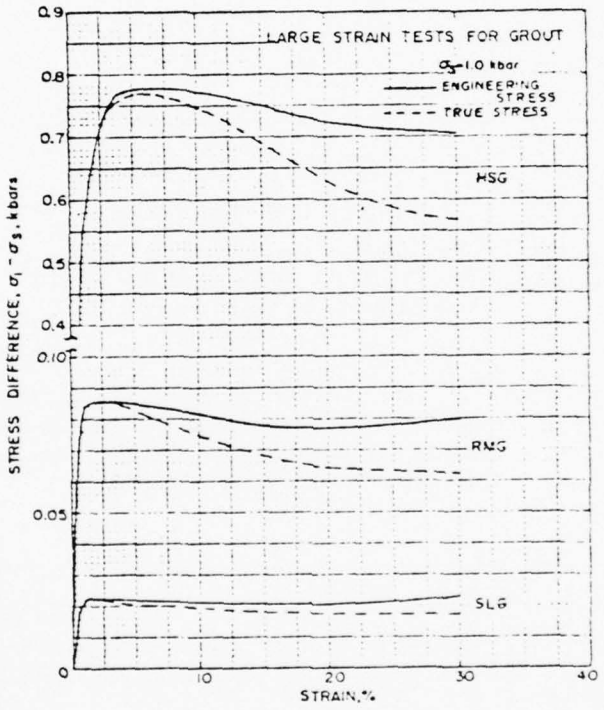

Figure 3.47 Stress difference vs percent axial strain for large axial strain tests on the three types of grout. (DNA 3870F)

The effect of pore water migration and its potential importance in cable tests was also revealed by the extrusion tests. The pre-test shear strength of the superlean grout loaded into the upstream extrusion chamber was 6.4 bars, but the post-test strength of the grout remaining in the upstream chamber was 14.9 bars. The increase in strength is attributed to the squeezing of water from the upstream to the downstream extrusion chamber. Based on the Terra-Tek work it is concluded that tests of cable interactions with grout must duplicate the in-situ stress state, the strain rate, and the total strain.

10.2 DNA4201F "A Viscometric Study of the Properties of Grout," Blake, T.R., Day, E.A. and Patch, D.F., Nov. 1974.

Based on post-shot evidence it had been suggested that the grouts used in underground tests may have a viscous behavior. Using a rotary viscometer no evidence was found for the viscous behavior of superlean grout, but rather plastic (rate independent) yieldings is observed and measured. The grout tested was HSSL-1 superlean with components mixed on the following percentage weight basis: 72.55 percent sand, 21.98 percent water, 3.2 percent cement, 2.3 percent bentonite gel, and 0.036 percent polymer friction reducer. Tests were performed at strain rates to 50 per second and pressures to 1 kbar. An initial failure strength thought to be comprised of the chemical bond strength and static friction is dependent on the strain rate, but is independent of the hydrostatic pressure. The value of the initial shear strength is 2.7×10^6 dynes/cm^2 (39 psi). After the initial failure the shear resistance decreases to a rate and pressure independent level of 0.9×10^6 dynes/cm^2 (13 psi). Terra-Tek data (Section III.10.1) indicate that the shear strength of HSSL-1 $(\sigma_1-\sigma_3)/\sqrt{3}$, is 5.3×10^6 to 2.3×10^7 dynes/cm^2 or about a factor of two greater than the triaxial values referenced in the S^3 report. Based on the Terra-Tek data the S^3 viscometer results appear to be somewhat low. The pressure independence of the failure strength is not in agreement with the Terra-Tek triaxial data, Figure 3.45. Most of the S^3 tests were performed on samples cured 18 to 30 days. One test grout cured for only one day indicated a 25 percent reduction in dynamic shear strength. By measuring the dynamic friction over a large number of revolutions of the viscometer the dynamic friction

AD-A071 369 H-TECH LABS INC SANTA MONICA CA F/G 18/3
THE DESIGN OF SUBTERRANEAN INSTRUMENTATION CABLES TO SURVIVE LA--ETC(U)
JUL 78 B A HARTENBAUM DNA001-77-C-0213
UNCLASSIFIED DNA-4636F NL

2 OF 2
AD
A071369

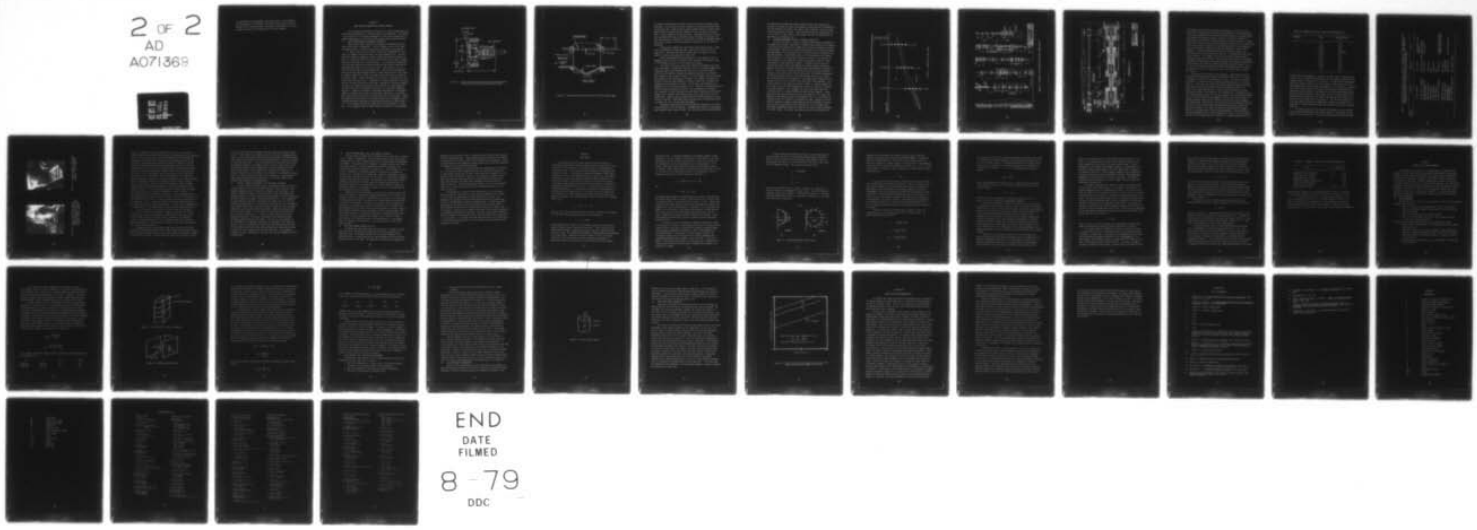

END
DATE
FILMED
8-79
DDC

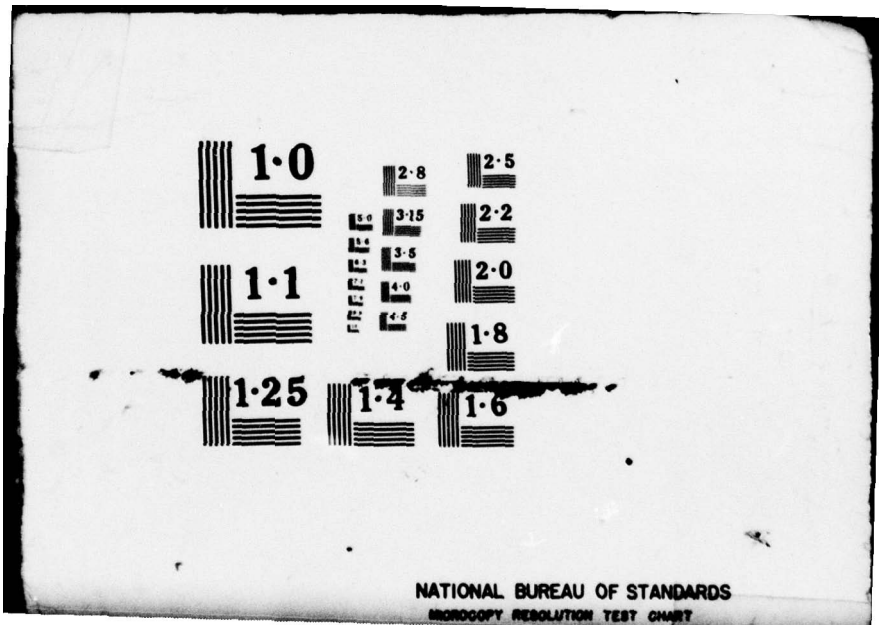
1·0
1·1
1·25
2·8
3·15
3·5
4·0
4·5
1·4
2·5
2·2
2·0
1·8
1·6
NATIONAL BUREAU OF STANDARDS
MICROCOPY RESOLUTION TEST CHART

was determined to be independent of the shear strain. The viscometer data are valuable to the present study because they indicate the rate insensitivity of superlean grout, the range of uncertainty of the yield strength in shear, and the magnitude of the shear strength.

SECTION IV

CABLE PRACTICES EMPLOYED BY FIELDING AGENCIES

In this Section the results of discussions on cable fielding practices with several experimenters at different agencies are documented. The purpose of this Section is to allow one experimenter to extend the learning curve of another experimenter at a different agency without duplicating past efforts.

11. SANDIA LABORATORIES, ALBUQUERQUE, NEW MEXICO

Two different cable techniques are employed in underground tests by Sandia Laboratories, Albuquerque. A third technique, used in an oil shale fracturing project, is also of interest and is described in this Section.

H. Miller and W. Cook use 4-wire shielded cable (ERDA-NV-MC-9, Rev 1, 5HLD, 4C) commonly called "blue quad" run inside hydraulic hose. The blue quad outer jacket is impervious to water (some cable jackets may leak, e.g., RG213). The hydraulic hose has a metal braid exterior and a rubber interior. Three quad cables may be run inside one hose. It is believed at Sandia that the crush space between the electrical cable and the hydraulic hose affords additional protection to the electrical cable. Cables must be run in a radial direction away from the working point. Most successful measurements have had the instrument package placed no closer than about the 1 kbar range. At greater ranges, say 0.5 kbar, any cable failure that does occur seems to be caused by shear. Cable connectors can be a source of failure both at canisters and at gas block seals. Transducers are usually hardwired to the blue quad and the wires are potted in hard foam. Although no electrical connector is used at the canister the hydraulic hose connector is a weak element and has been protected by a hollow steel cone with a 0.5 inch wall thickness, Figure 4.1. Based on time domain reflectometry measurements a considerable number of failures have occured at the gas-seal connectors, e.g. on Mighty Epic a 50% failure rate occured at the gas-blocks in the main tunnel. Sandia has departed from the practice of mounting connectors on a bulkhead, and has instead protected the gas-seals by installing them inside the TAPS, Figure 4.2. At the present time the new design has not been subjected to a field test. It is suggested that the reader obtain the results of the performance

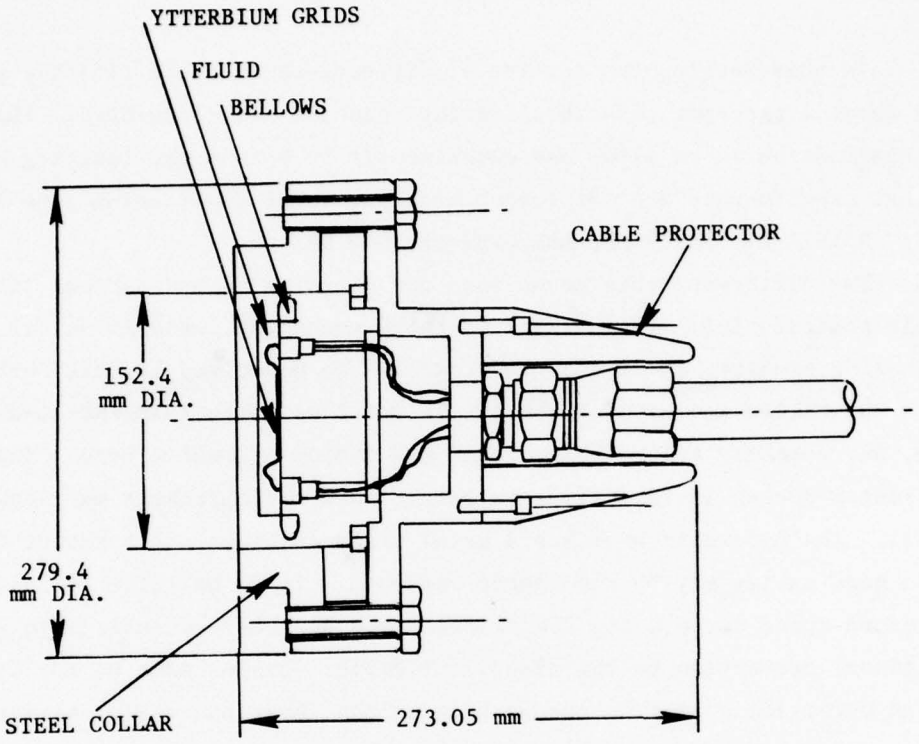

Figure 4.1 Sandia hardwired cable connection with cable protector (installed on fluid-coupled plate pressure gage).

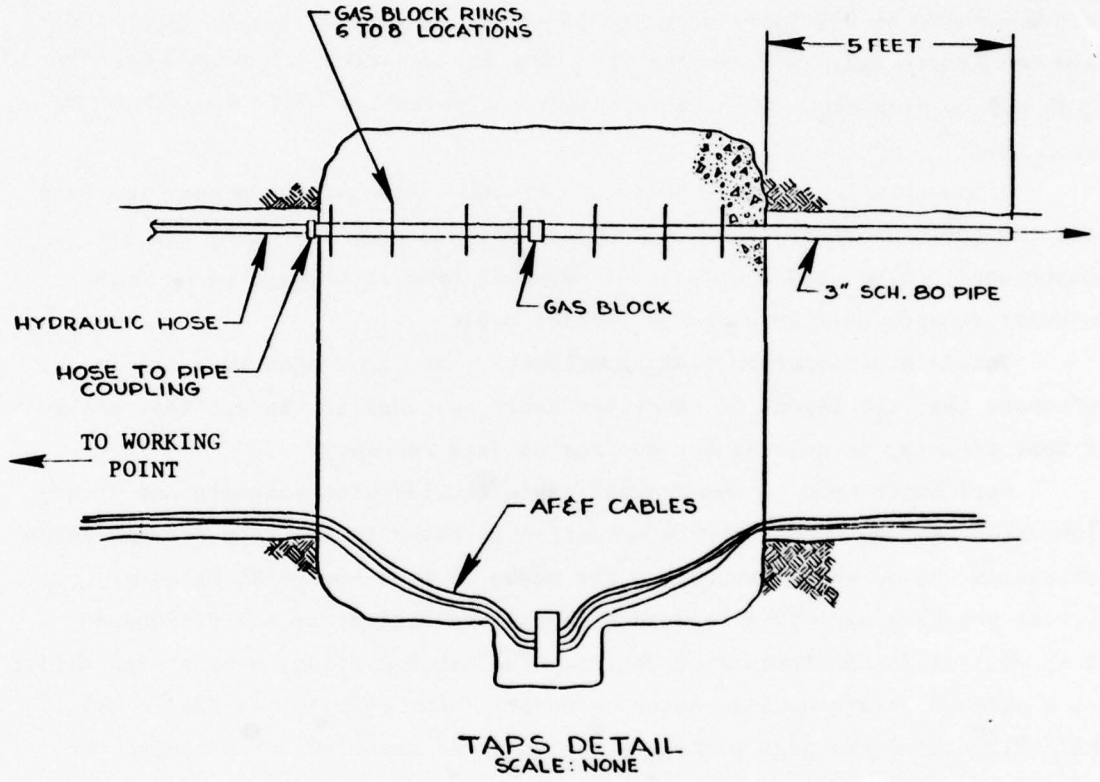

Figure 4.2 Sandia gas-blocks located inside the TAPS on Diablo Hawk.

of gas-seals located within the TAPS of the as-yet-to-be-fired Diablo Hawk experiment. Coal tar may be used as required as a gas-block material within the hydraulic hose. Based on the electrical characteristics of buried cable, Sandia reports no adverse reaction between the coal tar and the blue quad cable. Visual inspection has not been made. Sandia believes that the acetic acid liberated by RTV has a deleterious effect on cables, but no lab tests have been performed. Because coal tar contains a variety of compounds, some of which may be hazardous, the health dangers attendant with its use should be determined.

Although well logging cable and stretch cable have been used in years past the performance of these two cable types was such that they are no longer used. Blue quad protected by hydralic hose is thought to be much superior to both well logging and stretch cable.

Sandia experimenters (and experimenters at other agencies) are in agreement that the layout of favorable cable routings at the earliest stage of test planning is crucial for successful data recovery.

Carl Smith uses 50 ohm coaxial cable (RG213) with manganin and ytterbium stress gages. Considerable attention is given to the gage package-cable transition region which experience has shown to be a source of failure. Current practice employs a tapered polyethylene dielectric and Flexane 60 Epoxy potting in the transition region. The cable topology uses strain relief and a minimum strain configuration as needed. For example, on Middle Gust, the RG213 exited the gage package at an angle of about 40^{o} to minimize the tangential strain acting on the cable. The minimum strain geometry is in agreement with our calculations (Section II.2). The RG213 is embedded directly in grout without any special protection. The experimental data indicate that a pressure of tens of kilobars does not unduly distress solid dieclectric coaxial cable. However, cable failures may occur at some point on the unloading wave. Based on time-of-arrivals some of the failures appear to have occured in regions of large shear where the cable exits a borehole and enters a by-pass drift e.g., the Dido Queen experiment.

Ray Reed's experience with shale rubbleization experiments is of qualitative interest to the UGT program. Instrumentation cables are installed in open boreholes--grout cannot be used. The electrical cables (usually RG22B/U)

are protected by placing them inside aluminum tubing, which minimize compressing or pinching the cable and smoothes the loads produced by rubbleizing. The open boreholes can subject the cable to spall fragments, and may in some cases collapse about the cable. Shear offsets produced by rubbleization are of the order of 1 inch, which is considerably less than the maximum offests observed on an underground test.

12. WATERWAYS EXPERIMENT STATION, VICKSBURG, MISSISSIPPI

An intensive effort at securing a hardened cable plant was expended on the Mighty Epic interface experiment. Although several agencies were involved in the design and fielding of the Mighty Epic interface experiment, the Waterways Experiment Station had the prime responsibility for the detailed design and emplacement of the cable plant up to a location several feet ahead of the gas-seal bulkhead. The Waterways effort will be discussed in this Section. Partly because of cost and partly because of the nature of the geology the cable topology for the Mighty Epic interface experiment, Figure 4.3, was unfavorable for long term cable survival. To assist their survival the cables were heavily armored with 6061-T6 and 2024-T4 flanged conduit and employed slip joints to provide piecewise axial compressibility, Figures 4.4 and 4.5. Sandia stretch cable was installed inside the conduit above the interface and 16 TSP was used below the interface. The limited availability of 7075-T6 prevented the use of this high strength alloy for the conduit, but 7075-T6 was used for the canisters. The conduit wall thickness was 0.75 inches in the tuff and 0.5 inches in the relatively strong quartzite. The outside diamter of the conduit was either 2 inches or 3 inches between the slip joints. The slip joint housings were either 4.5 inches or 5.5 inches in outside diameter. In the downhole run, slip joint shear rings with activation forces of between 25,000 and 53,000 lbf were employed. In the drift the shear ring activation force was only 5000 lbf. The conduit was embedded in rock matching grout in the downhole runs, but in the drift the conduit was laid in a trench and surrounded with sand. (Based not only on pre-shot analyses of backfill compressibility and the buckling of the conduit, but also on post-shot reentry observations it is our opinion that additional consideration needs to be given to the type of backfill employed in a cable trench.) To protect the conduit elbow at the intersection of

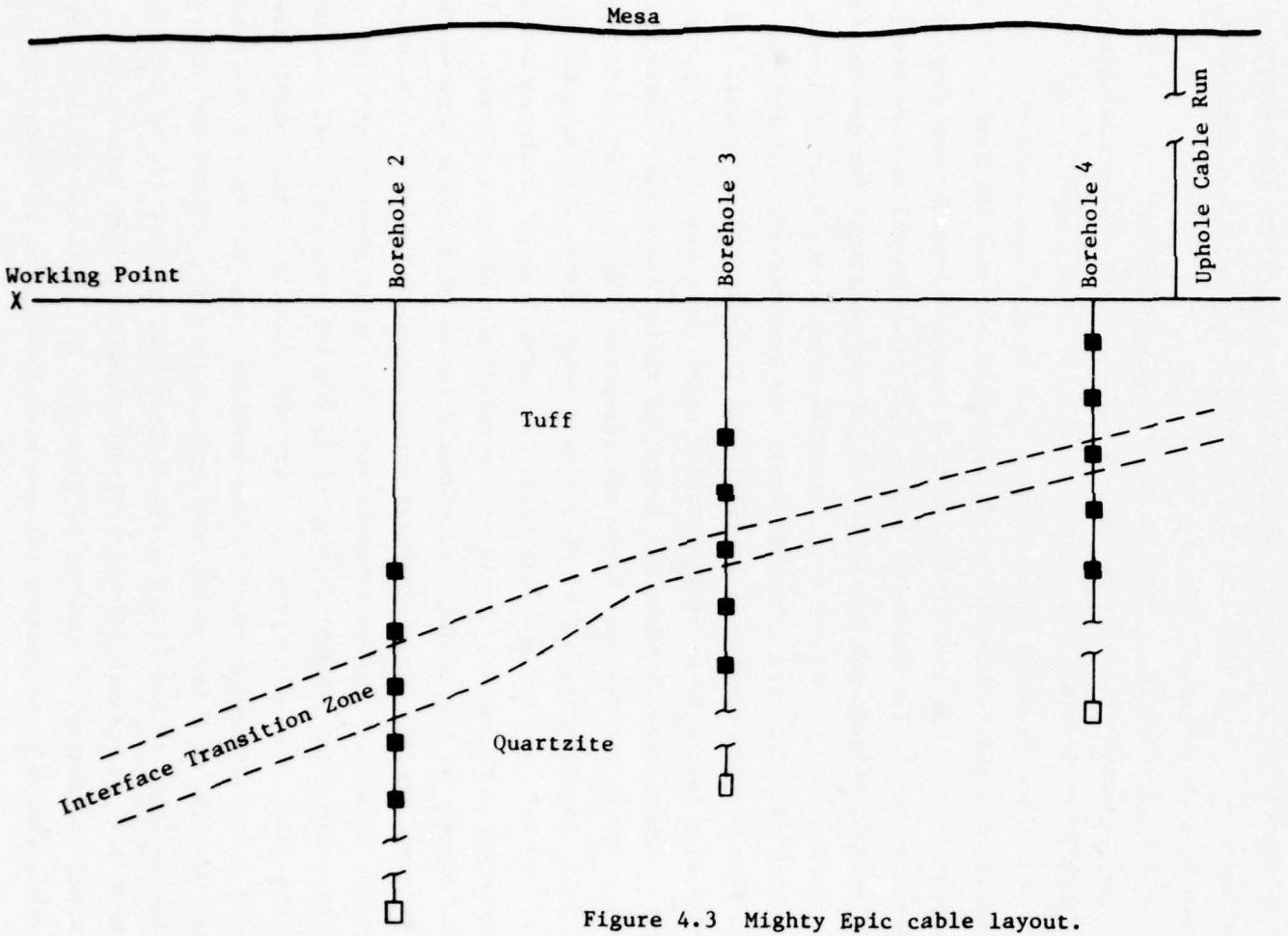

Figure 4.3 Mighty Epic cable layout.

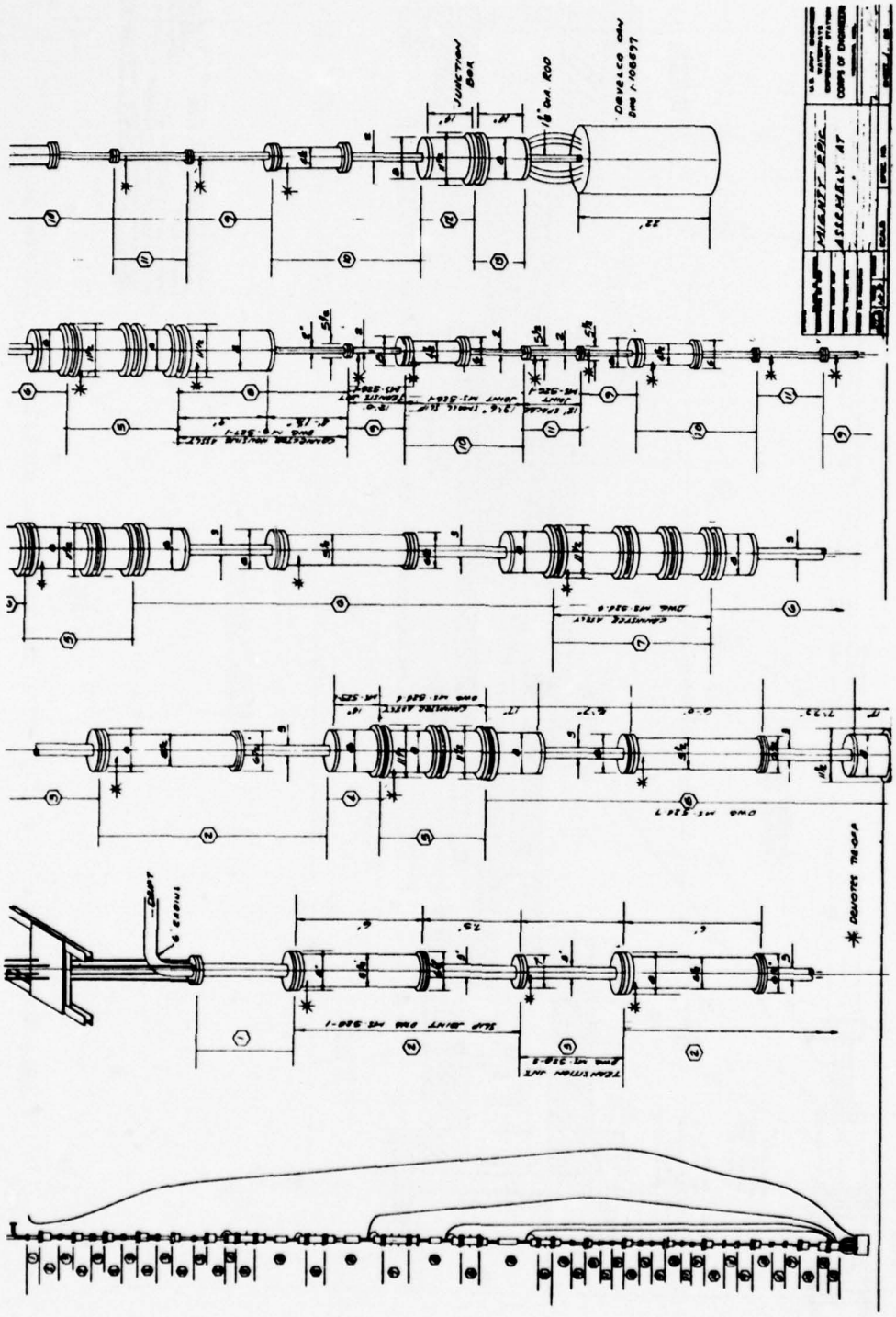

Figure 4.4 Detail of the downhole cable armor (Reference 15)

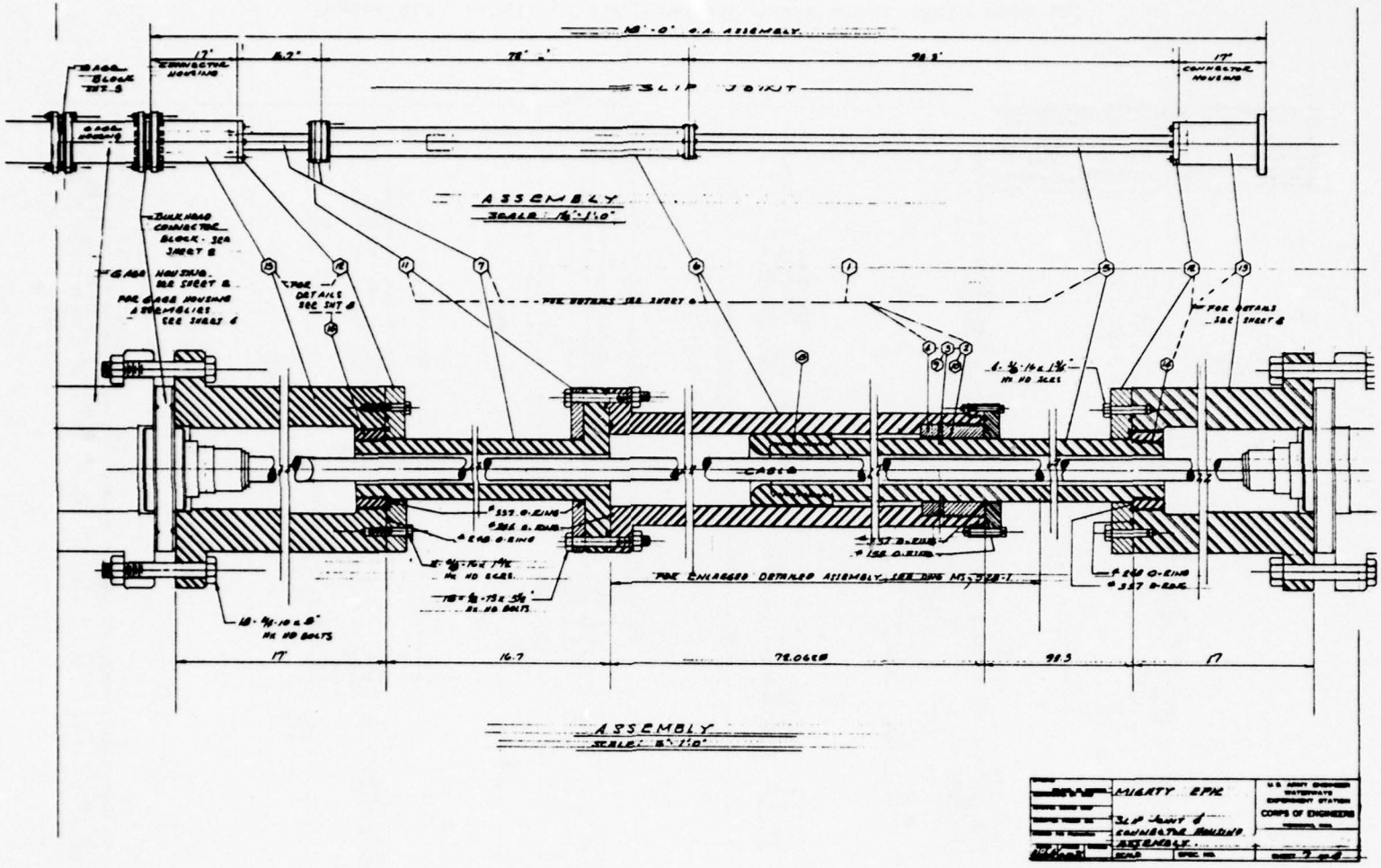

Figure 4.5 Detail of a slip joint and connector protection. (Reference 15)

each borehole and the drift the conduit was encased in a 4 feet x 4 feet x 8 feet block of high strength grout which was keyed into the surrounding tuff. To allow the instruments to record the free-field motion in the region around the interface no attempt was made to reinforce the conduit or limit the differential motion that was expected between the tuff and quartzite. Rather than relying on the survival of cable crossing the interface for the acquisition of data from below the interface an experimental device for the storage and the wireless (radio) transmission of data was emplaced at bottom of each borehole. A few feet beyond borehole number 4 the massive conduit was terminated and the cables were laid in coal tar. The Waterways design ceased at this location. Just beyond the coal tar the cables entered gas-block connectors mounted on a bulkhead. The gas-block connectors were not designed to withstand a high pressure environment although the downhole instrumentation string employed high pressure connectors manufactured by Envirocon. On the far side of the gas-seal bulkhead the cables were embedded in grout without any additional protection and made their way to the mesa inside a stemmed steel pipe.

We now proceed to examine circuit failures. Data obtained from the Waterways Experiment Station indicate simultaneous failure of all circuits in borehole 2 at 28 ms and in borehole 4 at 66 ms. The failure of circuits in borehole 3 occured over a time interval extending from 55.3 to 99.3 ms, Table 4.1. Post-shot time domain reflectometry (TDR) measurements indicated cable failures at various locations which are summarized in Table 4.2. Based on the signal waveforms all of the circuits from borehole 2 failed after shock arrival at the borehole - drift intersection. Although the post-shot TDR measurements reveal five failure locations, the time interval between wave arrival and circuit failure suggests that the first failure occurred through a shearing action at the borehole collar prior to the attainment of peak displacement. The design of the elbow section needs additional analysis. The use of a high strength grout section may have increased, rather than decreased the shear, e.g., recall the problem of passing cables through a TAPS at a much lower level of stress and displacement. Current thoughts on TAPS design suggest that if a high strength grout section is used it should be tied to the rock matching grout with rebar. A similar problem occurred on

Table 4.1 Mighty Epic circuit failure times (Reference 15)

Borehole	Gage	Time-of-Failure ms
2	all	27.8
3	3-1-uh	98.9
	3-1-uv	98.7
	3-2-uh	90.4-99.3
	3-2-uv	92.7
	3-3-uh	98.9
	3-4-uh	85.3
	3-4-uv	94.7
	3-5-uh	55.3
	3-5-uv	56.4
4	all	66.0

the Husky Pup cable experiment. The use of a drill collar is controversial. A steel collar is supposed to add support, yet the evidence suggests that the cables were cut at the location of the collar. We believe that reinforcement should be provided by rebar. The collar should be relied upon only to prevent sloughing and should be made of fiberglass. It is important to recognize that even if shear failure in the high stress region at the borehole-drift intersection were prevented it is unlikely that late-time measurements would have been obtained because of cable failure in the low stress region of the uphole cable run to the mesa. The uphole cable may have been severed less than 40 ms after signal arrival at borehole 2. The slip joint stroke in the drift just beyond the elbow was insufficient to take up the ground strain, resulting in a severed conduit and both open and short circuits in the cable, Figure 4.6.

The times-of-failure of the circuits from borehole 3 do not coincide with any first times-of-arrival at failure locations. The location of the initial failure is uncertain. All of the failures were relatively late-time

Table 4.2 Cable failure locations & type of failure. (Reference 15) Field Command asserts that the gas-seal connectors did not fail, but rather soft cables behind the bulkhead were severed. The Mighty Epic interface experiment.

Borehole	Location	Failure	Note
2	13 feet downhole	open circuit	steel casing & grout interface
	204 feet fwd. of bulkhead	open & short circuit	conduit severed
	65 feet fwd. of bulkhead gas-seal bulkhead	open circuit	one-pair only
	1080 feet below mesa	open circuit	
3	56 feet downhole	low Z	
	69 feet downhole	open circuit	
	74 feet downhole	low Z	
	33 feet fwd. of bulkhead	open circuit	conduit deformed against bulkhead located at fault
	1080 feet below mesa	open circuit	
	1292 feet below mesa	"discontinuity"	
4	4 feet downhole gas-seal bulkhead	short circuit	top of steel casing
	1065 to 1080 feet below mesa	open & short circuit	

Figure 4.6 Buckled and severed conduit where ground strain exceeded take-up capacity of slip joint 200 feet forward of gas-seal bulkhead. (Field Command)

Figure 4.7 Conduit passing through fault 33 feet forward of gas-seal bulkhead. (Field Command)

effects. Although the gas-seal connector did not fail for the borehole 3 cable the Waterways group reported that based on TDR measurements the connectors did fail for the other cables. DNA Field Command discounts the Waterways measurements and asserts that on the basis of visual observations the soft cables were severed behind the gas-block bulkheads.[16] Whether or not the gas-seals open-circuited under ground shock loading was never ascertained. Whichever group is correct, we note that data were lost and that more attention must be focused on designing a complete system, no one part of which will fail. Prior to emplacement, both the gas-seals and soft cables were recognized as sources of failure, and the fanning-out of soft cables from massive armoring in a high stress region was recognized as an illogical design. Under the pressure of meeting a test schedule and test budget, corrective action was not taken. Locating a secondary bulkhead at a fault resulted in the conduit and cable being damaged as it was forced against the steel bulkhead, Figure 4.7. The fault motion in itself did not damage the conduit. Such was not the case at the gas seal bulkhead. Generally unknown to the groups involved in the design of Mighty Epic, a fault traversed the gas-seal bulkhead and the resulting explosion induced offset was responsible for the aforementioned cable failure. The cable failure behind the gas-seals points out two needs. First, an integrated design is required rather than having different agencies patch their designs together. Second, better communications are needed between Field Command and the other design and fielding agencies.

The first failure of the borehole four cable could have occured at any one of the three failure locations. Failure at the top of the casing is most likely because the time interval between first arrival and failure was sufficient to allow a large shear offset to develop. The 1080 foot location in the uphole mesa run is also a possible first failure location because an analysis of arrival times has indicated a several ms delay between wave arrival and cable failure.

Considerable effort was expended to make cables survive in the high stress, large displacement region. Heavy walled conduit was employed to ensure that slip joints would work effectively to take up axial strain without binding or pinching off the cable. (We have noted many times that pressure in itself

up to at least a few tens of kilobars will not cause solid dielectric cable to fail -- the conduit is not needed to protect cable from a uniform pressure field.) Even if better high stress designs were available, late-time measurements almost surely would not have been obtained because of failure in regions of relatively low stress. It is our opinion that the low stress regions also need greater attention. For example, surveys for fault planes must be made, and appropiate designs must be implemented to prevent cable shear by low stress fault offsets. In the uphole run to the mesa the boring must be surveyed through the use of corings or logs (calipers or televiewer) to locate faults. At fault locations the cables must be protected. Under-reaming or heavy reinforcement may provide protection in a low stress region, but a workable method remains to be demonstrated.

13. SYSTEMS, SCIENCE AND SOFTWARE, (S^3) SAN DIEGO, CALIFORNIA

H. Kratz's group at Systems, Science and Software employs a variety of cabling techniques with no one technique enjoying a favored position. The methods employed are said to depend on the needs of each experiment. Most cables are embedded directly in backfill: RG213, RG22B, well logging, and Whitmore armored. The latter cable is built by Whitmore to an S^3 specification. The cable contains four number 22 twisted shielded pairs. For our purposes the most important features of the design are an inner jacket of 0.03 inch urethane surrounding the TSP, a double armor consisting of 0.015 inch diameter hard stainless steel wire, and an outer jacket of 0.040 inch thick urethane. Subminiature coaxial cables, RG174/U and Endevco 3090B, have been protected by a 1/4 inch OD conduit. The performance of these cables in field tests have been noted in Section III.4. Splices are protected by epoxy-filled Pomona junction boxes. The cables are anchored to the boxes with Bates and Thomas compression-type cable clamps. Test data are not available on the performance of the Whitmore cable and on the strength of the Pomona box splices. Data are available which demonstrates that RG22B taken from stock at the Nevada Test Site has a porous outer jacket which allows water to seep in between the outer conductor and the inner dielectric. Upon reaching a connector the shunt conductance of the water can cause high impedance circuits to malfunction.

14. PHYSICS INTERNATIONAL, (PI), SAN LEANDRO, CALIFORNIA

Two main cable techniques have been employed by F. Sauer and C. Vincent's group at Physics International. Based on their experience with above ground cratering shots, a double braided armored TSP has been employed on underground experiments. The braided cable is composed of a tightly wrapped inner stainless steel mesh with a loosely wrapped outer stainless steel mesh. The braided cable concept is discussed in Section III.7. The performance of the cable on stemming and containment diagnostic experiments is discussed in Section III.4. Recently (on the Mighty Epic structures experiments) schedule 160 steel pipe was used to protect soft TSP cables. To accomodate longitudural strains, slip joints were employed. The success of the steel conduit design prompted its adoption for the yet-to-be-fired Diablo Hawk experiment. At the present time the use of strong conduit is heavily favored, although the problem of fanning-in and fanning-out cables to and from the conduit has not been addressed in a critical manner.

Junction boxes are not thought to be a source of failure provided that they are filled with a relatively incompressible material such as epoxy. The joining of cables to canisters is considered to be critical. The outer braid of the double armored cable is clamped to the canister while the inner braid is epoxied to the canister. Pull-out tests to ensure that the connection of the cable to the canisters is at least as strong as the cable itself have been performed, but the results have not been documented. To prevent relative motion between the TAPS and the surrounding grout from severing cables that pass through the TAPS, a foam-filled rattle space is provided on both sides of the TAPS. Gas-seal connectors are thought to be a source of failure, partly because of the short pins used in the connectors, e.g., even during grout cure pins have open-circuited -- a condition thought to arise from thermal strains.

15. DNA FIELD COMMAND, NEVADA TEST SITE

The Nevada Test Site group under the direction of J. LaComb is responsible for many of the designs and construction techniques employed on an underground test. Of paticular interest are the gas-seal connectors and uphole cable runs. The gas-seals used by Field Command are 1000 psi hermetic commectors with 31 to 60 pins. The connectors are mounted on a bulkhead, are

provided shear protection by use of a concentric steel ring, and use a Kellem grip over a waterproof boot. Field Command believes that failures attributed to connectors have occured, in fact, in the cables near the connectors. Unlike the experimenters, Field Command personnel believe that the gas-seal connectors are adequate for the job they must perform.

Many experimenters are concerned about the survivability of the uphole run to the mesa, but Field Command states that no cables have been lost at a range greater than 800 feet and with a good sand stem, the uphole run will survive as close as 500 feet. However, it is difficult to achieve a good sand stem during the winter months using current practices because of the great amount of water condensate which accompanies the updraft from the tunnel to the mesa. It was noted that large offsets can occur in the uphole cable run: a 15 inch offset was measured on the Ming Blade cable run at a range of 700 feet.

The importance of laying out cable routes early in the experiment plan was stressed. Quite often so called "add-on" experiments are fielded at a late date and consequently may have unfavorable cable runs. The importance of cooperation and good communication between Field Command and the other fielding agencies cannot be overemphasized. Although some experimenters are of the opinion that steel borehole collars can sever cables, Field Command believes that the collars provide protection to cables. For the collars to be effective any multiple pours must be tied together adequately and impedance matching must be observed. The steel conduit cable protection system is thought to be technically sound, but costs more than six times that of a soft system. It is evident that some current practices are controversial. It is equally evident that most of the controversy could be resolved by good diagnostic experiments.

SECTION V

CABLE SHEAR

In Sections III and IV we have seen that the shear failure of cables that cross planes of weakness, whether they be construction discontinuities or natural faults, is a crucial problem in the measurement of late-time motions. In this section we shall analyze the transverse loads imposed on a cable. In particular we address the question of what force is required to move a cable through backfill so that not only can loads be determined, but so that the effects of backfill material properties can also be ascertained. We characterize the flow of the backfill material as governed by the maximum shear stress which the material can sustain and under which the material will flow, e.g., a perfectly plastic material or a Mohr-Coulomb material. A simple model of cable motion through backfill postulates that the normal stress, σ, is uniform over the projected area of the cable in the forward-facing direction and zero in the lateral and backward directions. The principal normal stress is related to the maximum shear, S_o, as

$$S_o = \frac{1}{2}(\sigma - 0) = \frac{1}{2}\sigma .$$

The force F per unit length on the cable is directly related to the diameter d of the cable and the maximum shear stress in the backfill,

$$F = \sigma d = 2S_o d .$$

The maximum shear may depend on the mechanical properties of the backfill material and the state of stress in the material. A full solution to the problem would include a complete description of the stress and flow field around the cable. The constitutive properties of grout backfill are described by a plastic model. Laboratory tests have failed to detect any viscous behavior of grout, rather the tests have confirmed the existence of a maximum shear type of criterion and the associated plastic flow response

(Section III.10). It has been customary to use analyses similar to that expressed in the above formula in the design of cable systems. The stress distribution used in the model was chosen in a rather ad hoc manner and the uniqueness of the stress distribution was not demonstrated. If we choose a different stress distribution we get quite a different answer. For example, using a similar model but allowing a background state of stress σ_n, σ_t, with σ_n in the direction of motion of the cable and σ_t in the transverse direction, the above relations are modified to

$$S_o = \frac{1}{2}\left[(\sigma + \sigma_n) - (0 + \sigma_t)\right]$$

and

$$F = (2S_o - \sigma_n + \sigma_t)d \ .$$

An analogous relationship is obtained using the von Mises yield condition. This result implies that the state of stress and not just a constant value of the yield stress in shear influences the loads on a cable. This second calculation thus indicates that a more complex dependence is possible, and suggests that a more careful analysis is warranted. We are concerned with whether it is the details of the stress distribution in a failed material (for a fixed value of the yield strength) that controls the load on a cable or whether the material properties themselves are altered. Recent data indicate the yield surface itself is altered by large deformations (Section III.10).

To clarify the type of dependence on material parameters we resort to the theory of elasticity. Even though the materials of interest are not linearly elastic, the theory of elasticity is useful for gaining insight into nonlinear problems and to suggest the forms of the dependence on material properties. Furthermore, in the more general plastic case a piecewise linear theory of elasticity can be used to determine the incremental deformation about a general state of stress[17]. Even if the moduli of the material are varying at a particular state of loading, the linear theory of elasticity can be used to determine the response to an increment of loading.

A simple model relating backfill stresses to the transverse force per unit length of cable can be developed from Boussinesq's problem[18], which is one of relating the stresses within a semi-infinite solid to a concentrated line load, F, on the free surface of the solid. The stress field is remarkably simple: All stresses are purely radial,

$$\sigma_r = \frac{-2F}{\pi} \frac{\cos \theta}{r}$$

$$\sigma_\theta = 0 ,$$

$$\sigma_\theta = 0 .$$

Two cases can be related to cable loads. In Figure 5.1, one-half of a cable of diameter d is embedded in the half space. The radial stress is a maximum on the axis of symmetry. Yielding first occurs at $\theta = 0$; thus, using the maximum shear stress or Coulomb yield condition, the force which just induces first yielding is

$$F = \frac{\pi}{2} S_o d .$$

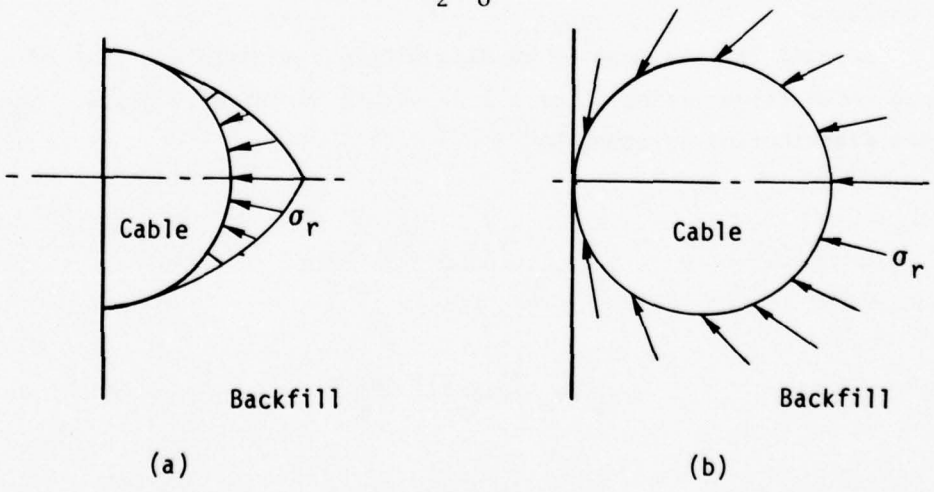

Figure 5.1. Boussinesq models of cable loads.

Inasmuch as the half-space has yielded at only one place, this force should be smaller than that derived from the other models. It turns out that this is indeed the case. In Figure 5.1(b) an entire cable cross-section of diameter d is buried tangent to the free surface. The magnitude of the stress is constant on the surface of the cable, $\sigma_r = -2F/\pi d$. In this topology all of the material yields simultaneously. Employing the Coulomb yield condition,

$$F = \pi S_o d \ .$$

It can be observed from the above formulas that the stress distribution is independent of the elastic parameters. Prager has shown that for plane elastic problems if the stresses are specified on the boundaries of the material, then the stresses are determined throughout the material independent of the elastic parameters provided that the topology is simply connected[19]. If the topology is multiply connected then the resultant force on each of the multiple boundaries must be zero for the stresses to be independent of the elastic constants. The mathematical representation of the transverse motion of a cable through the surrounding material is one of a doubly connected topology; thus, dependence on material properties is possible.

A model for the case of loading within a material is that of a concentrated force acting along a line within an infinite plate. The stress distribution is given by[20]

$$\sigma_r = -\frac{(3 + \nu)F}{4\pi}\frac{\cos\theta}{r}$$

$$\sigma_\theta = \frac{(1 - \nu)F}{4\pi}\frac{\cos\theta}{r}$$

$$\tau_{r\theta} = \frac{(1 - \nu)F}{4\pi}\frac{\sin\theta}{r} \ .$$

It can be seen that the stress distribution depends on Poisson's ratio, and so a dependence on material parameters has been uncovered for this case of a doubly connected topology. (Reference 20 discusses the problem of plane stress, but as is well known plane strain and plane stress solutions are identical in the absence of body forces.) The maximum shear stress is given by

$$\tau_{max} = \frac{F}{2\pi r} ,$$

and is thus independent of Poisson's ratio. Assuming incipient yielding and calculating the net force on a circle of radius equal to that of the cable we obtain,

$$F = \pi S_o d .$$

Not only is the load independent of the elastic parameter, but it is identical with the second form of Boussinesq's solution.

As suggested throughout, we expect our results for the cable motion to depend more on the theory of plasticity than on the theory of elasticity. We have used the theory of elasticity not only to obtain particular numerical results for the condition of incipient yielding, but also to indicate the form of dependence on material parameters, such as Poisson's ratio. Furthermore, the linear theory of elasticity can be applied incrementally for gross deformations with a more complex total dependence on material parameters. However, in this case the material parameters for the incremental loading will be determined by the state of stress produced by all of the previous loads. For a resolution of such complex dependence it is generally necessary to resort to numerical solutions obtained with a digital computer.

Turning now to the theory of plasticity, we have uncovered two analytic solutions and one numerical solution which can be applied to the problem of transverse cable loads. One of the analytic solutions was devised by Karagozian (Section III.7.3) specifically for investigating loads on cables. The other analytic solution is the classical one of

Prandtl for the deformation of a semi-infinite solid produced by a flat punch. It is thought that the application of Prandtl's solution to the cable problem must surely result in an upper bound estimate. Because Boussinesq's first solution of incipient yielding is a lower bound, it is of value to place an upper bound on the loads using Prandtl's solution. The numerical solution is a finite element treatment of the yielding and fracture in the matrix material surrounding a solitary reinforcing fiber. Deformation of the fiber itself can also be calculated. The composite problem is very close analog of the cable problem, and has already been described in Section III.9.

To continue, Karagozian has proposed a solution in which the shear stress acting on the circular outline of the surface of the cable has a constant magnitude equal to the maximum shear stress. On one-half of the cable the shears act in a clockwise direction and on the other in a counter-clockwise direction to reinforce one another in retarding the motion of the cable. The shear stress distribution, which is considerably different from the other stress distributions which have been considered in this section, satisfies the plasticity yield condition at the surface of the cable and presumes a rough rather than a smooth boundary condition at the surface of the cable, since the maximum shear occurs there. Using the no-slip condition at the cable-backfill interface and resolving the shear in the direction of motion, the force on the cable is

$$F = 2S_o d \ .$$

This, of course, is exactly the same as our introductory estimate which, however, was based on an entirely different distribution of stress.

The classic problem of Prandtl's is that of a flat punch of width d resting on the surface of a semi-infinite solid, and being forced into the solid by a normal load. The problem is two dimensional (plane strain) with the material extending indefinitely in the third dimension. The description of this problem is given in various texts[21,22], and the treatment is based on more recent results by Hill[23]. In Prandtl's original solution a triangle of solid material in uniform flow, just below the flat

punch, moves with the (rigid) punch as a rigid body. On each side of the triangle is a centered fan of material in plastic flow with yet another uniform flow triangle on each side to connect the fans to the surface. Unlike the five other estimates the plastic solution does not exhibit a surface of cylindrical symmetry that can be thought of as a cable. With this distribution of plastic flow the force on the punch turns out to be

$$F = (\pi + 2)\, S_o d \ .$$

The work of Hill has suggested another flow field, but the force on the punch is the same as that just given. It has not been demonstrated rigorously that the punch problem is an upper bound to the cable problem; the results themselves indicate that this is quite likely the case. The same result that was found from the elastic solutions, namely, that the transverse loads are independent of the elastic constants, also holds from the plastic solutions.

The results of elastic analyses and plastic analyses for the transverse loads applied to a cable by backfill all have the same form:

$$F = CS_o d \ ,$$

where the coefficient, C, depends upon the details of the analysis. The numerical value of the coefficient is listed in Table 5.1. As would be expected on physical grounds the Boussinesq "half buried cable" is a lower bound estimate because it treats only incipient yielding at $\theta = 0$. The plastic punch problem provides an upper bound estimate.

For design purposes a value of the coefficient between 2.00 and 3.14 is recommended; a conservative design would use C = 3.14. The uncertainty in the value of the coefficient is less than the uncertainty in the value to be used for the shear strength of backfill material. It is important to recognize the limitations of the simple analyses summarized in Table 5.1. For a large fraction of the duration of explosion induced ground motion the cable does not induce failure of the backfill as assumed by the models but rather the stress wave sweeping over the cable

Table 5.1. Summary of results for cable load coefficient.

Model		Coefficient
Boussinesq "half buried cable"	$\pi/2$	1.57
Simple plasticity estimate	2	2.00
Karagozian shear estimate	2	2.00
Boussinesq "tangent buried cable"	π	3.14
Line force within material	π	3.14
Plastic punch on surface	$\pi + 2$	5.14

location induces failure in the surrounding geologic material. That this is so has been suggested by machine calculations of explosions in tuff[24].

It is concluded that two sets of experiments are necessary. The first set should be a close analog of the models summarized in Table 5.1; that is, load-deformation measurements of a pipe embedded both fully and partially in grout should be made. The second set of experiments should place the grout in a failed state and then make load-deformation measurements.

SECTION VI

THE DESIGN OF CABLE EXPERIMENTS

The purpose of this Section is to address means for improving field designs. The main thrust will be experimental; simple analyses are already available and their applicability needs to be tested. Before reformulating or improving the analyses, experimental observations on the performance of cable systems are necessary. Research experiments are needed to shed light on problems caused by shear and by large axial deformations. Test engineering experiments are needed to resolve uncertainties in the performance of certain components. The value of a third class of experiments; namely, small scale replicas of a field test, is uncertain at present. It is believed that the research experiments will resolve some of the uncertainties in the design of small scale experiments.

16. SHEAR EXPERIMENTS

The questions to be resolved by shear experiments (which will be described forthwith) are as follows:

a. What is the relative motion between cable conduit and backfill?

b. How does the conduit elongation depend upon the offset across the plane of weakness?

c. What is the offset that causes conduit failure?

d. What is the effectiveness of rebar in tying together two media, at least one of which has failed?

Parameters to be varied during the course of the experiments include:

a. Backfill type: superlean grout, rock matching grout, high strength grout, and sand.

b. The state of stress, e.g., prior to loading a cable in shear the backfill is either initially unstressed or on the failure surface.

c. The yield strength of the backfill (which, of course, is related to (a.) and (b.).

d. The material inside the conduit, e.g., either empty or filled with a viscous fluid.

To set ideas we indicate schematically a test setup in Figure 6.1. The principal feature is a plane of weakness at the interface between material one and material two. Material two is displaced along the interface relative to material one, and the deformation of the conduit is observed. The observations may employ active instrumentation or take a rather simple and direct approach; namely, visual inspection obtained by sectioning the test block.

As noted in Section III.10.1 the strength of grout is logarithmically dependent on the strain rates. If the laboratory tests are to have a one-to-one correspondence with field tests then the strain rates must be similar. A one-to-one correspondence is not essential for understanding the phenomena of interest, but it is vital that the backfill properties under load be known accurately. Attention also must be paid to the problem of pore water migration. To prevent the test results from being influenced by end conditions the conduit should be long enough so that if the conduit were made any longer the test results would remain invariant. The critical L/d can be estimated by equating the force exerted on the conduit by surface tractions to the tensile force within the conduit at the yield point of the metal,

$$\pi d L S_o = \frac{\pi(d^2-d_i^2)\sigma_y}{4},$$

$$\frac{L}{d} = \frac{\left[1-(d_i/d)^2\right]}{4}\frac{\sigma_y}{S_o}.$$

As an example, for 6061-T6 conduit and both superlean and tuff matching grouts the critical L/d is:

σ_y	S_o	L/d	$(L/d)^*$
40,000 psi	86.6 psi	87	260
40,000 psi	866 psi	8.7	26

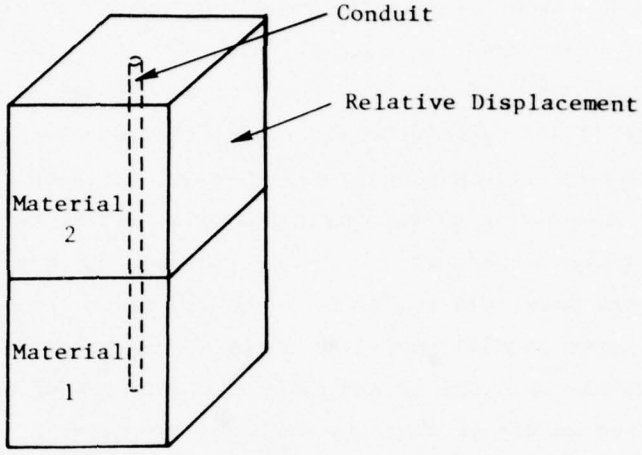

Figure 6.1 Conduit strain at plane of weakness.

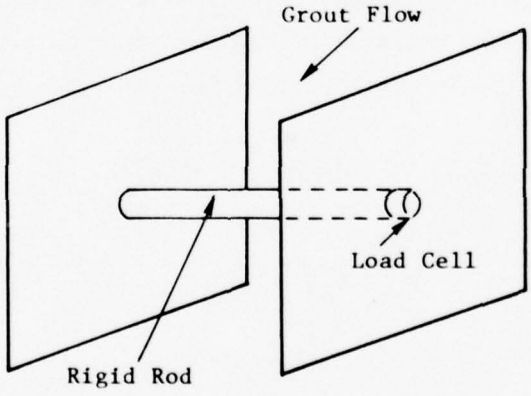

Figure 6.2 Transverse conduit loads.

If a reduction in the yield strength of grout is experienced at large strains, then the L/d ratios must be increased in the same proportion as the strength is decreased. Using the data of Section III.10.2 the L/d is increased by a factor of three and is denoted by $(L/d)^*$. The yield strength of the conduit in tension is not a free parameter because it is directly related to the crucial elongation to failure. Although it is not the intent of this study to design hardware, we note that for an initial set of experiments a savings in money might be effected by restricting the experiments to weak materials such as superlean grout and sand at low confining pressures.

The apparatus for testing conduit is the same as would be designed for testing the effectiveness of steel reinforcing bar (rebar) in tying two different materials together and should be so used. The problem is one in which large strains, material failure, and rebar debonding all play a role. In a simple analysis of the effective strength of a steel reinforced grout interface we assume that the weaker grout is fixed to the stronger grout if the sum of shear strength of the rebars plus that of the weaker grout, S_{o1}, is equal to the shear strength of the stronger grout, S_{o2}. For the full shear strength of a rebar to come into play the surface tractions exerted on the rebar by the weak grout must just equal the resisting force within the bar at the shear yield point of steel, S_{or}. Taking the total cross sectional area of the rebars as A_r and the area of the interface as A we equate the shear strength of the composite with that of the stronger medium,

$$A_r S_{or} + (A-A_r)S_{o1} = AS_{o2}$$

$$\frac{A_r}{A} = \frac{S_{o2}-S_{o1}}{S_{or}-S_{o1}}.$$

The critical length of reinforcing rod needed to develop the required shear force is

$$2S_{o1}dL = \frac{\pi d^2}{4} S_{or},$$

$$\frac{L}{d} = \frac{\pi}{8} \frac{S_{or}}{S_{o1}}.$$

As an example, for superlean grout, S_{o1}, tuff matching grout, S_{o2}, and steel rebar, S_{or}, the area of steel to that of grout and the critical L/d are:

S_{o1}	S_{o2}	S_{or}	A_r/A	L/d
86.6 psi	866 psi	23,100 psi	0.034	104

Superlean grout is so weak compared to tuff that the rebar must provide 90 percent of the shear strength. Either the L/d must be great enough to allow the rebar to pick up the necessary surface tractions or A_r/A must be adjusted accordingly.

A second type of shear test, which we shall call a direct shear test, is useful for testing the simple analytic models and for acting as a check on the tests of shear at a plane of weakness. In concept the test is simple; in practice care must be exercised to ensure accurate measurements. The purpose of the experiment is to measure the force on a rigid rod produced by the motion of backfill. The experimental setup is indicated schematically in Figure 6.2. The parameters to be varied are the type of backfill, the yield strength, and the state of stress. Problems involving strain rate and pore-water migration will have to be solved and this presumably will have been done by the experiments for testing conduit strain at a plane of weakness. The design of a good seal between the pressure vessel and rigid rod that will at the same time allow a good force measurement and prevent grout extrusion may prove troublesome. A simple silastic ring may prove to be adequate.

17. AXIAL LOADING, SLIP, AND BUCKLING EXPERIMENTS

The questions to be resolved by axial loading experiments (which will be described in short order) are as follows:

a. What is the magnitude of the axial surface tractions transmitted to conduit as the backfill suffers axial compression?

b. What is the amount of slip between the conduit and backfill?

c. Under what circumstances will buckling occur?

d. How do end, surface, and joint conditions affect the conduit response?

e. How do slip joints compare with slack or "meander" conduit?

The parameters to be varied are the same as those for the shear tests, i.e., backfill, stress state, yield strength, and conduit filling material. The test setup is indicated schematically in Figure 6.3. Several different end conditions need to be investigated. At the far end of the grout chamber, near the fixed back plate, the conduit can be either free-floating or fixed to the back plate. At the near end the conduit should be capped a few centimeters below the surface of the grout. Two different caps should be used: one with the same diameter as the conduit to keep the end load at a minimum and the other with a larger diameter to increase the axial load on the conduit. With the conduit in contact with the ram and with a long L/d ratio the effects of compression on a canister-conduit joint can be studied experimentally. The effect of a tapered transition can also be studied. Having designed canister and cable systems without the benefit of reentry observations we believe that these scaled tests will prove extremely useful. Some thought should be given to the feasibility of extending these tests to the problem of fanning-in and fanning-out many cables to and from a single conduit.

The last research test that we shall discuss is a direct pull-out test of conduit embedded in backfill. The question to be answered by this test is: what is the force required to pull conduit through backfill? It is of interest to initially have the backfill both in the unstressed state and on the yield surface. The parameters to be varied are the same as in the other tests. Because of the uncertainties that arose in the Husky Pup cable experiment it would be of value to test straight conduit with the far end free and to test slack or meander cable with the far end both fixed and free. Practical details concerning the best way to build the pressure vessel and to effect a low drag, non-leaking conduit feed-through need to be worked out.

18. TEST ENGINEERING EXPERIMENTS

Because of the controversy that exists concerning the performance of gas-seal connectors we believe that tests of electrical continuity and noise-generation in gas-seal connectors under shock loading are necessary. The

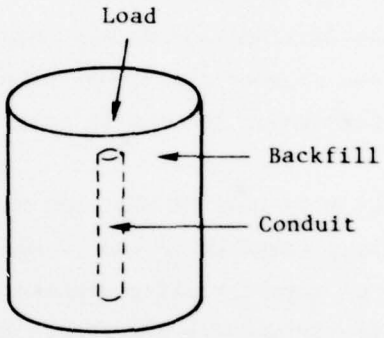

Figure 6.3 Axial conduit loading.

initial set of tests can be simple impact or drop tests. If the connectors pass the shock tests then more sophisticated pressure loading tests should be considered. To provide design specifications, junction boxes and canisters should be subjected to cable pull-out tests. The pull-out force should be no less than the force which causes the cable to fail.

19. SMALL-SCALE MODEL EXPERIMENTS

Based simply on geometrical scaling the group of tests comprising the Diamond Mine HE, the Mine Dust HE, the Husky Pup cable add-on experiment, and the Mighty Epic interface experiment suggests that scaled tests might be a useful way to test a hardened cable plant prior to full-scale deployment. The two nuclear tests and the Diamond Mine HE shot experienced failures that appear to be shear induced at one or more locations. The Mine Dust HE cables maintained their integrity throughout the entire event and remained operative after the shot.

The success of the Mine Dust HE shot may have resulted either from a more advantageous cable topology compared to the Diamond Mine HE test and to the nuclear tests, or based on simple scaling arguments the improved topology may have been aided by relatively massive armoring. Full scale cable armor dimensions, based on the 1/4 inch diameter Mine Dust armor, as a function of nuclear yield are plotted in Figure 6.4. The full-scale armor dimensions are greater than have been employed on nuclear tests. (Moreover, to load gages in boreholes the explosive tests employed aluminum angle which was left in place, thus providing additional cable support.) The basic theoretical idea behind the concept of scaled tests, that identical strains occur at scaled locations so that the response of full-scale cable armor can be tested in small-scale experiments, needs to be supported by more detailed analyses. The scaling argument might be persuasive were it not for the results of Dido Queen (Section III.4.4) which demonstrated the value of 1/4 inch OD 6061-T6 aluminum armor in extending the recording time on a full-scale test. It is clear that the analysis has not progressed to the point where geometric scaling can explain the performance of cable armor.

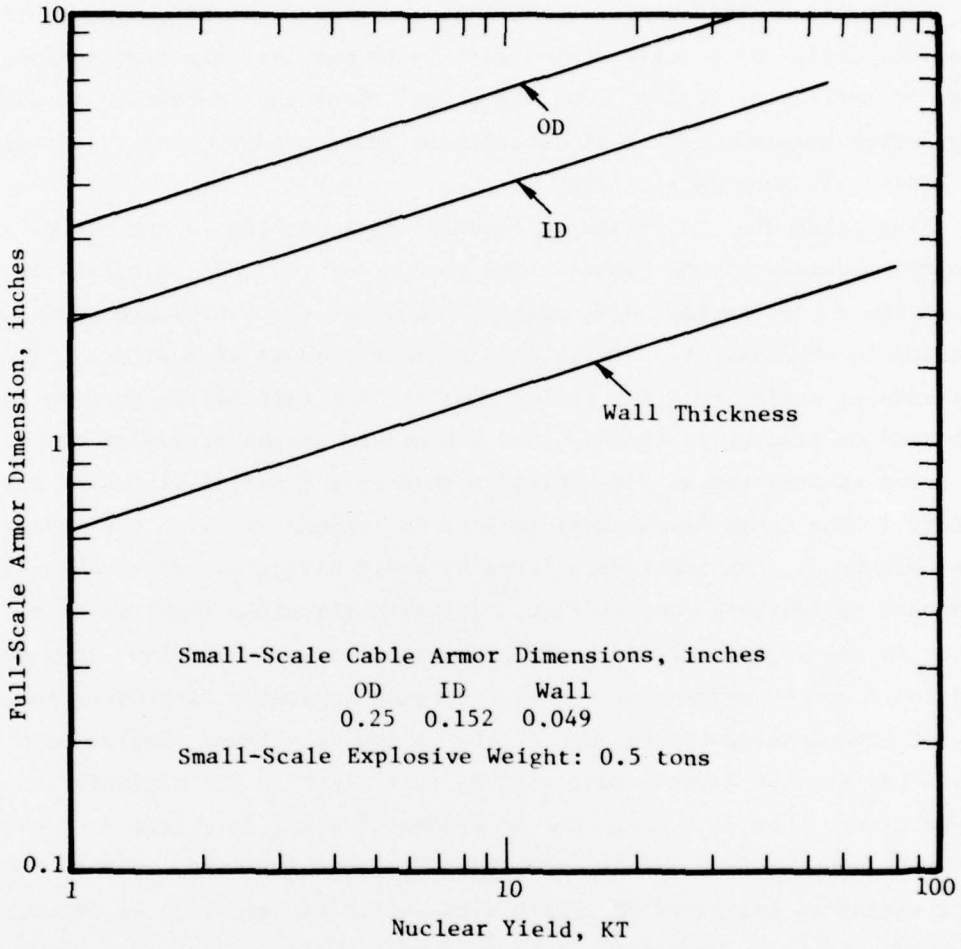

Figure 6.4 Full-scale cable armor dimensions vs nuclear yield based on Mine Dust and Diamond Dust HE tests.

SECTION VII

CONCLUSIONS AND RECOMMENDATIONS

To conclude this report we outline the procedures that are needed for the logical design of a cable system that is to survive late-time motions in the two to three kbar region. Not all of the steps can be carried through to completion because of lack of data; these shortcomings constitute areas where additional work is required.

The first step in designing a cable system is the laying out of the mechanical topology of the cables. The purpose of the cable topology is to minimize shear offsets and axial strains. Whether the cables are radial or non-radial is of lesser importance than avoiding planes of weakness. (It goes almost without saying that for cables that are not expected to survive for a long period of time it is crucial that the ground motion arrive at the transducer prior to arriving at the cable; in this case a radial placement may be mandatory.) The cable layout must be done in conjunction with the layout of drifts, bulkheads, and other structures to avoid having an unfavorable cable run imposed by existing construction. The as-built cable topology should be included in the Project Officer's Report. The entire cable plant must be considered from the transducer to the recording apparatus to prevent one weak component from causing the failure of the entire data link. Cables must be isolated from the differential motions that occur in the vicinity of most structures. Axial strains can be estimated using data from past experiments or if need be (and not as desirable) from machine calculations. Shear offsets cannot be estimated ab initio with sufficient accuracy to be useful for design purposes. Past data might be used to estimate an upper bound for the offsets at all planes of weakness, but such estimates tend to be quite rough. We have not studied the economics of allowing for large offsets at all planes of weakness. Additional research on offset motion is needed. Offsets produce shear loads on cables which can be estimated by the procedures of Section V. The accuracy of the estimates needs to be established by experiments as discussed in Section VI. At the present state-of-the-art a workable method for protecting cables from shear failure at an unavoidable plane of weakness is uncertain. The shear experiments of Section VI should provide

insight into the interactions between a cable and backfill and also give guidance to design techniques. Where construction has created a weak zone, the possibility of limiting shear by tying different media together with reinforcing bars needs further development and experiments to provide design data are suggested in Section VI.

Different experimenters use different cables for similar applications. Some experimenters either employ or have suggested the employment of cable types that have been tried and discarded by other experimenters. A variety of cables have been used to attain limited goals, but no technique has demonstrated the ability to survive late-time motions on a full-scale test in the two to three kbar region. Several experiments have suggested the value of strong conduit in protecting relatively soft cables and this technique has been taken up by recent cable hardening design. The value of the conduit resides not in protecting the cable from the pressure field (such protection is unnecessary), but in improving the axial strain capabilities and in resisting shear. The shear resistance has arisen not by design, but by virtue of the stoutness of the design which is needed to prevent collapse of the conduit. The use of slip joints has been shown by experiment to be one method of taking up axial strain. If the axial strain exceeds the capacity of the slip joints the cable is subject to catastrophic failure imposed by buckled conduit (Section IV). The axial slippage between backfill and conduit, and the lateral support against buckling afforded to conduit by backfill needs clarification. Experiments to investigate axial loading effects are discussed in Section VI.

Inattention to detail or faulty components can cause the failure of an entire data link system. Some experimenters (but not all) have subjected the connection of the cable and the canister to a tensile test, demanding that the force to fail the connection at least equal the tensile strength of the cable. All designs that find their way to the field should be subjected to such a test and the results documented in the Appendix to the Project Officer's Report. Shear and compression tests of connections are also necessary (Section VI). Evidence has not been found of failures at junction boxes, provided that the junction boxes are filled with a relatively incompressible material, such as epoxy. Although junction boxes to not seem to

be a source of failure we believe that the effectiveness of cable grips at the boxes needs to be documented by experiment. The danger (which happens all too often in experiments) is that a seemingly minor change to a workable design, say the substitution of one grip for another, can result in failure. The most controversial component is the gas-seal and its mount. Many experimenters state in that the hermetic gas-seal used on underground tests is responsible for many failures; Field Command believes that the connectors are adequate. We believe that shock and pressure tests are needed to help resolve the controversy. Better control on the locating of cable faults in the field may also be required to distinguish between connector failure and cable failure.

SECTION VIII

LIST OF REFERENCES

1. Teller, E., et al, The Constructive Uses of Nuclear Explosives, 1968, McGraw-Hill, pp. 136-7.

2. Perret, R. and Bass, C., Free-Field Ground Motion Induced by Underground Explosions, February, 1975, SAND74-0252.

3. Shunk, R., Personal communication.

4. Vincent, C., Personal communication.

5. Ibid.

6. Ibid.

7. Ibid.

8. Kratz, H., Personal communication.

9. Ibid.

10. Lindberg, H. and Senseny, P., "Theoretical and Laboratory Investigation of Deep-Based Structures--Support of Diablo Hawk", Monthly Progress Report No. 16, Contract DNA 001-76-C-0385, SRI International Project PYU 5762.

11. Bowles, J., Foundation Analysis and Design, 1977, McGraw-Hill, 2nd Ed.

12. Burland, J. B. and Wroth, C. P., "Settlement of Buildings and Associated Damage", Settlement in Structures, April, 1974, British Geotechnical Society Conference, Wiley, 1975, pp. 611-54.

13. Butters, S., Personal communication.

14. Avitzur, B., Metals Forming: Process and Analysis, 1968, McGraw-Hill, N. Y., p. 153.

15. Smith, D., Unpublished notes, Waterways Experiment Station.

16. LaComb, J., Personal communication.

17. Biot, Maurice A., Mechanics of Incremental Deformations, 1965, Wiley.

18. Den Hartog, J. P., Advanced Strength of Materials, 1952, McGraw-Hill.

19. Prager, W., On Plane Elastic Strain in Doubly Connected Domains, 1946, Applied Mathematics, Volume 3, pp. 377-81.

20. Timoshenko, S. and Goodier, J. N., Theory of Elasticity, 1951, Mc-Graw-Hill.

21. Den Hartog, J. P., loc. cit.

22. Prager, William and Hodge Jr., Philip G., Theory of Perfectly Plastic Solids, 1968, Dover.

23. Hill, R., "The Plastic Yielding of Notched Bars Under Tension," Quarterly Journal of Mechanics and Applied Mathematics, 1949, Volume 2, pp. 40-52.

24. Hartenbaum, B. and Schuster, S., Unpublished machine calculations of Mighty Epic ground motions.

APPENDIX A

NOMENCLATURE

a	exponent in formula for displacement
B	coefficient (random displacement)
C	coefficient (shear loading)
c	coeffient in formula for displacement
d	diameter of cable
E	Young's modulus
F	force per unit length on cable
G	coefficient in formula for cavity radius
h	depth of burial
I	moment of inertia
L	length
M	mass of spherical element of earth
M_p	plastic moment
n	porosity or void fraction
P	resisting pressure
R	final radial coordinate
R_c	radius of cavity
r	initial radial coordinate
S	final position of element
S_o	maximum shear stress
s	initial position of element
T	tensile force
u	displacement
w	load per unit length
Y	yield of explosion
α	angular offset from a radial line
ϵ	strain
γ_{max}	maximum shear strain
ρ	density
σ	normal stress component

θ	polar angle
Δ_c	deflection of cable
Δ_λ	random displacement
λ	wavelength
ν	Poisson's ratio
σ_y	yield strength in tension
τ	shear stress
$(\ )_c$	cavity
$(\ )_o$	initial value
$(\ )_r$	radial
$(\ )_t$	tangential
$(\ )_1$	final value

DISTRIBUTION LIST

DEPARTMENT OF DEFENSE

Atomic Energy
ATTN: Executive Assistant

Defense Advanced Rsch. Proj. Agency
ATTN: TIO

Defense Civil Preparedness Agency
ATTN: Hazard Eval. & Vul. Red. Div.,
G. Sisson

Defense Documentation Center
12 cy ATTN: DD

Defense Intelligence Agency
ATTN: DB-4E
ATTN: DB-4C, E. O'Farrell

Defense Nuclear Agency
ATTN: DDST
2 cy ATTN: SPSS
4 cy ATTN: TITL

Field Command
Defense Nuclear Agency
ATTN: FCTMOF
ATTN: FCPR

Field Command
Defense Nuclear Agency
Livermore Division
ATTN: FCPRL

Interservice Nuclear Weapons School
ATTN: TTV

Joint Strategic Tgt. Planning Staff
ATTN: NRI-STINFO, Library

NATO School (SHAPE)
ATTN: U.S. Documents Officer

Under Secretary of Defense for Rsch. & Engrg.
ATTN: Strategic & Space Systems (OS)

DEPARTMENT OF THE ARMY

BMD Advanced Technology Center
Huntsville Office
Department of the Army
ATTN: 1CRDABH-X
ATTN: ATC-T

Chief of Engineers
Department of the Army
ATTN: DAEN-RDM
ATTN: DAEN-MCE-D

Deputy Chief of Staff for Ops. & Plans
Department of the Army
ATTN: MOCA-ADL, Technical Library

Harry Diamond Laboratories
Department of the Army
ATTN: DELHD-N-TI
ATTN: DELHD-N-NP

DEPARTMENT OF THE ARMY (Continued)

Redstone Arsenal
U.S. Army R&D Command
ATTN: RSIC

U.S. Army Ballistic Research Labs
ATTN: DRDAR-BLE, J. Keefer
ATTN: DRDAR-BLV
ATTN: Technical Library
ATTN: DRDAR-BLT, W. Taylor

U.S. Army Engineer Center
ATTN: DT-LRC

U.S. Army Engineer Div., Huntsville
ATTN: HNDED-SR

U.S. Army Engineer Div., Ohio River
ATTN: ORDAS-L, Technical Library

U.S. Army Engr. Waterways Exper. Station
ATTN: W. Flathau
ATTN: J. Ingram
ATTN: L. Ingram
ATTN: G. Jackson
ATTN: Library

U.S. Army Material & Mechanics Rsch. Center
ATTN: Technical Library

U.S. Army Materiel Dev. & Readiness Command
ATTN: DRXAM-TL, Technical Library

U.S. Army Nuclear & Chemical Agency
ATTN: Library

DEPARTMENT OF THE NAVY

Civil Engineering Laboratory
Naval Construction Battalion Center
ATTN: Code L51, S. Takahashi
ATTN: Code L51, R. Odello
ATTN: Code L08A

Naval Electronic Systems Command
ATTN: PME 117-21

Naval Facilities Engineering Command
ATTN: Code 03T
ATTN: Code 09M22C
ATTN: Code 04B

Naval Material Command
ATTN: MAT 08T-22

Naval Postgraduate School
ATTN: Code 0142

Naval Research Laboratory
ATTN: Code 2627

Naval Surface Weapons Center
White Oak Laboratory
ATTN: Code F31

Naval Surface Weapons Center
ATTN: Technical Library & Info. Svcs. Br.

DEPARTMENT OF THE NAVY (Continued)

Naval Underwater Systems Center
ATTN: Code EM, J. Kalinowski

Naval War College
ATTN: Code E-11

Naval Weapons Evaluation Facility
ATTN: Code 10

Office of Naval Research
ATTN: Coe 474, N. Perrone
ATTN: Code 715, Technical Library

Office of the Chief of Naval Operations
ATTN: OP 03EG
ATTN: OP 981

Strategic Systems Project Office
Department of the Navy
ATTN: NSP-43

DEPARTMENT OF THE AIR FORCE

Air Force Geophysics Laboratory
ATTN: LWW, K. Thompson

Air Force Institute of Technology, Air University
ATTN: Library

Air Force Systems Command
ATTN: DLW

Air Force Weapons Laboratory
ATTN: SUL
ATTN: DE, M. Plamondon

Assistant Chief of Staff
Intelligence
Department of the Air Force
ATTN: INT

Deputy Chief of Staff
Research, Devleopment, & Acq.
ATTN: AFRDQSM

Deputy Chief of Staff
Logistics & Engineering
ATTN: LEEE

Foreign Technology Division, AFSC
ATTN: NIIS

Rome Air Development Center, AFSC
ATTN: TSLC

Space & Missile Systems Organization
Air Force Systems Command
ATTN: MNN

Strategic Air Command
Department of the Air Force
ATTN: NRI-STINFO, Library

DEPARTMENT OF ENERGY

Department of Energy
Albuquerque Operations Office
ATTN: CTID

Department of Energy
ATTN: Doc. Con. for Classified Library

DEPARTMENT OF ENERGY (Continued)

Department of Energy
Nevada Operations Office
ATTN: Doc. Con. for Technical Library

OTHER GOVERNMENT AGENCIES

Central Intelligence Agency
ATTN: OSI/NED, J. Ingley

Department of the Interior
Bureau of Mines
ATTN: Technical Library

DEPARTMENT OF ENERGY CONTRACTORS

Lawrence Libermore Laboratory
University of California
ATTN: Technical Information Dept. Library
ATTN: L-96, L. Woodruff
ATTN: D. Oakley

Los Alamos Scientific Laboratory
ATTN: MS364
ATTN: R. Bridwell
ATTN: M. Peek

Sandia Laboratories
ATTN: L. Hill
ATTN: Orgn. 3141
ATTN: A. Chabai

Sandia Laboratories
ATTN: Library & Security Classification Div.

DEPARTMENT OF DEFENSE CONTRACTORS

Aerospace Corporation
ATTN: Technical Information Services

Agbabian Associates
ATTN: M. Agbabian

Applied Theory, Inc.
2 cy ATTN: J. Trulic

Avco Research & Systems Group
ATTN: Library, A830

BDM Corporation
ATTN: Corporate Library
ATTN: T. Neighbors

Boeing Company
ATTN: Aerospace Library

California Research & Technology, Inc.
ATTN: S. Shuster
ATTN: Library
ATTN: K. Kreyenhagen

Calspan Corporation
ATTN: Library

Civil Systems Corporation
ATTN: J. Bratton

University of Dayton
Industrial Security Super., KL-505
ATTN: H. Swift

DEPARTMENT OF DEFENSE CONTRACTORS (Continued)

University of Denver
Colorado Seminary
Denver Research Institute
ATTN: Security Officer for J. Wisotski

EG&G Washington Analytical Services Ctr., Inc.
ATTN: Library

Eric H. Wang
Civil Engineering Rsch. Facility
The University of New Mexico
ATTN: N. Baum

Gard, Inc.
ATTN: G. Neidhardt

General Electric Company-TEMPO
ATTN: DASIAC

H-Tech Laboratories
ATTN: B. Hartenbaum

IIT Research Institute
ATTN: Documents Library

University of Illinois
Consulting Services
ATTN: N. Newmark

Institute for Defense Analyses
ATTN: Classified Library

Kaman AviDyne
Division of Kaman Sciences Corp.
ATTN: E. Criscione
ATTN: N. Hobbs
ATTN: Library

Kaman Sciences Corp.
ATTN: Library

Lockheed Missiles and Space Co., Inc.
ATTN: Technical Information Center, D/Coll.
ATTN: T. Geers

McDonnell Douglas Corp.
ATTN: R. Halprin

Merritt CASES, Inc.
ATTN: J. Merritt
ATTN: Library

Oak Ridge National Laboratory
Union Carbide Corporation
Nuclear Division
ATTN: Civil Def. Res. Proj.
ATTN: Doc. Con for Technical Library

Physics International Co.
ATTN: F. Sauer
ATTN: L. Behrmann
ATTN: Technical Library
ATTN: E. Moore
ATTN: J. Thomsen

DEPARTMENT OF DEFENSE CONTRACTORS (Continued)

R & D Associates
ATTN: C. MacDonald
ATTN: R. Port
ATTN: Technical Information Center
ATTN: W. Wright, Jr.
ATTN: J. Lewis
ATTN: H. Brode
ATTN: A. Latter

R & D Associates
ATTN: H. Cooper

Science Applications, Inc.
ATTN: Technical Library

Science Applications, Inc.
ATTN: D. Maxwell
ATTN: D. Bernstein

Southwest Research Institute
ATTN: W. Baker
ATTN: A. Wenzel

SRI International
ATTN: G. Abrahamson
ATTN: B. Gasten

Systems, Science & Software, Inc.
ATTN: Library
ATTN: T. Cherry
ATTN: D. Grine
ATTN: T. Riney

Terra Tek, Inc.
ATTN: A. Abou-Sayed
ATTN: Library
ATTN: S. Green

Tetra Tech, Inc.
ATTN: L. Hwang
ATTN: Library

TRW Defense & Space Sys. Group
ATTN: P. Bhutta
ATTN: Technical Information Center
2 cy ATTN: P. Dai

TRW Defense & Space Sys. Group
San Bernardino Operations
ATTN: F. Wong

Universal Analytics, Inc.
ATTN: E. Field

Weidlinger Assoc., Consulting Engineers
ATTN: M. Baron

Weidlinger Assoc., Consulting Engineers
ATTN: J. Isenberg

Westinghouse Electric Corp.
Marine Division
ATTN: W. Volz